Theses and Dissertations--Chemistry   Chemistry

2018

Assembly and Trafficking of the Cystic Fibrosis Transmembrane Conductance Regulator and Associated Proteins

Zhihui Zhang

University of Kentucky, zhihui.zhang@uky.edu
Author ORCID Identifier:
https://orcid.org/0000-0002-4896-0559
Digital Object Identifier: https://doi.org/10.13023/etd.2018.380

Recommended Citation

Assembly and Trafficking of the Cystic Fibrosis Transmembrane Conductance

Regulator and Associated Proteins

DISSERTATION

A dissertation submitted in partial fulfillment of the requirements for the degree of
Doctor of Philosophy in the College of Arts and Sciences at the University of Kentucky

By

Zhihui Zhang

Lexington, Kentucky

Director: Christopher I. Richards, Associate Professor of Chemistry

Co-Director: Yinan Wei, Associate Professor of Chemistry

Lexington, Kentucky

2018

ABSTRACT OF DISSERTATION

**ASSEMBLY AND TRAFFICKING OF
THE CYSTIC FIBROSIS TRANSMEMBRANE
CONDUCTANCE REGULATOR AND ASSOCIATED PROTEINS**

Cystic Fibrosis (CF) is an autosomal recessive genetic disease that leads to severe malfunction in many organs, but particularly the lungs. The primary cause of this malfunction is the decrease of the airway surface liquid layer on the lung epithelium. The lack of hydration leads to mucus build up on the epithelial lining, leading to blockage of airways. The underlying cause of CF is the dysfunction of the cystic fibrosis transmembrane conductance regulator (CFTR), which results from mutations in the protein. Almost 90% of CF patients are caused by the deletion of the phenylalanine at position 508 of CFTR, which is believed to affect the folding and stability of CFTR. The misfolded ΔF508-CFTR undergoes ER associated degradation (ERAD), causing the failure of ΔF508-CFTR trafficking to the cell surface. Small molecule correctors yield moderate improvements in the trafficking of ΔF508-CFTR to the plasma membrane. It is currently not known if correctors increase trafficking through improved cargo loading of transport vesicles or through direct binding to CFTR. In this dissertation, real-time measurements of trafficking were utilized to identify the mechanistic details of chemical, biochemical, and thermal factors that impact CFTR correction, using the corrector molecule VX-809, a secondary mutation (I539T), and low temperature conditions. Each individually improved trafficking of ΔF508-CFTR to approximately 10% of wild-type levels. The combination of VX-809 with either low temperature or the I539T mutation increased the amount of CFTR on the plasma membrane to nearly 40%, indicating synergistic activity. The number of vesicles reaching the surface was significantly altered; however the amount of channel in each vesicle remained the same. Therefore, a 2 step therapeutic approach might be an ideal treatment for CF. The first step would be composed of a compound that mimics the mechanism of stabilization provided by low temperature or the I539T mutation, while the second step would be VX-809 or a similar corrector compound. These studies suggest that understanding how low temperature and second site suppressors alter ΔF508-CFTR could be key to the development of future therapeutics for the effective treatment of CF.

The precise pathophysiology of cystic fibrosis is not well studied. The involvement of another transport protein, epithelial sodium channel (ENaC), makes the situation more complicated. ENaC and CFTR are colocalized on the apical surface of epithelia cells. With our fluorescence microscopy techniques, we explored the effects of CFTR on the residence time of ENaC on the cell membrane. A reliable approach measuring the half-life of protein on the cell membrane is required for this study. We present a new approach to quantify the half-life of membrane proteins on the cell surface, through tagging the protein with the photoconvertible fluorescent protein, Dendra2. Total internal reflection fluorescence microscopy (TIRF) is applied to limit visualization of fluorescence to proteins located on

the plasma membrane. Photoconversion of Dendra2 works as a pulse chase experiment by monitoring only the population of protein that has been photoconverted. As the protein is endocytosed the red emission decreases due to the protein leaving the TIRF field of view. The half-life of the protein on the plasma membrane was calculated upon imaging over time and quantifying the change in red fluorescence. Our method provides a unique opportunity to observe real-time protein turnover at the single cell level without addition of protein synthesis inhibitors. This technique will be valuable for the future protein half-life study.

KEYWORDS: cystic fibrosis, membrane protein half-life, TIRF, real-time measurement

Zhihui Zhang

08/01/2018

Assembly and Trafficking of the Cystic Fibrosis Transmembrane Conductance Regulator

and Associated Proteins

By

Zhihui Zhang

Dr. Christopher I. Richards
_____
Director of Dissertation

Dr. Yinan Wei
_____
Co-Director of Dissertation

Dr. Mark A. Lovell
_____
Director of Graduate Studies

08/01/2018
_____
Date

ACKNOWLEDGEMENTS

TABLE OF CONTENTS

v

LIST OF FIGURES

CHAPTER 1: BACKGROUND INFORMATION

1.1.Membrane Protein Trafficking and Endocytosis in Cells

Proteins on the cell membrane are associated with many aspects of cellular function and convert extracellular stimuli into intracellular signals. Proteins on the cell membrane undergo a complicated process from the initial transcription to the final delivery to the cell surface. In addition, proteins have limited life time on the cell membrane as they return to the interior of the cell after finishing the mission on the cell surface. The failure of trafficking or endocytosis has been connected to several diseases, such as cystic fibrosis and Liddle's syndrome. Therefore, it is essential to understand trafficking and endocytosis for the development of new therapeutic approaches of these diseases.

1.1.1 Transcription and Translation

Eukaryotic cells have three classes of RNA polymerase, RNA polymerase I, II, III. RNA polymerase II is responsible for the transcription of the protein-encoding gene, and thus mRNA is transcribed by RNA polymerase II[1]. Initially, RNA polymerase II interacts with the transcription factors, a DNA binding protein, which is capable of recognizing and accurately initiating transcription at specific promoter sequence. During transcription, RNA polymerase II first generates long mRNA containing untranslated 5'region, multiply

exons, multiply introns, and an untranslated 3' region. Then, introns are removed (splicing) to create mature mRNA consisting of exons as well as 5' and 3' noncoding regions[2-4]. A gene can produce multiple forms of mature mRNA by using different promoters, selection of different polyadenylation sites, or alternative splicing. Transcription occurs in the nucleus.

Translation converts the language of genetic information in the sequence of mRNA into the amino acid sequence of a polypeptide chain. Message RNAs export from the nucleus to cytoplasm and then protein are synthesized on ribosomes by linking amino acid together in a specific order. Protein biosynthesis in all cells includes three distinct phases: (1) Initiation: mRNA binding by the small ribosomal subunit (40S) triggers the protein synthesization. Then, an initiator aminoacyl-tRNA (tRNA$_i^{Met}$) recognizes the first codon followed by the large ribosomal subunit (60S) joining the initiation complex, which prepares for the next stage. (2) Elongation: the ribosome remains binding with the mRNA and moves along it in the 5' to 3' direction, recruiting aminoacyl-tRNAs whose anticodons match with the successive codons. In this manner, the polypeptide grows one amino acid at a time and eventually forms a whole polypeptide chain. (3) Termination: This step occurs when the ribosome reaches a "stop" codon on the mRNA. At this time, the ribosomal subunits release from the mRNA and the primary structure of a protein forms. Cytosolic protein are translated on free ribosomes, and secretory protein are translated on ribosomes attached to rough endoplasmic reticulum (ER)[5-6].

1.1.2   Protein Trafficking

Membrane proteins need to go through the secretory membrane system to eventually arrive at the cell membrane. The secretory membrane system is made up of organelles including the endoplasmic reticulum (ER), the Golgi complex, and tubulovesicular transport intermediates that regulate intracellular membrane transport between them. The linear polypeptide chain gives rise to a three dimensional conformation in the ER and then the protein is loaded to a secretory cargo and transported to the Golgi complex for further processing and maturation. It is sorted and packaged into post-Golgi carriers that move through the cytoplasm to fuse with the cell membrane[7].

1.1.2.1 Protein Translocation from Ribosome to the ER

In higher eukaryotic cells, the translocation of many proteins across the ER membrane occurs co-translationally. Protein intended for functioning in membranous organelles or exporting from the cells carry an extra amino acid residue at the N-terminus that is the signal sequence serving as the reorganization site for sorting and dispatching the protein to their proper destination. The protein with the extra N-terminal sequence is called a precursor. Signal recognition particles (SRPs), together with signal receptors (SRs), associate with the N-terminal sequence of a polypeptide as it undergoes polypeptide chain elongation. If the polypeptide N-terminal sequence is a signal sequence, the nascent chain will be translocated into ER. The N-terminal signal sequence is clipped off by membrane-bound signal peptidase after the whole polypeptide chain enters the lumen ER[8-10].

1.1.2.2 Protein Folding in the ER

Protein folding is the process through which a linear polypeptide chain acquires its three dimensional conformation for its proper biological function. Previous studies showed that the linear amino acid sequence was only the information required for proper folding of a polypeptide[11-13]. The driving force for protein folding is the burial of hydrophobic side chains from the aqueous solvent, which places the whole system in the lowest Gibbs free energy state. Therefore, a folded protein usually has a buried hydrophobic core and a hydrophilic surface.

Protein folding is often assisted by molecular chaperones. Protein folding in *E. coli* has both chaperone independent and chaperone dependent pathways, while protein folding in eukaryotic cells is more complicated[14]. Many molecular chaperons are heat shock proteins (Hsp). The principle Hsp chaperones are Hsp70, Hsp60 and Hsp90[15]. In the chaperone dependent pathway, Hsp70 protein binds with an unfolded nascent polypeptide emerging from ribosome. Hsp70 protein such as DnaK is made up of two domains: an N-terminal ATP-binding domain, and a central domain that binds with the exposed hydrophobic regions of the nascent polypeptide. The DnaK : ATP complex receives an unfolded (or partially folded) polypeptide chain from the a Hsp40 family member DnaJ. The formation of the DnaK : DnaJ complex with the unfolded polypeptide sufficiently prevents unfolded protein aggregation. The substitution of ADP with ATP on DnaK is catalyzed by Grp releasing the polypeptide chain form the complex, which gives the unfolded polypeptide the opportunity to fold. Partially folded intermediates or, in some cases, completely folded proteins are formed with multiple cycles of Hsp70 interaction. The partially folded

intermediates may be passed to the Hsp60 chaperonin system to complete the protein folding. Hsp60 provides an enclosed environment to the partially folded protein, allowing for protein folding proceeding spontaneously in a protective space. Hsp60 chaperones are divided into two classes based on the source and structure. Group I Hsp60 chaperones are found in bacteria, named GroES-GroEL complex. Group II Hsp60 chaperones, CCT/TRiC, exist in archaea and eukaryotic cells and are analogs of GroEL. After the conformational regulation done by Hsp70 and Hsp60, some molecules such as transduction molecules require the additional interaction with Hsp90 to be fully functional. Transduction molecules include receptor tyrosine kinases, soluble tyrosine kinases, and steroid hormone. Cystic fibrosis transmembrane conductance regulator (CFTR) is Hsp90 dependent as well[16-17].

1.1.2.3 Protein Transport from the ER to the PM

Secretory proteins crossing of the ER membrane through ER exit sites is usually accomplished by the activities of cytosolic coat protein complex (COP II), which are scattered over the ER membrane[18]. The assembly of COP II is initiated by a GTP binding protein, Sar1, which is capable of activing the ER membrane. Sec23/24 and Sec13/31 are assembled onto the activated ER membrane to form a COP II bud loading with the cargo protein. The COP II buds are delivered to pre-Golgi intermediates that are recognized as transport vehicles for protein delivery to the Golgi complex[19-21].

Pre-Golgi intermediates first merge with the cis-face of Golgi, which exists as an elaborate tubular network. The cargo proteins then go through polarized stacks of Golgi cisternae to

the trans-Golgi network (TGN) where they are packaged into membrane-bound carriers destined for the plasma membrane[22]. The post-Golgi carrier formation requires 3 steps: (1) the secretory proteins initially segregate into discrete domains on Golgi membranes; (2) The domains elongate into tubules; (3) the initial segregated domains detach from the Golgi body and form post-Golgi carriers[23-24].

After detaching as tubules from the Golgi complex, post-Golgi carriers move toward the cell membrane. They remain stationary for a variable period (15–30 s) and then rapidly fuse with the plasma membrane. Fusions occur randomly across the cell surface[7].

1.1.3 Endocytosis

Endocytosis is thought as the process that nutrients and other molecules are taken up from the extracellular milieu[25], while it is critical in maintaining the balance of protein on the cell membrane as well. Extracellular materials transporting to the cytoplasm is usually called pinocytosis or phagocytosis depending on the size of the cytoplasmic vesicle and the property of the cargo molecules. Molecules on the cell surface mostly internalize to the cytoplasm via clathrin-dependent or caveolae-dependent pathways. Clathrin-dependent pathways are the major route [26-27] and the mechanism is well studied.

Clathrin-mediated endocytosis is the uptake of molecules from the cell surface to the interior of the cell via clathrin-coated vesicles, which are formed from the cell membrane[26, 28-29]. It has been identified by electron microscopy images that clathrin is the major protein making the lattice-like coat around vesicles [30]. The clathrin-mediated pathway is so far the

best characterized endocytosis route. Clathrin does not directly bind with the cargo protein or cell membrane. In contrast, the clathrin coating process relies on adaptor protein 2 (AP2) and other accessory proteins[27-28, 31]. The formation of clathrin-coated vesicle requires 5 stages: **(1) Nucleation.** The first stage demands the formation of a putative nucleation module that defines the sites on the plasma membrane where clathrin will be recruited and vesicles will bud. This process calls for plasma membrane-specific lipid phosphatidylinositol-4,5-bisphosphate (PtdIns(4,5)P$_2$), including FCH domain only (FCHO) proteins, EGFR pathway substrate 15 (EPS15) and intersectins. These factors work together to initiate the formation of clathrin-coated pits by recruiting AP2. **(2) Cargo selection.** Cargo is specifically selected by AP2. AP2 binds both cargo and PtdIns(4,5)P$_2$, and then recruits several classes of cargo-specific adaptor. **(3) Clathrin coat assembly.** Clathrin coat is formed through AP2 or accessory adaptor proteins recruiting more clathrin triskelia around the pit. **(4) Vesicle scission.** The vesicle budding process depends on dynamin, a mechanochemical enzyme. Dynamin binding at the neck of the vesicle triggers membrane scission. This process requires GTP hydrolysis. **(5) Uncoating and clathrin component recycling.** As soon as the vesicle is detached from the cell membrane, the clathrin coat is disassembled. The uncoated vesicles move to fuse with their target endosomes. The cargo protein in endosomes will be eventually sent to either lysosome for degradation or the cell membrane for recycling.

1.2.Cystic Fibrosis and Cystic Fibrosis Transmembrane Conductance Regulator

1.2.1. History of Cystic Fibrosis

Cystic Fibrosis appeared about 3,000 BC caused by the migration of people, gene mutations and new conditions in nourishment. It is most common among people of eastern European ancestry and least common in Africans and Asians[32]. Although cystic fibrosis was not yet recognized as a specific disease, literature from Germany and Switzerland in the 18th century reported the association between salt loss and illness[33]. In 1938 Dorothy Hansine Andersen published an article, "Cystic Fibrosis of the Pancreas and Its Relation to Celiac Disease: a Clinical and Pathological Study", in the American Journal of Diseases of Children. She is the first one to describe the characteristic cystic fibrosis of the pancreas and correlate it with the previously known lung and intestinal symptoms[34]. Since then, it has been learned that Cystic Fibrosis (CF) is an autosomal recessive disease caused by the presence of mutations in both copies of the gene encoding the Cystic Fibrosis Transmembrane Conductance Regulator (CFTR). Those with a single working copy are carriers. In the United States, about 1 in 3300 newborns are diagnosed with CF and about one in 25 people are carriers[35].

1.2.2. Pathology of Cystic Fibrosis

Cystic Fibrosis (CF) is an autosomal recessive genetic disease that leads to severe malfunction in many organs, and particularly the lungs[36]. The primary cause of this malfunction is the decrease of the airway surface liquid layer (ASL) on the lung

epithelium[37]. The lack of hydration leads to mucus build up on the epithelial lining and the blockage of airways[37-40]. This condition is exacerbated by the inability to remove the bacteria trapped in this mucous layer, resulting in chronic infection of the respiratory system. The underlying cause of CF is the dysfunction of the cystic fibrosis transmembrane conductance regulator (CFTR), which results from mutations in the CFTR gene[41-42]. CFTR serves as an ion channel, regulating anion secretion and thereby playing a crucial role in maintaining proper fluid volume in the lumen of many organs, including the lungs, pancreas, and intestines. Nearly 2000 different mutations can cause CF exist and the most prevalent mutation is the deletion of the phenylalanine at position 508 (ΔF508) of nucleotide binding domain 1 (NBD1)[43]. Approximately, 90% of those suffering from CF have this mutation on at least one allele. ΔF508 is believed to affect the folding and stability of CFTR. As shown in Figure 1.1, the deletion of this single amino acid prevents CFTR from undergoing anterograde coat protein complex II (COPII) dependent transport from the ER to the Golgi and on to the cell surface; instead the channel undergoes ER associated degradation (ERAD)[44-47]. Evidence points toward local misfolding of ΔF508-CFTR and destabilization of the protein once folded[48-49]. For example, ΔF508-CFTR is more susceptible to proteolytic digestion, has a lower open probability once it is on the plasma membrane (PM), and unfolds at lower temperature and lower urea concentrations than wild-type CFTR[50-52]. The change in stability of ΔF508-CFTR likely results from a combination of decreased structural stability in NBD1 itself and an interruption of normal domain-domain interactions[48, 53-54].
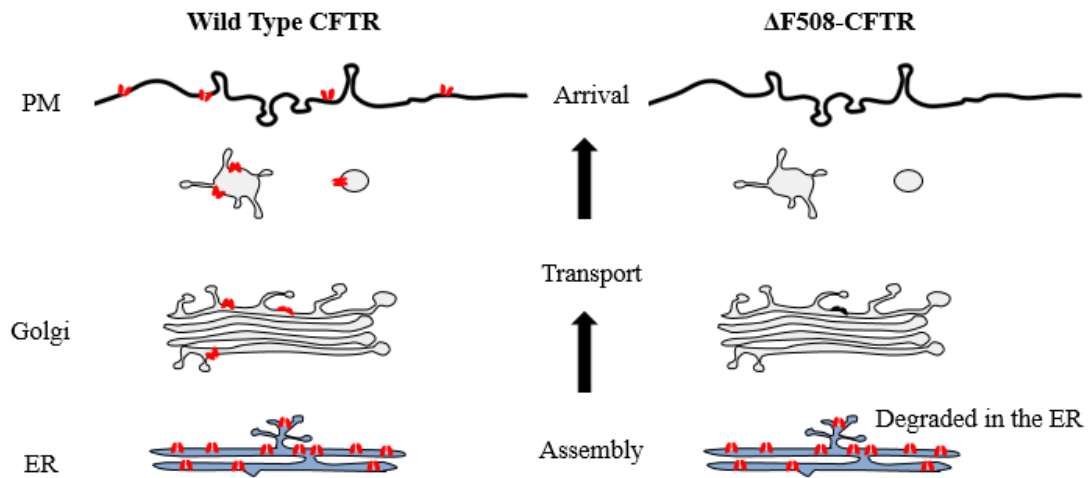
Figure 1.1: Comparison of Wild-type CFTR with ΔF508 CFTR. Left: The regular pathway for wild-type CFTR that get transported from the Endoplasmic Reticulum (ER) to the Golgi and on to the cell surface. Right: The pathway for ΔF508 CFTR, which undergoes ER associated degradation.

1.2.3. Structure of Cystic Fibrosis Transmembrane Conductance Regulator

CFTR is the only one in the ABC (ATP-binding cassette) transporter family that works as an ion channel on the apical membrane of epithelial cells. It primarily regulates chloride and bicarbonate transport across the cell membrane[55-57]. CFTR is a single polypeptide chain consisting of 1480 amino acid residues. CFTR has a conserved ABC transporter structure of 2 Membrane Spanning Domains (MSD) and 2 Nuclear Binding Domains (NBD), but an additional regulatory domain (R domain) is unique for CFTR. All these domains arranged from N- to C-terminus are MSD1, NBD1, R, MSD2 and NBD2. Each membrane spanning domain consists of 6 membrane spanning α-helices and two MSDs can form a pore through which ions cross the membrane[58]. The 4th extracellular loop is glycosylated at residues 894 and 900[59]. The R domain seems to be mostly random coil with 5% α-helical structure based on NMR and other biophysical approaches[60]. The R domain has target sites for Protein Kinase A for phosphorylation, which initiates the CFTR channel ion transport cycle[61].

A

Structure of CFTR

Extracellular

Intracellular

Plasma Membrane

NH$_2$

NBD1

R

NBD2

COOH

B

Out

TMD2

TMD1

In

R domain

Lasso motif

NBD2

NBD1
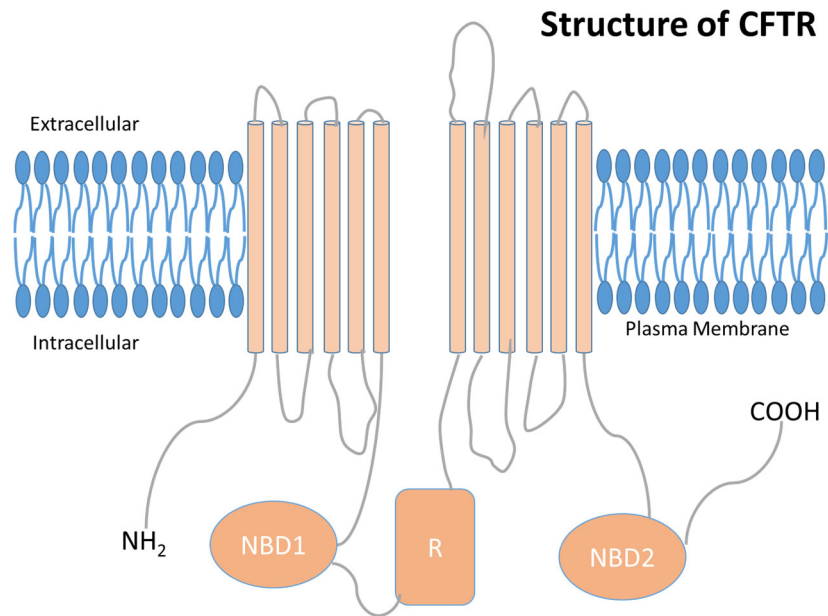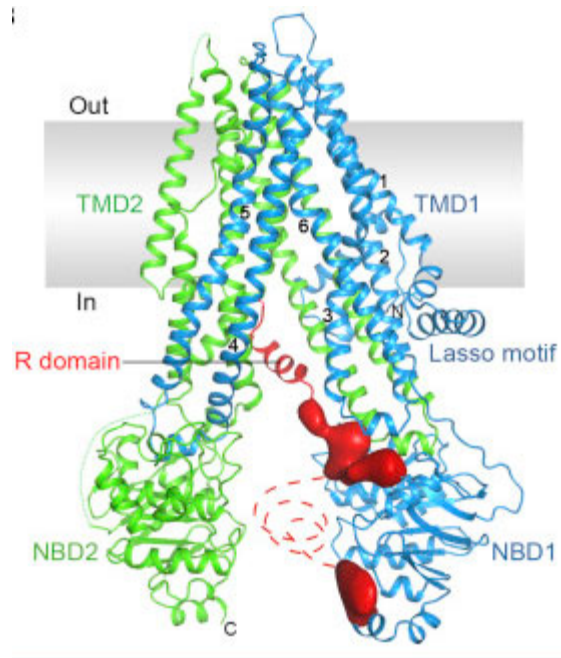
Figure 1.2: Structure of Cystic Fibrosis Transmembrane Conductance Regulator (CFTR) Structure. (*B* is reprinted with permission from Liu, F.; Zhang, Z.; Csanády, L.; Gadsby, D. C.; Chen, J., Molecular structure of the human CFTR ion channel. *Cell* 2017, *169* (1), 85-95. e8.)

1.2.4. Life Cycle of CFTR

In the life cycle of CFTR, four broad pathways have been identified: (1) biosynthesis, folding and trafficking from the ER to the PM; (2) endocytosis from the PM to the early endosomes; (3) recycling of endocytosed CFTR back to the cell surface; (4) endocytosed CFTR for degradation (Figure 1.3).

The folding of CFTR is primarily through a co-translational mechanism and the post-translation modification makes moderate changes to the conformation of CFTR. Initially, the co-translational folded CFTR inserts into the lipid bilayer of ER, where post-translational folding takes place. CFTR is core glycosylated in the ER and the glycans attached to CFTR are essential for the CFTR interactions with different lectins (in particular, calnexin). In the post-translation stage, CFTR binds with molecular chaperones and ubiquitin ligase enzymes, which play key roles in degrading the misfolded CFTR. Correctly folded CFTR moves to the Golgi complex where it undergoes further glycosylation to be fully folded. The mature native CFTR goes through the trans-Golgi network and then traffics to the PM. When ΔF508-CFTR is rescued from the ER by correctors such as VX-809 or reduced temperature, it is capable of accumulating on the plasma membrane. However, the rescued ΔF508-CFTR still folds improperly and it cannot function well as an ion channel[62]. Additionally, it is not as stable as wild-type CFTR on the plasma membrane. It has been shown that the half-life of ΔF508-CFTR on the plasma membrane is ~4 h, while it exceeds 48 h for wild-type CFTR[63].

The endocytosis of CFTR is primarily through the clathrin-mediated mechanism[64]. Initially, a putative nucleation module is formed on the site of CFTR molecule on the plasma membrane. An endocytic motif on the C-termini of protein is essential for the incorporation into clathrin-coated vesicles. CFTR contains a conserved YXXU motif—1421YDSI at the C-termini, which works as the endocytic motif recognized by adaptor protein 2[65]. When CFTR is specifically selected, the clathrin coating around CFTR starts to form followed by the clathrin coating vesicle splitting from the cell membrane. As soon as the vesicle is detached from the cell membrane, the clathrin coat is disassembled. The uncoated vesicle either forms an early endosome or immediately moves back to the cell membrane for recycling. The early endosome could be for recycling or degradation. Classifying of CFTR from the cell membrane into different routes is determined by small GTPases of the Rab family. Rab 5 regulates the cargo CFTR to enter to the early endosome followed by either Rab 7 facilitating the early endosome to form a late endosome for degradation or Rab 4 assisting the early endosome to recycle back to the cell surface[65]. Approximately 50% of wild-type CFTR is recycled back to the cell membrane rapidly within 5 minutes, while those that are not immediately recycled undergo the endosome recycling pathway for a slower recycling[66]. The balance of CFTR on the PM is maintained through anterograde trafficking, endocytosis, recycling and lysosomal degradation.
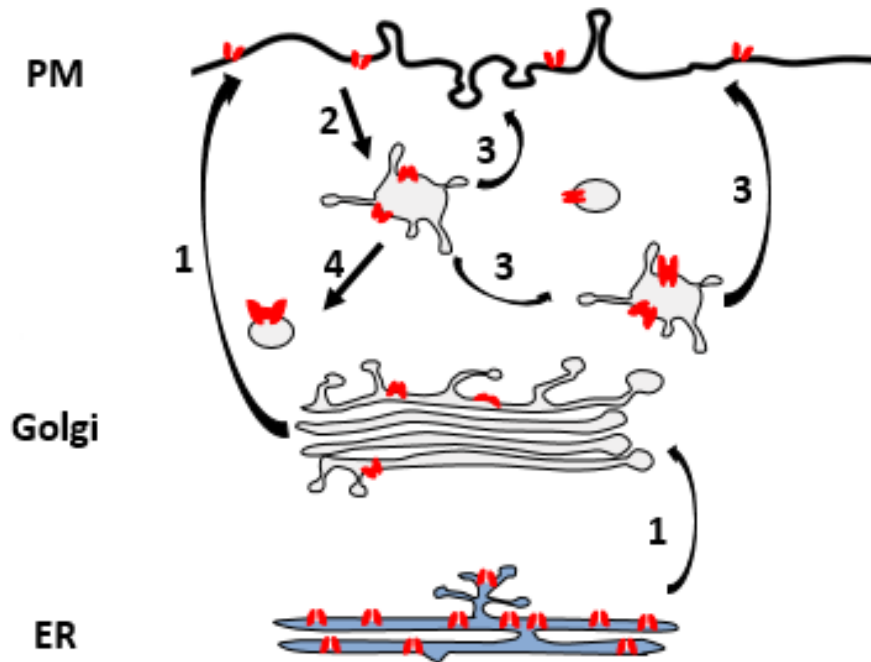
Figure 1.3: Life Cycle of CFTR. (1) CFTR is core glycosylated in the ER and then traffics to the cell membrane. (2) CFTR is endocytosed from the cell mmebrane through the clathrin-mediated pathway and forms an early endosome. (3) The early endosome can either immediatelly recyle back to the cell membrane or undergo the endosome recycling pathway for a slower recycling. (4) The early endosome forms a late emdosome for degradation.

1.2.5. Cystic Fibrosis Symptoms and Therapies

CFTR mainly regulates chloride across the membrane of epithelial cells. ΔF508-CFTR causes the failure of chloride transportation, which disrupts salt and water homeostasis. This causes thick, sticky mucus building up in essential organs and further leads to inflammations in the lungs and complications in digestive system and reproductive system.

Currently, there is no cure for CF, and treatments can only relieve symptoms. Antibiotics are used for lung infections; mucus-thinning drugs can help patients cough up the mucus to improve the lung function; bowel surgery is able to remove the blockages in the bowel; other procedures include feeding tube, lung transplant, chest physical therapy and so on. The mentioned therapy eases CF symptoms but fails to alter the fundamental cause of CF.

In recent years, new CF drugs were developed aiming at the defect CFTR. VX-770 is the first FDA approved CFTR corrector and was marketed in 2012. It was initially approved for CF patients caused by the G551D mutation, which results in a dysfunction of CFTR on the cell membrane. G551D-CFTR is able to traffic to the cell membrane, while its function is significantly reduced[67-70]. VX-770, a CFTR potentiator, facilitates G551D-CFTR channel function by directly binding to the channel to induce a non-conventional mode of gating, which increases the channel open probability[68, 70-71]. VX-809 and VX-770 conjugated treatment was approved by FDA in 2015 to treat homozygous ΔF508-CFTR, which accounts for approximately 70% of CF. ΔF508-CFTR not only reduces the channel function, but also leads to its degradation in the ER. In the VX-770/VX-809 combination, VX-809 increases the number of ΔF508-CFTR on the cell membrane, and VX-770

promotes its channel function[42, 60, 72-74]. VX-809 is believed to improve ΔF508-CFTR cell surface expression, but its action mechanism is not well studied. In 2018, the combination of VX-661 and VX-770 was approved by FDA for homozygous ΔF508-CFTR and heterozygous ΔF508-CFTR patients. Similarly, VX-661 increases the amount of CFTR delivered to the cell surface, and VX-770 enhances the chloride transport[75-78]. Different from VX-770/VX-809, VX-770/VX-661 can also be applied for heterozygous ΔF508-CFTR patents. Clinical trials showed that VX-770/VX-661 was effective for those who were with the F508del mutation and a second mutation predicted to be responsive to VX-770/VX-661, but it was not shown to be effective in patients who were with the F508del mutation and a second mutation not predicted to be responsive to VX-770/VX-661[79].

1.3. Epithelial Sodium Channel and Epithelial Sodium Channel Related Diseases

The Epithelial Sodium Channel (ENaC) is selectively permeable to Na^+. It is primarily responsible for the reabsorption of sodium ions at the collecting ducts of the kidney. ENaC is assembled as a heterotrimer composed of three homologous subunits α, β, and γ[80]. Each subunit contains two transmembrane spanning domains, and a large extracellular loop. The α, β, and γ subunits are encoded by SCNN1A, SCNN1B, and SCNN1G, respectively. The α subunit is required for a functional ENaC channel, while homosubunit structures can still be expressed on the cell surface.

Water makes up of 60-70% of human body weight and ENaC plays a key role in maintaining Na^+ and water hemostasis. Dysregulation of ENaC channel activity, localization on the cell membrane, and residence time on the cell membrane is associated

with severe human diseases. Some ENaC related diseases are caused by the mutations in the genes encoding ENaC subunits.

Multi-system pseudohypoaldosteronism type 1 (PHA1B) is an autosomal recessive disease, resulting from homozygous or heterozygous mutations in the gene encoding for α, β, and γ subunits. The mutations lead to the loss of ENaC function causing recurrent salt wasting episodes in multiple organs[80]. PHA1B patients suffer from metabolic acidosis and hypertension during recurrent salt wasting episodes. Impaired Na^+ reabsorption also results in severe salt loss in kidney. Other influences include increased chloride in sweat and salivary, impaired fertility and recurrent lower pulmonary tract infections. The symptoms are seen in patients from infant age and relieved as patients getting older. The current therapy is supplying high NaCl (up to 45 g/day) to the patients lifelong[77, 81-82].

Liddle syndrome is another ENaC associated disease. Liddle syndrome is an autosomal dominant disease cause by mutations in PY motif at the C-terminus of β, or γ subunits. The mutations lead to the gain of ENaC function, which attributes to the extended residence time of ENaC on the cell membrane. Liddle syndrome patients also show metabolic acidosis and hypertension due to breaking the homeostasis balance. Gained Na^+ reabsorption results in over fluid reabsorption in kidney[81-82]. This disease is mainly found in people in their childhood or young adulthood, and it is rare in infants. The therapies include using diuretics to block ENaC and low salt diet for the patients.
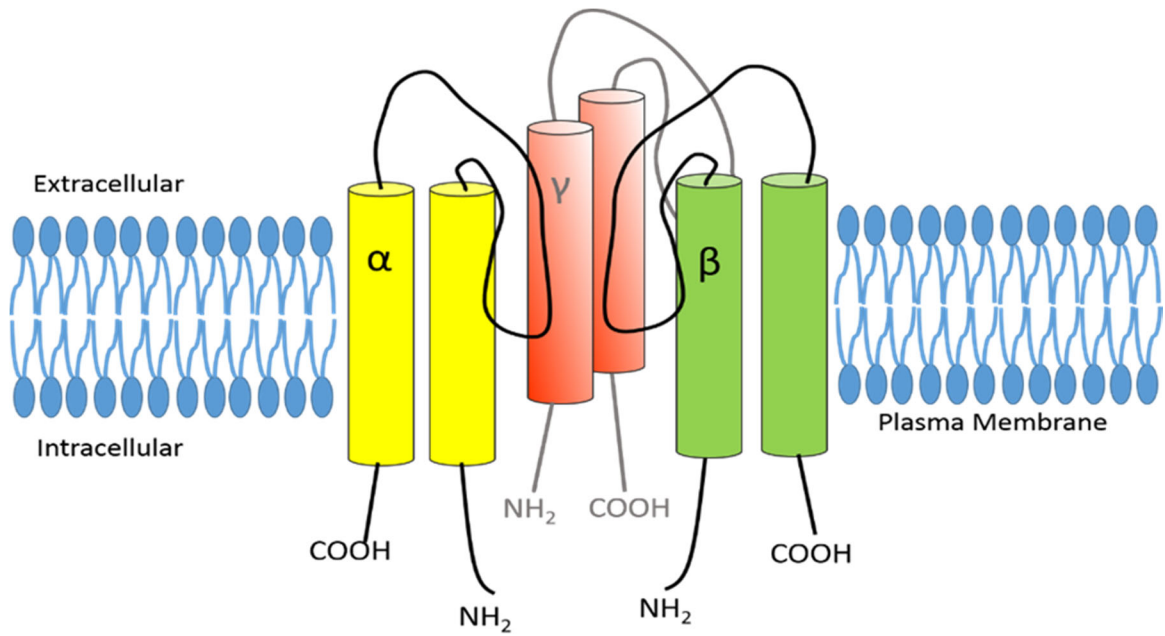
Figure 1.4: Diagram Demonstrating the Arrangement of the ENaC Subunits. A functional ENaC channel is consisted of α, β, and γ subunits. Each subunit contains two transmembrane spanning domains, and a large extracellular loop.

1.4.Fluorescence Microscopy in Biological Systems

Fluorescence microscopy is currently one of the most powerful and widely used techniques for biological studies. Fluorescence microscopy employs fluorophores which are able to absorb light at a specific wavelength and emit light at a longer wavelength. Fluorophores are very bright under a microscope and thus they are easily distinguishable from the background signals. This optical property makes it straightforward to obtain images of the fluorophores labeled molecules with high contrast and observe biological activities in living conditions. Though the spatial resolution is not as high as that of electron microscope, fluorescence microscope allows for observing a living sample without damaging it. Fluorescence microscopy can be used to visualize fundamental cellular processes such as membrane protein expression, ion channel activities, and membrane receptor/ligand interaction.

1.4.1 Principles of Fluorescence

Fluorescence is the emission of light that occurs after fluorophores absorb energy from excitation light. In most cases, the emission light is of longer wavelength than the absorption light. The wavelengths of absorption and emission are both closely associated with the outermost electron orbitals in the fluorophore molecules. After absorbing energy (photos), a fluorescent molecule in the ground state moves an electron into a higher energy level orbital and alters the electronic, vibrational and the rotational states. The molecule is in the so-called "excitation state". Eventually, the absorbed energy is released mostly due to vibrational relaxation or fluorescence emission and the fluorophore returns back to the

ground state. Fluorophores typically contain ring structures (aromatic groups) with π bonds. These compounds are selected for fluorophores as the energy differences between the ground state orbitals and the excited state orbitals is relatively small. Thus, the relatively low energy photons in the visible light region are capable of being used to excite fluorophores from the ground state to the excitation state[83-84].

The Jablonski diagram (Figure 1.5) is useful to understand the excitation and emission process. Molecules could be in the singlet or triplet electronic state based on the angular momentum of the electrons. Electrons usually stay paired with opposite spins ($+ \frac{1}{2}$ and $- \frac{1}{2}$) in a single orbital, resulting in the cancellation of the magnetic moments. S_0 is the ground state with the lowest energy level. S_1 and S_2 are excited singlet states in which the outer electron is excited to a higher energy level orbital; S_2 contains more energy than S_1. An electron is able to quickly relax from the upper vibrational (rotational) energy level to the lowest vibrational (rotational) energy level in the same excitation state. Then, the electron has three pathways to release energy to the ground state: 1) the fluorescence decay pathway; 2) the nonradiative decay pathway; 3) intersystem crossing. Intersystem crossing describes a pair of electrons undergoing transition from the singlet state to the triplet state[85-86]. The triplet state is that a pair of nonbonding electrons exist in two separate orbitals with the spin of electrons parallel to each other and the triplet state is not allowed according to quantum theory. Therefore, transition of electrons directly from the ground singlet state to the triplet state is forbidden. However, intersystem crossing makes the forbidden transition possible. An electron can be excited from the ground state S_0 to the S_1 excitation state first, then goes through the intersystem crossing from S_1 to T_1 state, and eventually goes back to the ground state from the T1 state[85, 87].
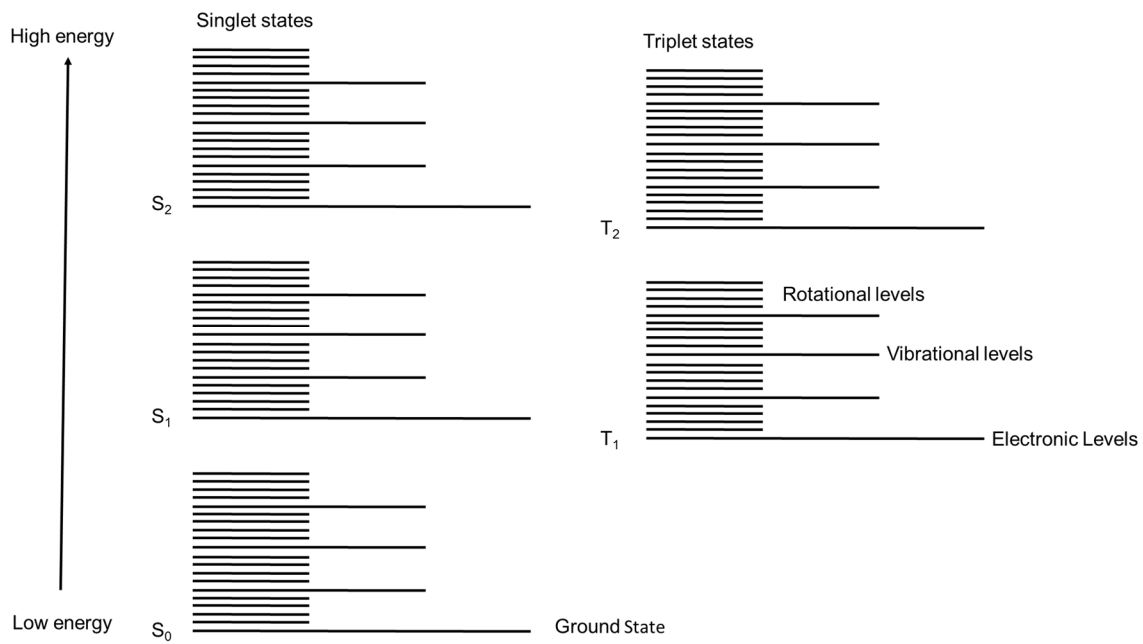
Figure 1.5: Jablonski Diagram.

1.4.2 Epifluorescence

Epifluorescence is the most common technique used in fluorescence microscopy. In this technique, an excitation beam is used to illuminate the whole specimen and emissions are all collected by a camera or seen by eye. In epifluorescence, the excitation light first passes through a filter to remove the unwanted wavelength from the excitation light. Then, it directly illuminates the sample through an objective, resulting in fluorescence. A dichroic is used to separate the emitting fluorescence from the reflected excitation light. Furthermore, an emission filter is utilized to transmit specific wavelengths of the emitted light before it is collected by the camera.

The major advantage of wide-field epifluorescence is the big illumination area. Other advantages include low cost, simple instrumentation and flexibility. The disadvantage of epifluorescence is the low image contrast and low spatial resolution[83, 85]. As emissions generated from the entire specimen are all collected, the presence of out of focus emission results in the low spatial resolution. In addition, exposing to high intensity excitation beam may cause photodamage to the living tissues and photobleach the fluorophores[88-89].

1.4.3 Total Internal Reflection Fluorescence (TIRF) Microscopy

Total Internal Reflection Fluorescence (TIRF) Microscopy is a wide-field illumination technique that illuminates only the fluorophores near the glass coverslip[90]. It has been widely used in biological imaging as it significantly minimizes the fluorescence background and has high spatial resolution[91].

As the excitation beam enters from a high index of refraction medium to a low index of reflection medium, the angle of the beam changes in accordance with the Snell's law:

$$\theta_c = \sin^{-1}(n_1 / n_2),$$

n_1 and n_2 are the refractive indices of the sample and the cover slip, respectively. The refractive index must be less than that of cover slip.

If the incident angle is less than the critical angle (θ_c), the excitation light can pass the sample-cover slip interface and be reflected by the sample-cover slip interface. When the incident angle is greater than the critical angle, the excitation light is only reflected off the sample-cover slip interface back into the cover slip. In this case, some of the incident energy penetrates the sample-cover slip interface, creating the evanescent field. This is the excitation field employed in TIRF microscopy. The intensity (*I*) of the evanescent field decays exponentially with the distance from the interface (*z*). The intensity of the evanescent field at any position z is described by:

$$I_z = I_0^{-z/d},$$

Where, I_0 is the intensity of the evanescent field at *z*=0. I_0 is related to the intensity of the incident beam by a complex function of θ and polarization. The depth of the evanescent field, *d,* is the distance from the cover slip at which the excitation intensity decays to 1/e, or 37%, of I_0. Depth *d* is defined by:

$$d = (\lambda_0 / 4\pi) *(n_2^2 \sin^2\theta - n_1^2)^{-1/2},$$

Where, λ_0 is the wavelength of the excitation light in a vacuum, θ is the incident angle[92].

Epifluorescence

TIRF

Sample
Coverglass
Incident Beam

Evanescent Field
Sample
Coverglass
Incident Beam
Θ_c
Reflection Beam
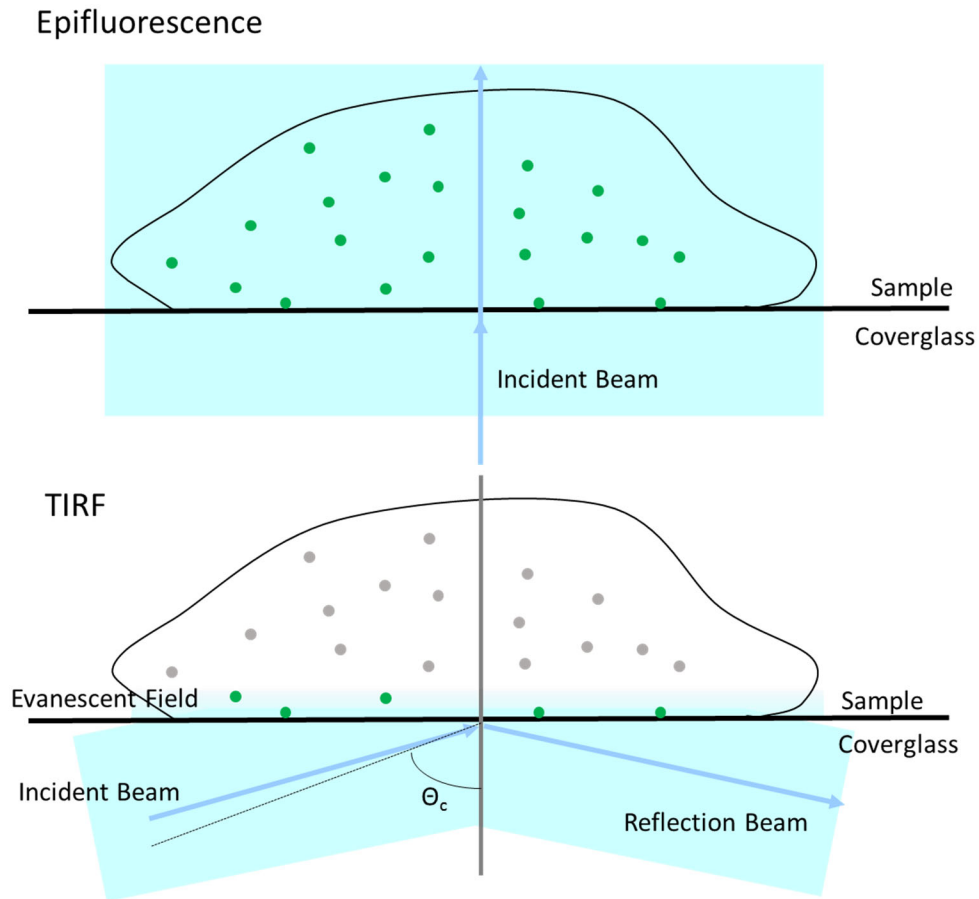
Figure 1.6: Epifluorescence and Total Internal Reflection Fluorescence. Top: Epifluorescence. The incident beam is perpendicular to the cover glass and all the fluorophores are illuminated by the incident beam. Bottom: Total internal reflection fluorescence. The incident angle is above the critical angle and the incident bean is reflected off the cover glass surface. Energy passed through the coverslip creates the evanescent field, which decays exponentially into the sample. Evanescent field is usually less than 200nm above the glass coverslip.

1.4.4   Confocal Microscopy

In a wide-field microscopy system, the presence of out of focus emission beam results in low spatial resolution. This problem can be solved by adding a pinhole to the light pathway, and the new system is called confocal microscopy. A laser is used as the excitation source in a confocal microscopy system is as it is brighter and smaller in size than the mercury lamp used in wide-field microscopy. There are two possible instrumental setups: (1) a pinhole in the excitation pathway (The left diagram in Figure 1.7 shows this setup); (2) a pinhole in the emission pathway. In the first setup, the excitation light is directed toward a sample through a pinhole. Thus, only the light passing through the pinhole hits the sample, restricting the illumination size in the specimen. In the second setup, the specimen is illuminated by the excitation beam in the way of wide-field microscopy, and a pinhole is placed in the emission light pathway. Only emission light passing through the pinhole can be received by the detector[93-94]. In confocal microscopy, a pinhole removes all of the out of focus emission light and improves the spatial resolution of images. On the other hand, the pinhole leads to a very small illumination size, which limits its application to a big size sample. The problem can be overcome by developing a scanning confocal microscopy where a stage holding the sample moves [95] or a laser source moves [96] to record a whole image of the sample.
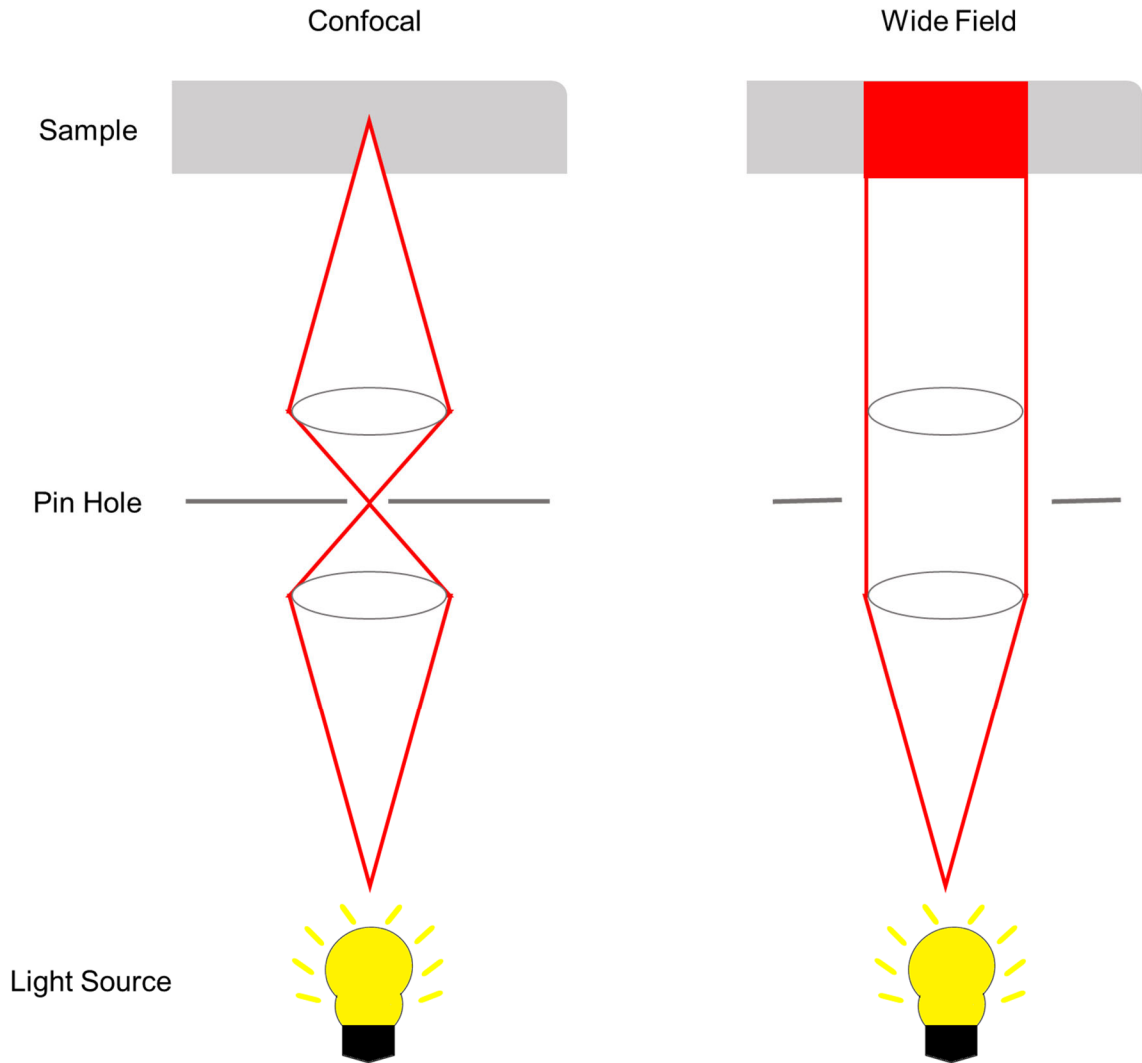
Figure 1.7: Comparison of Confocal Microscopy with Wide-Field Microscopy. Lift: Confocal Microscopy. Before hitting the sample, the excitation light passes through a pin hole to narrow the illumination volume in the sample. In this manner, the emission lights are all focused on the camera resulting in high resolution images. Right: Wide-field Microscopy. The whole sample is illuminated by the excitation beam. Out-of-focus emission lights are all detected by the camera.

1.4.5   Single Molecule Fluorescence Microscopy

The existence of millions of molecules in a biological system makes it possible to have millions of reactions occur at the same time. A better understanding of these biological reactions can provide essential information to understand the secret of life. Ensemble techniques that simultaneously detect multiple fluorophores have been widely used and provided valuable information for biological studies[97]. However, owing to the detections of multiple fluorophores, the dynamic information of each single molecule is lost. Recent development of fluorescence microscopy makes it possible to study the individual molecules. In single molecule fluorescence microscopy, biological molecules are labeled with fluorophores, and the dynamic of the biological molecule is detected by resolving measurements from the affiliated fluorophore[98].

One of the common single molecule techniques is single molecule FRET. There are two experimental setups for single FRET studies: the first one is immobilizing the fluorophores (a FRET pair) labeled biological molecules on a cover slip and utilizing the TIRF instrumental setup to image the molecules on the glass; the other one is having the fluorophores (a FRET pair) labeled biological molecules in solution and applying confocal instrumental setup to look at the biological molecules diffusing through the focal point. In my work, the diffusion style single molecule FRET approach is utilized. To perform this experiment, two fluorophores (one is donor; the other is acceptor) are required to tag on a protein molecule. When the protein molecule is denatured or unfolded, the distance between the two fluorophores is not in the FRET distance range (1-10nm)[99]. Therefore, the energy transfer between the FRET pairs is not efficient and only low FRET efficiency

events are observed. When the protein is fully folded, the two fluorophore distance is reduced resulting in high FRET efficiency events. A single fluorescent burst is observed as a single protein molecule tagged with a FRET pair freely diffuses through the detection volume of a confocal microscopy. A pulsed laser excitation system coupled with time-correlated single-photon counting electronics recording the arrival time and fluorescence delay of each photon, is applied to alternately excite the donor and acceptor. The yield fluorescence signals are collected by avalanche photodiode (APD). A burst gives rise to a FRET efficiency, *E*. Thousands of fluorescent bursts are accumulated and a histogram of FRET efficiencies are plotted resolving the folded and unfolded protein subpopulations[100-101].

1.4.6 Förster Resonance Energy Transfer (FRET)

1.4.6.1 Principle of Förster Resonance Energy Transfer

Förster resonance energy transfer (FRET) is the process in which energy is transferred between two sufficiently close fluorescent molecules through non-radiative dipole-dipole coupling. Förster resonance energy transfer is named after Theodor Förster, who first developed the theory of resonance energy transfer in 1948[102]. FRET occurs when (1) the distance between the donor and the acceptor is in the range of 1-10 nm; (2) there is a substantial overlap of the donor emission spectrum and the acceptor absorption spectrum; (3) the appropriate alignment of orientation of the donor emission dipole moment and the acceptor absorption dipole moment; (4) a donor has a high quantum yield (Φ_d). (Figure 1.8)

The FRET efficiency (E) is the quantum yield of the energy transfer, the fraction of energy transfer per donor excitation event.

$$E = \frac{K_{ET}}{K_f + K_{ET} + \Sigma K_i}$$

Where K_{ET} is the rate of energy transfer, K_f is the radiative decay rate, and the K_i is the rate constants of any other decay excitation pathway.

E depends on the donor-acceptor distance r with an inverse the sixth power law.

$$E = \frac{1}{1 + (r/R_0)^6}$$

Where R_0 is the distance at which the energy transfer efficiency is 50%[103]. R_0 depends on the overlap of donor emission spectrum and acceptor absorption spectrum, and the orientation of the donor emission dipole and acceptor absorption dipole.

$$R_0 = 2.8 \times 10^{17} \cdot \kappa^2 \cdot \Phi_d \cdot \varepsilon_A \cdot J_{(\lambda)} \quad ^{1/6}$$

Where κ^2 represents the angle of the donor and acceptor dipoles; Φ_d is the quantum yield of the donor, which is defined as the ratio of the number of photons emitted to the number of absorbed. Φ_d depends on the environment of the donor and the acceptor[104]. ε_A is the maximal acceptor extinction coefficient ($mol^{-1} cm^{-1}$). $J_{(\lambda)}$ is the overlap of donor emission spectrum and acceptor absorption spectrum.

FRET is unique and capable of providing signals sensitive to intra- and intermolecular distances in the range of 1-10nm. Therefore, FRET is widely used to study molecular interaction and conformation with a spatial resolution far beyond the diffraction limit ($\sim \frac{\lambda}{2NA}$, NA is the numerical aperture of the objective) of optical microscopy.

1.4.6.2 Intensity Based FRET Method

Since the rate of energy transfer cannot be determined directly (because it is a dark process), the efficiency of energy transfer can be calculated from altered parameters, such as fluorescence intensity, lifetime or bleaching kinetics[105]. In my work, the intensity based FRET is utilized.

In case of FRET, the donor quantum yield is diminished (Q_{DA}<Q_D, donor in presence of acceptor, DA), resulting in reduced donor fluorescence intensity (I_{DA}<I_D). Energy transferred from the donor to the acceptor increases the acceptor fluorescence intensity, which is defined as sensitized emission. This method uses only one laser to excite the donor and records the emission from both donor and acceptor. The FRET efficiency is basically calculated by comparing the measured fluorescence intensities in the donor and the acceptor channels after donor excitation.

$$E = \frac{f_{Dex}^{Aem}}{f_{Dex}^{Dem} + f_{Dex}^{Aem}}$$

Where f_{Dex}^{Dem} is the number of photons in the donor channel after donor excitation, f_{Dex}^{Aem} is the number of photons in the acceptor channel after donor excitation.

However, single laser excitation has spectral cross-talk problems as the emission spectrum of donor fluorophores is often so broad that it is impossible to avoid the detection of donor emitted photons in the acceptor emission channel. This problem is solved by the development of alternating-laser excitation (ALEX). In an ALEX microscopy system, the excitation of the donor is alternated with the excitation of acceptor[106]. We are capable of detecting the number of photons in the acceptor channel after acceptor excitation (f_{Aex}^{Aem}) for each burst. The three parameters $f_{Dex}^{Dem}, f_{Dex}^{Aem}, f_{Aex}^{Aem}$ provide a way to verify the presence of the acceptor in a fluorescent active form by defining the raw stoichiometry.

$$S^{raw} = \frac{f_{Dex}^{Dem} + f_{Dex}^{Aem}}{f_{Dex}^{Dem} + f_{Dex}^{Aem} + f_{Aex}^{Aem}}$$

For donor only species, S^{raw} is 1; for acceptor only species, S^{raw} is 0. With the proper alternating excitation of donor and acceptor, a molecule tagged with a donor and an acceptor shows a stoichiometry that is distinguishable from the donor-only and acceptor-only species. Thus, S^{raw} allows us to determine the labeling stoichiometry[106]. By having a two dimensional ES histogram, we are able to separate low FRET species from donor only species based on the respective stoichiometry. In this manner, low FRET molecules can be studied using ALEX microscopy.

A
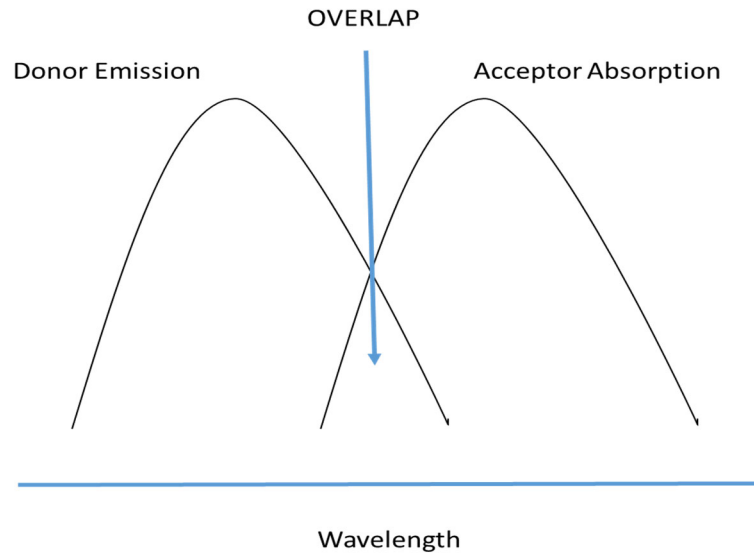
B
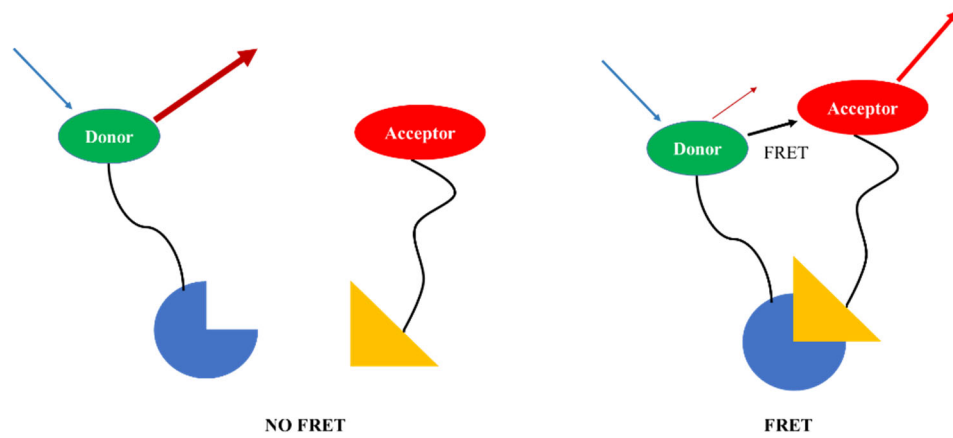
Figure 1.8: Schematic Mechanism of FRET. (A) In a FRET pair, the donor emission and the acceptor absorption must partially overlap with each other to have FRET occur. (B) The donor and acceptor excitation and emission with/without FRET.

1.5.Fluorescent Proteins

1.5.1   pH Sensitive Fluorescent Protein

Wild-type green fluorescent protein (GFP) has a bimodal absorption spectrum with two peak maxima, at 395 and 475 nm[107]. The two maxima is caused by the protonated and deprotonated states of Tyr 66, which forms part of the chromophore. A given GFP is trapped in either of two alternative states: in the protonated state, the chromophore is excited at 395 nm; in the deprotonated state, it is excited at 475 nm. Miesenbock et al, tried to convert wild-type GFP to a pH sensitive fluorescent protein though making mutations that facilitate conformers exchange, or switch changes in pH to changes in the electrostatic environment of the chromophore[108]. Two classes of pH sensitive fluorescent protein are generated: Ratiometric pHluorins and ecliptic pHluorins. Ratiometric pHluorin shows a reversible excitation ratio change between pH 7.5 and 5.5 with a response time of <20 ms (Figure 1.9 B). Ecliptic pHluorins do not show fluorescence quench until pH is lower than 6, where the excitation peak at 475nm vanishes but the 395 nm excitation peak remains. Fluorescence returns within 20 ms after exposing to neutral pH[108] (Figure 1.9 C).
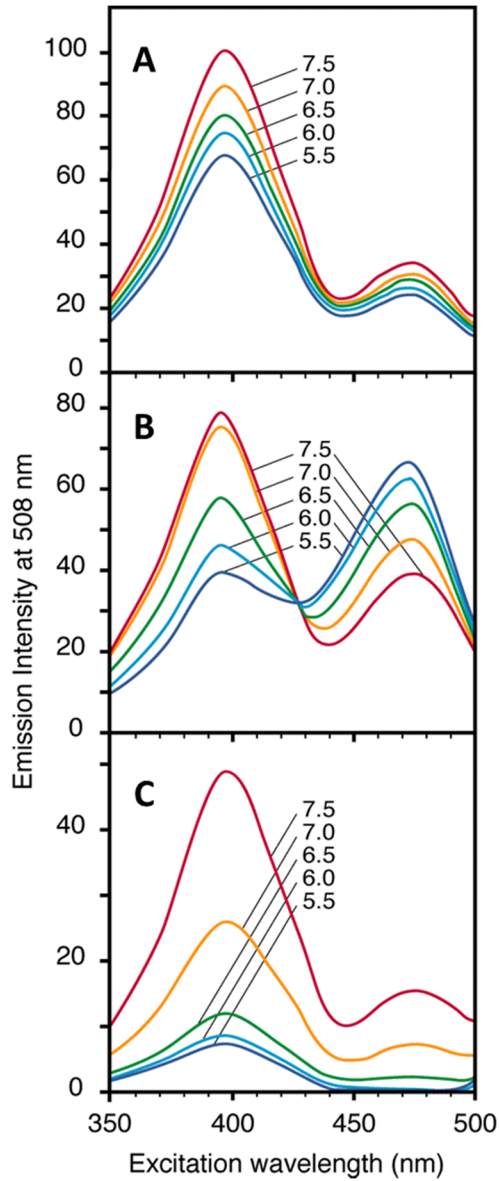
Figure 1.9: Fluorescence Excitation Spectra. (A): Wild-type GFP (B): Ratiometric pHluorin (C): Ecliptic pHluorin. (Reprinted by permission from Miesenböck, G.; De Angelis, D. A.; Rothman, J. E.*Nature* **1998,** *394* (6689), 192.)

1.5.2 *Photoconvertible Fluorescent Protein: Dendra2*

Dendra, derived from octocoral Dendronephthya sp, is a mutant of the GFP-like protein (Figure 1.10)[109]. Dendra is capable of being irreversibly photoconverted from green emissive form to red emissive form by exposing to the UV-violet light (e.g. 405 nm) or blue light (e.g. 488 nm). Gurskaya et al showed that intense blue light ($0.5–0.7$ W/cm^2) activation resulted in the appearance of bright red fluorescence in Dendra-expressing cells, while low intensity blue light (<50 mW/cm^2) for the same time period or even prolonged exposure time failed to photoconvert Dendra[110]. This behavior makes it possible to select fluorescent cells without photoconverting them by using a low intensity 488 nm light. Dendra 2 is a mutational Dendra with alanine at position 224 replaced by valine, which leads to better maturation and brighter fluorescence both before and after photoconversion. In response to intense UV-violet or blue light, Dendra 2 undergoes irreversible photoconversion, causing a decrease of green fluorescence and the appearance of red fluorescence[56]. After complete photoconversion, red fluorescence increases about 100~300 fold and green fluorescence decreases about 10-15 fold, which results in up to 4000 fold red to green fluorescence contrast. The maturation time of Dendra2 (the $t_{1/2}$, or half-life for the immature state) is only 38 min[111]. The stability of Dendra2 has also been tested such that the fluorescence intensity of Dendra2 expressed in cells remains stable for several hours when cells are treated with protein synthesis inhibitor cycloheximide[112]. Thus, Dendra2 is an ideal fluorescent protein for labeling.
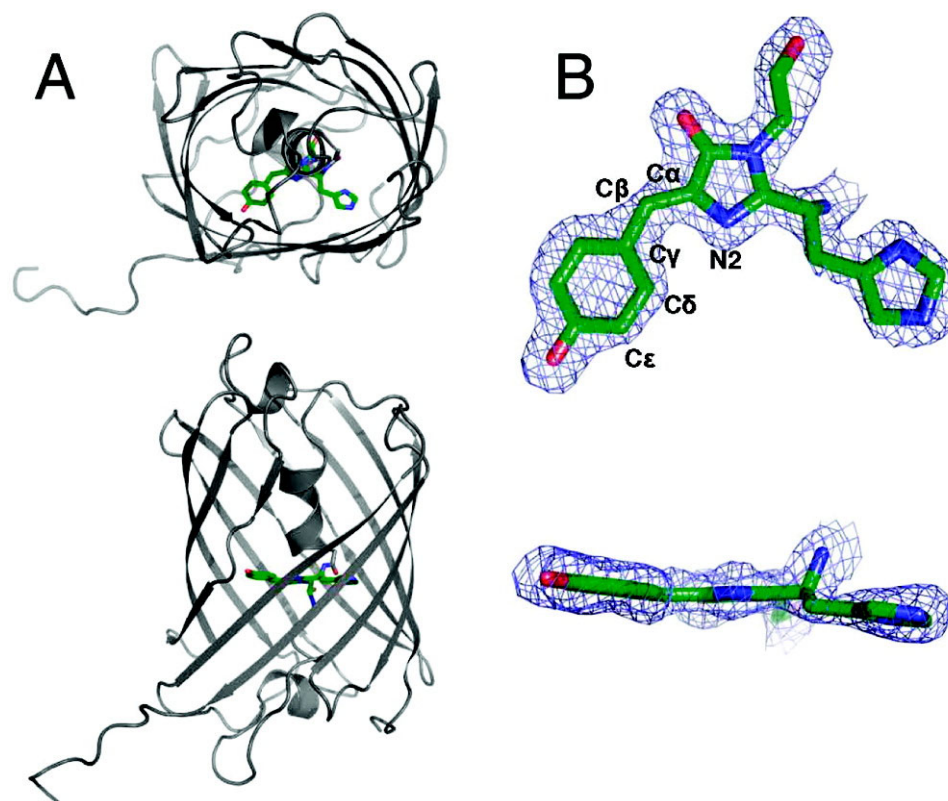
Figure 1.10 : Structure of Dendra 2. Top and side views of the overall fold of a Dendra2 monomer in cartoon representation, with the embedded chromophore shown as sticks. (B) Top and side views of the chromophore. (Reprinted with permission from Adam, V.; Nienhaus, K.; Bourgeois, D.; Nienhaus, G. U., Structural basis of enhanced photoconversion yield in green fluorescent protein-like protein Dendra2. *Biochemistry* **2009,** *48* (22), 4905-4915.)

CHAPTER 2: OVERVIEW AND STATEMENT OF PROJECTS

2.1.Motivation and Projects Overview

Almost 90% of CF patients are caused by the deletion of the phenylalanine at position 508 of CFTR, which is believed to affect the folding and stability of CFTR[50, 113]. The misfolded ΔF508-CFTR undergoes ER associated degradation (ERAD), causing the failure of ΔF508-CFTR trafficking to the cell surface[44-47]. Despite significant research interest, the exact mechanism of how the ΔF508 mutation causes the folding and functional defects is still unclear. A pharmacological approach that targets the underlying cause of the disease has led to the development of compounds that are partially effective[114-116]. One of these compounds, VX-809 acts as a chemical chaperone for ΔF508-CFTR, producing 10-15% of wild-type plasma membrane protein levels in cell based assays[114]. This is well below the required 25-50% needed for a therapeutic approach to relieve the majority of CF symptoms[117]. ΔF508-CFTR has a lower open probability on the plasma membrane compared to wild-type[118-119]; thus correction to above 50% of wild-type levels may be required to achieve sufficient functional activity to relieve symptoms. In addition to these small molecule chaperones, low temperature (27 °C) and secondary mutations within CFTR, such as I539T and G550E as well as others, have also been shown to increase the population of ΔF508-CFTR on the plasma membrane[52, 120]. However, full mechanisms of these correctors have not been resolved. Thus, one of the goals of my work was to elucidate the mechanism of the correctors (compound VX-809, low temperature and second site suppressor I539T) induced ΔF508-CFTR trafficking for the development of new cystic fibrosis therapeutics.

The fundamental cause of ΔF508 related cystic fibrosis is that the deletion of phenylalanine in position 508 affects the proper folding of CFTR and alters its stability[50, 113]. Whereas, the precise mechanism of ΔF508 is still elusive with many unanswered questions. Understanding the detailed wild-type CFTR folding and ΔF508-CFTR misfolding actions will be greatly beneficial to the development of CF therapies. Both experimental and theoretical methods have been utilized to intensely study the folding mechanism of protein. Owing to the extremely complex protein folding mechanism, no single technique so far is adequate for fully understanding it. Therefore, new technologies are developed to provide new and deeper insights into the folding mechanism. Although bulk measurements have been widely used, many essential aspects of protein folding information are lost due to the complexity of protein structures and the stochastic nature of these processes. For instance, "transition state" molecules do not belong to any state populations[121], which makes the study of intermediate states of folding more mysterious. Single molecule techniques offer new access to information unavailable from bulk measurements such that it is capable of providing dynamic information at the single molecule resolution. Hence, single molecule technique is ideal for the study of the dynamics of protein folding reactions.

The precise pathophysiology of cystic fibrosis is not well studied with many unanswered questions. The involvement of another transport protein, epithelial sodium channel (ENaC), makes the situation more complicated. ENaC and CFTR are colocalized on the apical surface of epithelia cells and have functional interactions. With our fluorescence microscopy techniques, we would like to explore the effects of CFTR on the residence time of ENaC on the cell membrane. A reliable approach measuring the half-life of protein on the cell membrane is required for this study. Recently, techniques to measure the half-life

of plasma membrane proteins on the cell surface include surface biotinylation with western blot analysis, ligand binding, and functional studies such as electrophysiology or calcium imaging [122-124]. These techniques suffer from low temporal resolution of membrane receptor half-life and can be low throughput. Additionally, the procedure is complicated by the need to use translation blockers or intracellular protein trafficking inhibitors to eliminate the insertion of newly trafficked protein into the plasma membrane [125-127]. This also increases the error as translation blockers could affect other cellular processes that may relate to membrane protein residence time at the cell surface. Therefore, another goal of my work was to develop a high temporal resolution approach to quantify the half-life of protein on the cell membrane.

2.2. Correctors Alter Expression and Trafficking of CFTR

The goal was to explore how reduced temperature, the second site suppressor I539T, and the small molecule corrector VX-809 work alone and in combination to affect the intracellular distribution and trafficking of CFTR. We determined the amount of protein on the cell surface, along with the rate of delivery of vesicles containing CFTR to the plasma membrane. These studies, for the first time, measured protein trafficking in real time. To perform the experiments, transiently transfected human embryonic kidney (HEK) 293T cells were used to express wild-type CFTR or CFTR mutations on the plasma membrane. The 4th extracellular loop of wild-type CFTR or CFTR mutations was genetically labeled with a pH-sensitive version of GFP, better known as superecliptic pHluorin (SEP). Total internal reflection fluorescence was used to measure expression and distribution of SEP-labeled CFTR.

2.2.1   Total Internal Reflection Fluorescence (TIRF)

TIRF microscopy is utilized to visualize the fluorophore-labeled CFTRs on the plasma membrane. This setup is capable of detecting fluorophores to a depth of 200 nm above the cell-glass interface when excited by total internal reflection laser. SEP-CFTRs localized on the PM, in the peripheral ER near the PM, and in the vesicles between PM and ER are within the TIRF excitation range. Super ecliptic pHluorin (SEP) was excited with a 488 nm diode-pumped solid-state (DPSS) laser through the objective (Olympus 1.49 NA 60x oil immersion). An electron multiplying charge coupled device (EMCCD) was employed to detect the SEP fluorescence signal. In order to obtain total internal reflection, the laser was focused on the back aperture of the objective lens and the angle of the beam was adjusted using a stepper motor. Since bulk of the cell is not illuminated, fluorescence background is decreased and thus the signal to noise ratio at the plasma membrane is increased.

2.2.2   Super-Ecliptic pHluorin (SEP) to Measure Expression

Super-Ecliptic pHluorin (SEP) is a pH sensitive fluorescent protein fluorescent with a 488 nm excitation at a neutral pH but not fluorescent under acidic conditions (pH<6). Previous studies showed that SEP-labeled proteins on the cell surface lost all detectable fluorescence upon exposure to low pH (5.4) extracellular solution, while those localized in the ER membrane were not affected. Thus, SEP labeling allows us to measure only the protein population localized on the cell surface[128].

The 4th extracellular loop of CFTR was genetically incorporated with SEP in order to have SEPs on the cell surface orient to the extracellular side. SEP excited by the 488 nm laser is fluorescent in a pH7.4 environment. Adjusting the pH to acidic condition (pH<6) prevents SEP fluorescence. When cells expressing CFTR were in pH 7.4 extracellular solution, CFTRs on the PM and in the peripheral ER (pH>7) were all fluorescent, but those localized in the Golgi and the trafficking vesicles at the lower pH condition were not visible. Then, the extracellular solution was changed to an identical solution except the pH was adjusted to 5.4. Since SEPs were oriented to the extracellular side of CFTR, they were exposed to an acidic environment and failed to fluoresce. Changing the pH of the extracellular solution does not alter the pH of the peripheral ER, Golgi or the trafficking vesicles. Therefore, the observed fluorescence was solely from CFTRs in the peripheral ER when cells were in the pH 5.4 extracellular solution. This process is illustrated in Figure 2.1.

CFTRs are not only on the PM or in the ER, but also located in vesicles between the PM and ER. The SEP assay can also be used to determine the population of CFTR located in the acidic vesicles. NH_4Cl is added to the extracellular solution to equilibrate the pH of the lumen vesicles to that of the extracellular solution, as the plasma membrane is permeable to NH_3. NH_3 moves to the intracellular side of the cell until NH_3 equilibrates the two sides of the plasma membrane. Initially, growth medium in the cell-seeded dish was replaced with pH 7.4 extracellular solution without NH_4^+. Images of the selected cells were taken and then the extracellular solution was changed to the same pH 7.4 extracellular solution with NH_4^+. When no NH_4^+ is in the extracellular solution, only SEPs on the PM and in the ER are exposed to the pH 7.4 environment and fluoresce. As the additional NH_4^+ increases

the pH of the lumen vesicles to above pH 6, SEPs on the PM, in the ER, and in the vesicles

are all visible. (Figure 2.2)
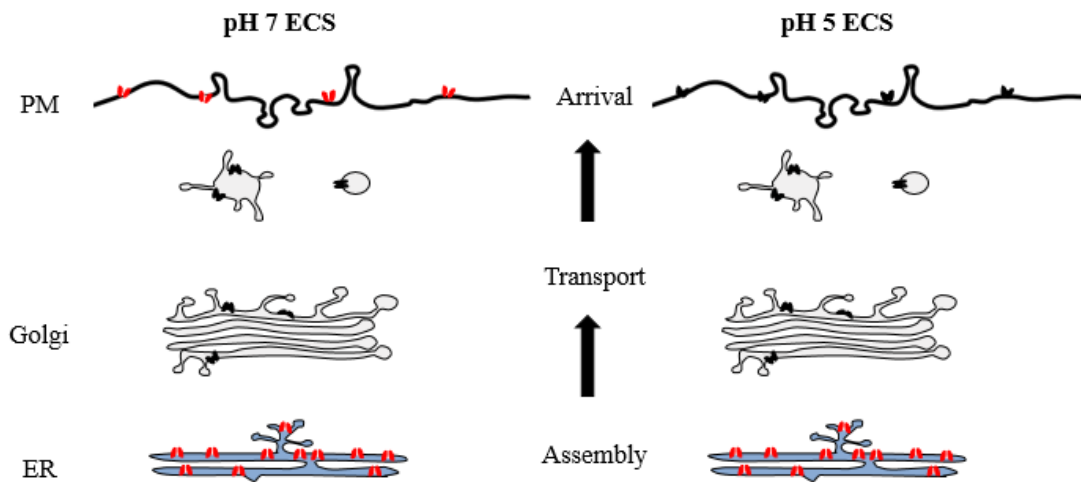
Figure 2.1: Cartoon Illustrating Changes in Membrane Fluorescence due to the change of the Extracellular Solution pH. When the extracellular solution is pH 7.4, SEP-labeled CFTRs on the PM and in the ER are fluorescent. (B) When the extracellular solution is pH 5.4, SEP-labeled CFTRs in the ER are fluorescent and SEP-labeled CFTRs on the PM fail to fluoresce.
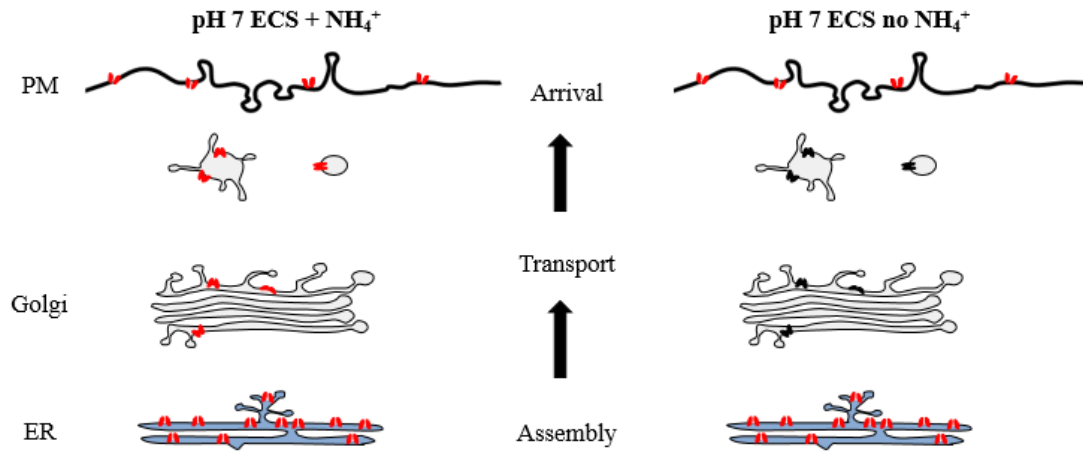
Figure 2.2: Cartoon Illustrating NH4+ Changing Fluorescence in the Interior of a Cell. When NH4Cl is added to the extracellular solution, SEP-labeled CFTRs on the PM, in the ER, and in the vesicles are fluorescent. (B) When extracellular solution does not contain NH4Cl, SEP-labeled CFTRs on the PM and in the ER are fluorescent.

TIRF images were collected for each cell at both pH 7.4 and pH 5.4 conditions. Figure 2.3 shows the fluorescence change of an individual cell upon exposure to the two pHs extracellular solutions. For quantitation, the integrated density (ID) for each image is determined. The ID is defined as the product of the average fluorescence intensity and the total number of pixels occupied by the cell. The plasma membrane integrated density (PMID) is a readout of the level of CFTR on the cell surface, where an increase in the PMID correlates to an increase in the number of SEP- CFTR on the plasma membrane.

$$PMID = ER + PM\ ID\ (pH\ 7.4) - ER\ ID\ (pH\ 5.4)$$

The vesicle integrated intensity (Vesicle ID) is a readout of the level of CFTR located in the vesicles, where an increase in the Vesicle ID correlates to an increase in the number of SEP- CFTR in the vesicles.

$$Vesicle\ ID = ER + PM + Vesicle\ ID\ (ECS\ with\ NH3) - ER + PM\ ID\ (ECS\ no\ NH3)$$

The ratio of CFTR on the plasma membrane is calculated from the integrated density of CFTR on the plasma membrane (pH 7.4 ID – pH 5.4 ID) divided by the total integrated density at pH 7.4. The ratio of CFTR on plasma membrane compared to the total (ER + PM) CFTR was used to quantify the distribution between the PM and peripheral ER. An increase in the percentage of CFTRs found on the plasma membrane (% PM) corresponds to a change in the distribution of CFTRs between the ER and PM.

$$\%\ PM = \frac{PMID}{ER + PM\ ID\ (pH\ 7.4)}\ x\ 100\%$$

pH7 (ER+PM)   **pH5 (ER Only)**   **pH7-pH5 (PM)**
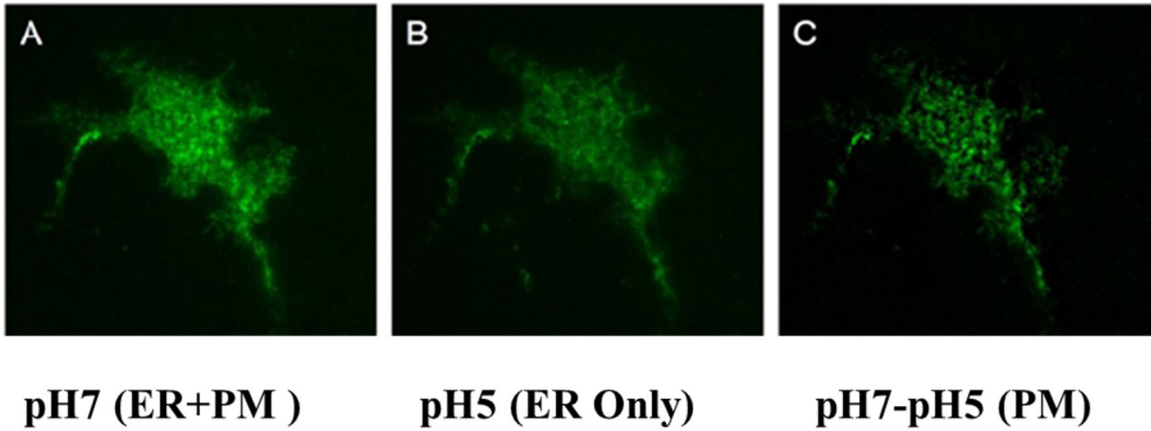
Figure 2.3: Example of an HEK293T Cell Expressing SEP-CFTR. (A) When the extracellular solution is pH 7.4, SEP-labeled CFTRs on the PM and in the ER are fluorescent. (B) When the extracellular solution is pH 5.4, SEP-labeled CFTRs in the ER are fluorescent, but SEP-CFTRs on the PM fail to fluoresce. (C) The fluorescence intensity in *B* subtracted from the fluorescence intensity in *A* equals the SEP-CFTR on the plasma membrane.

2.2.3   Detection of Single Vesicle CFTR Insertion Events

In trafficking vesicles, the SEP tag is oriented towards the low pH interior, resulting in quenching of the fluorescence signal. When the vesicles merge with the PM, SEP is exposed to a neutral pH extracellular solution, reactivating fluorescence. Hence, each vesicle insertion results in a burst of fluorescence. Figure 2.4 shows an example of an insertion event in cells expressing wild-type CFTR tagged with SEP. After the initial insertion and the burst of fluorescence, a spreading of the emission is observed and corresponds to full fusion of the vesicle with the PM. An insertion event experiment was performed to quantify the rate of CFTR trafficking to the cell membrane. Differences in the trafficking rates of CFTR upon exposure to different correctors were measured.

It is possible that the amount of CFTR loaded into each trafficking vesicle could also be different. To determine if this could be the case, we compared the relative fluorescence intensity of vesicles containing CFTRs upon exposure to different correctors. We selected a region of interest that encompassed the insertion event and determined the average fluorescence intensity of the frame before vesicle arrival and again at the brightest point of vesicle insertion. The difference between these values was used to calculate the fluorescence signal from the insertion event and thus represented the relative number of CFTR in the vesicle. Differences in the amount of CFTR loaded into each trafficking vesicle upon exposure to different correctors were measured.
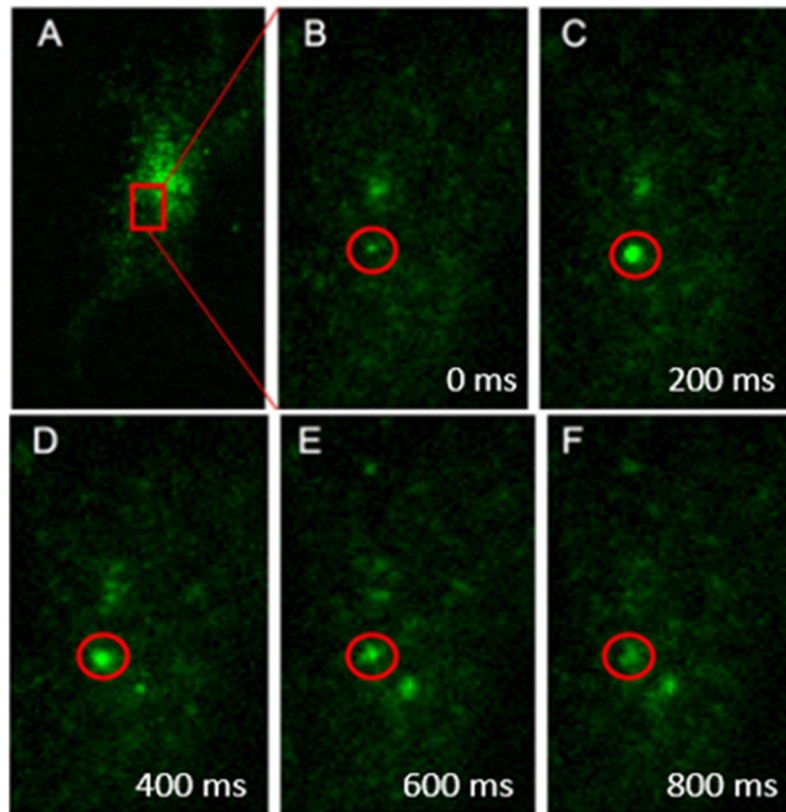
Figure 2.4: An Example of a Single Vesicle Insertion Event. (A) TIRF image of a whole cell. (B) - (F) the magnified red box in image *A*. At time 0, SEP labeled CFTR in a trafficking vesicle arrives at the cell surface. SEP exposure to a pH 7.4 extracellular solution turns on the fluorescence of SEP, and thus a burst of fluorescent is observed. As the vesicle fuses with the plasma membrane, the fluorescent burst spreads out.

2.3. CFTR-NBD1 Structure Study Using Single-Molecule FRET

Single –molecule FRET is well suited to investigate the structure and dynamics of a protein as it can resolve the folded and unfolded subpopulations to reveal protein structure information. To perform this experiment, two fluorophores (one is donor; the other is the acceptor) are required to tag the protein. As the protein is denatured, the distance between the two fluorophores is not in the FRET distance range (1-10nm). Therefore, the energy transfer between the FRET pair is not efficient, and only low FRET efficiency events are observed. With the protein fully folded, the two-fluorophore distance is reduced resulting in high FRET efficiency events (Figure 2.5). A pulsed laser excitation system, coupled with time-correlated single-photon counting electronics recording the arrival time and fluorescence delay of each photon, was applied to alternatively excite the donor and acceptor. As a single protein molecule labeled with a FRET pair freely diffuses through the detection volume of a confocal microscopy, a single fluorescent burst is captured by the APD and gives rise to a FRET efficiency, E (details have been explained in Chapter 1). Thousands of fluorescent bursts are accumulated and a histogram of efficiencies of those FRET events is plotted resolving the folded and unfolded protein subpopulations (Figure 2.6).

The most common mutation is a deletion of the phenylalanine at position 508 in NBD1. This mutation is associated with 90% of CF cases. Therefore, research of NBD1 is of significant interest. Our goal was to determine how the structural properties of NBD1 were altered due to the mutation and determine the effect of other conditions such as VX-809, reduced temperature and the second site suppressor I539. In this study, NBD1 was

expressed in *E.Coli*, and purified using Ni-NTA Agarose, as a His tag was added to the C-terminus. A FRET pair, Cy3 (donor) and Cy5 (acceptor), was incorporated at the two remaining cysteine sites of NBD1 using maleimide-thiol linker chemistry. Maleimide attached to the fluorescent dyes Cy3 and Cy5 can react with the sulfhydryl group of the cysteine on NBD1 resulting in labeling (Figure 2.7 A). Two cysteines at position 491 and 524 exist in NBD1. When NBD1 is fully folded, the distance between C491 and C524 is approximately 1.4 nm, resulting in an efficient energy transfer between the donor and acceptor. The distance between the two fluorophores, however, will be beyond the FRET distance range as the protein is unfolded. Energy from the donor cannot be transferred to the acceptor efficiently, and no high FRET efficiency event is observed. The properly labeled CFTR-NBD1 protein molecules were in diluted solution to ensure single molecules diffuse through the focused laser beam. As each NBD1 passed through the focal volume, the donor molecule was excited, and energy transfer was observed if the acceptor was in a close enough proximity. The structure information of NBD1 molecules was resolved by the FRET efficiency.
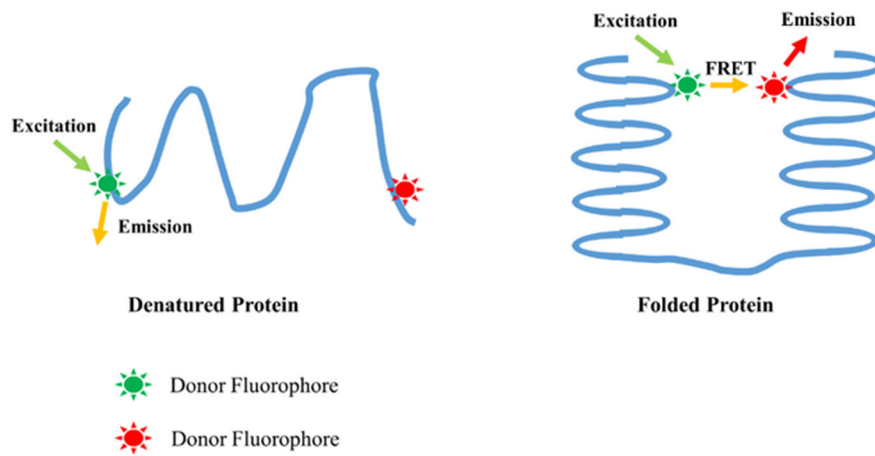
Figure 2.5: Comparison of FRET Event in Denatured Protein and Folded Protein. Left: The distance of FRET pair labeled on the denatured protein is beyond the FRET distance range. Energy cannot be transferred from the donor fluorophore to the acceptor fluorophore. Right: Though the FRET pair is far away from each other in the primary structure of the protein, energy is transferred between the FRET pair efficiently since the protein is folded.
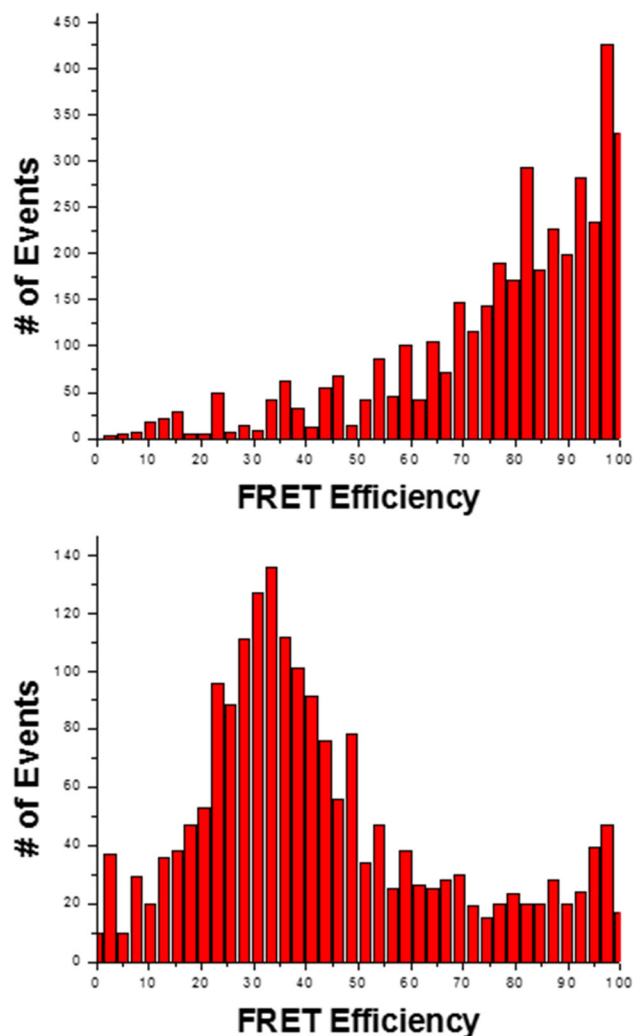
Figure 2.6: Representative FRET Efficiency Populations Showing the Protein Folding States. The two populations are collected from the same protein in two states. Top: protein in a buffer solution maintaining its native structure. A high FRET efficiency (80-100%) population is seen indicating the protein is fully folded. Bottom: protein in the same buffer solution but containing 6M GuHCl to fully denature the protein. FRET efficiency shifts to 30-50%. A FRET efficiency difference can be seen when the protein structure changes.

A
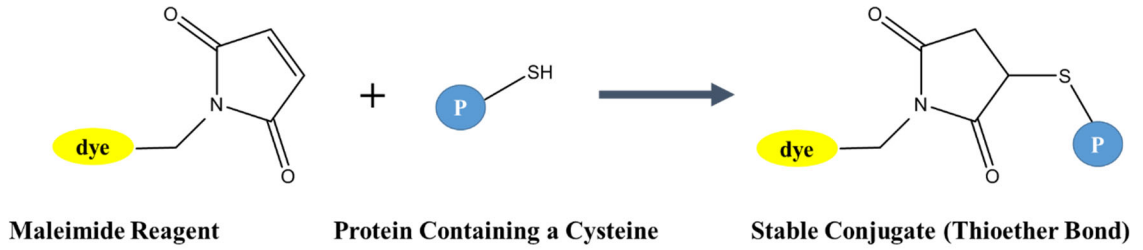
B
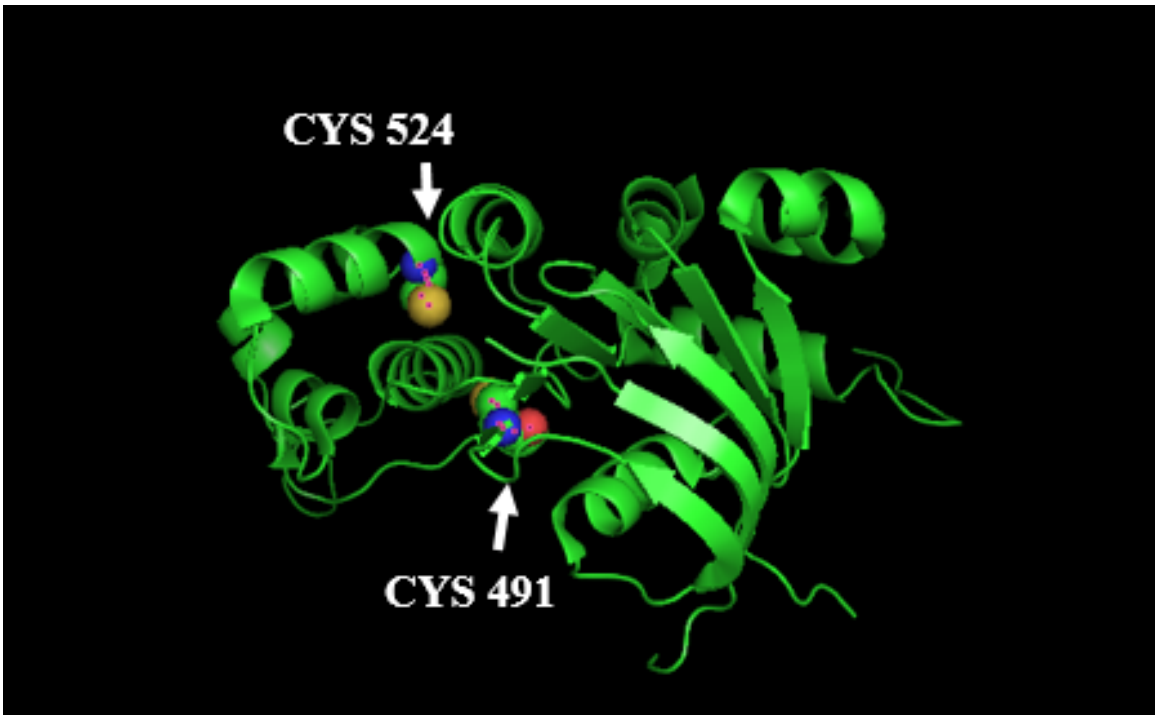
Figure 2.7: CFTR-NBD1 Fluorescent Labeling. (A) The maleimide – thiol chemistry reaction. (B) The structure of CFTR-NBD1 and the position of the two cysteines for fluorescent dyes labeling. *B* is created from PBD 2BBO.

2.4.A New Approach to Measure the Half-life of Protein on the Plasma Membrane

The goal was to develop a new pulse-chase approach utilizing total internal reflection fluorescence microscopy (TIRFM) to determine the half-life of protein on the cell membrane. A photoconvertible fluorescent protein, Dendra2, is applied in this approach as a fluorescent label. Dendra2, derived from octocoral Dendronephthya sp, is a mutant of the GFP-like protein[109]. Dendra2 is capable of being photoconverted from a green emissive form to red emissive form by exposure to UV-violet light (e.g. 405 nm) or blue light (e.g. 488 nm). Previous studies showed the appearance of bright red fluorescence in Dendra-expressing cells could be initiated by intense blue light (0.5–0.7 W/cm^2), while low intensity blue light (<50 mW/cm^2) for the same time period or even prolonged exposure time failed to photoconvert it[110]. This behavior makes it possible to select the fluorescent cells using a relatively low intensity (<50 mW/cm^2) 488nm laser without photoconverting them. The maturation time of Dendra2 (the $t_{1/2}$ or half-life for the immature state) is only 38 min[111]. The stability of Dendra2 has also been tested such that the fluorescence intensity of Dendra2 expressed in cells remains stable for several hours when cells are treated with protein synthesis inhibitor cycloheximide[112]. Thus, Dendra2 is an ideal fluorescent protein for labeling.

This new approach is utilized to quantify the half-life of epithelial sodium channel (ENaC) on the plasma membrane. HEK 293T cells expressing Dendra2 tagged ENaC were selectively photoconverted with 405 nm TIRF excitation to ensure the photoconvertion of protein occurs only at the plasma membrane (Figure 2.8 A). A population of Dendra2 on the cell surface with red emission was generated, and then time-lapse images of the same

field of view were taken to monitor endocytosis of ENaC (Figure 2.8 B). The half-life of the protein on the plasma membrane was calculated by quantifying the decay in the red fluorescence over time. Although new membrane protein is continuously delivered to the cell surface, it only exhibits green fluorescence not detectable in the red emission channel. As seen in Figure 2.9, cells are solely fluorescent in the green emission channel before exposure to 405 nm TIRF excitation. After the exposure, fluorescence is observed in both the green and red emission channels. The green fluorescence intensity is reduced after photoconvertion mostly due to a fraction of the population switched from green to red fluorophores.
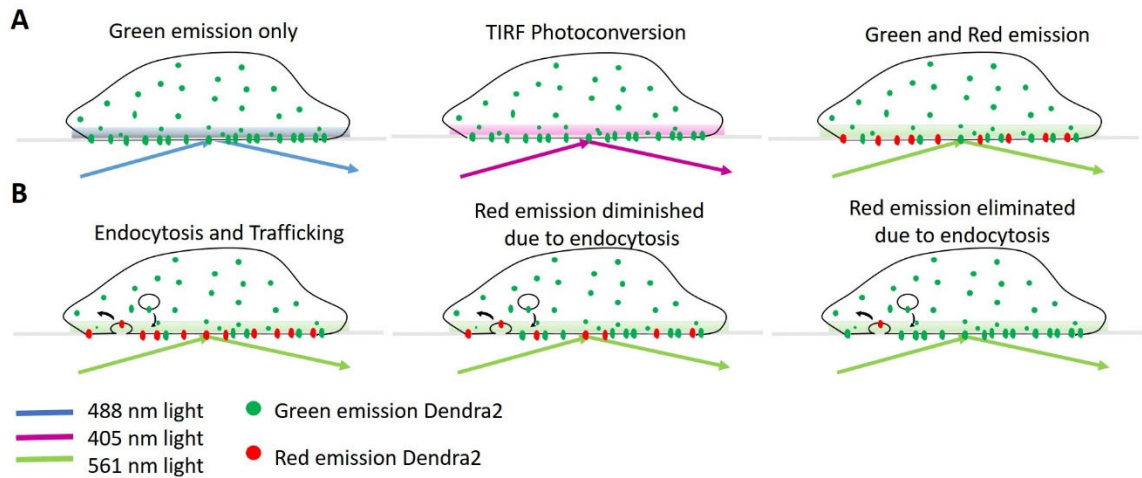
Figure 2.8: Cartoon Illustrating the Method Utilizing Dendra2 to Measure PM Protein Half-Life. (A) The fluorescent behavior of cells expressing Dendra2 before and after photoconversion. (B) The dynamic process of PM protein endocytosis and trafficking after a fraction of Dendra2 photoconverted to the red emissive form.
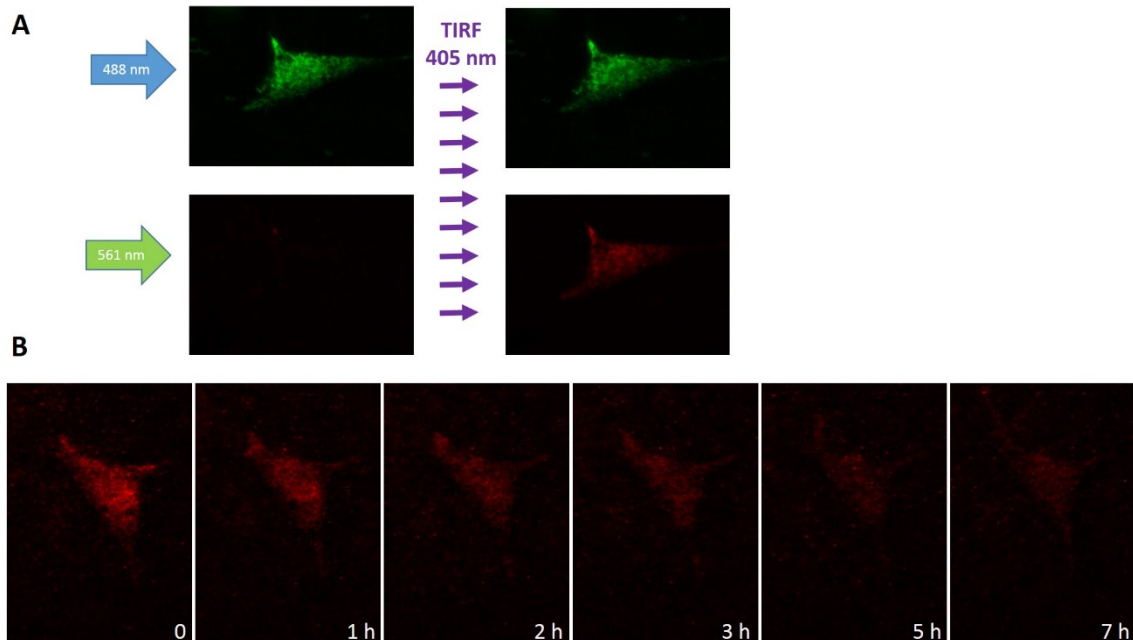
Figure 2.9: Example of TIRF Based Photoconversion and Fluorescence Decay. (A) TIRF images of a single cell before and after UV-violet photoconversion in both green and red emission channels with 488 nm and 561 nm excitation, respectively. (B) Representative time-lapse TIRF images in the red emission channel at different time points.

CHAPTER 3: MATERIALS AND METHODS

3.1. Materials

3.1.1   Reagents

Matrigel was purchased from Corning.   Lipofectamine 2000 transfection reagent was purchased from Invitrogen.   35 mm glass bottom petri dishes were obtained from Cell E&G. Cy3-maleimide and Cy5-maleimide were purchased from Lumiprobe. Azithromycin and L-ascorbic acid was purchased from Sigma Aldrich. Dynasore ≥98% was obtained from Enzo Life Science.

3.1.2   Plasmid Constructs

3.1.2.1 CFTR-SEP Plasmid Constructs

A pH-sensitive variant of GFP (Super ecliptic pHluorin; SEP) was utilized to quantify CFTR distribution on the plasma membrane (PM) and in the endoplasmic reticulum (ER). SEP was amplified by PCR using primers containing the AgeI and BsiWI restriction sites and cloned into a pcDNA 3.1 plasmid containing the gene for CFTR, which had AgeI and BsiWI restriction sites incorporated into the extracellular loop 4 of CFTR using the quikchange II site-directed mutagenesis kit. The cloning of SEP into the 4th extracellular loop of CFTR was carried out to ensure that SEP was oriented on the lumenal side of the ER and extracellular region of the cell when resident on the PM. The quikchange II site-

directed mutagenesis kit was also used to create the F508 deletion in CFTR. This construct was then used to incorporate the I539T mutation to generate I539T/ΔF508-CFTR.

3.1.2.2 CFTR-NBD1 Plasmid Construct

Wild-type CFTR-NBD1 gene consisting of 291 amino acids was cloned between NcoI and XhoI restriction sites of pET28 vector. His tag was incorporated into the C-terminal of NBD1 for the following protein purification. Kanamycin resistance gene existed in the vector for further colony selection.

3.1.2.3 ENaC Plasmid Constructs

Full length SCNNIA, SCNNIB and SCNNIG cDNA were purchased from Origene and cloned in pcDNA 4TO. The fluorescent protein Dendra2 was incorporated in to the C-terminus of each construct via NotI and XhoI restriction sites. The quickchange II site-directed mutagenesis kit (Agilent Technologies) was used to create the Y618A mutation in SCNNIB. The Y618A corresponds to a tyrosine to alanine change in position 618 in SCNNIB. All constructs were verified by sequencing.

3.2.Methods to Determine CFTR Expression and Trafficking

3.2.1   Cell Culture

Human embryonic kidney (HEK) 293T cells were cultured using standard tissue culture techniques at 37 °C and 5.6% CO_2. HEK 293T cells were maintained in growth media

consisting of Dulbecco's Modified Eagle Medium (DMEM), 10% fetal bovine serum, and 1% penicillin, and streptomycin [128-129]. Culture flasks were coated with a matrigel solution consisting of 1% matrigel in DMEM media. The matrigel solution added to the flasks and allowed to incubate for 5-10 min, then aspirated before the addition of cells. Cells were maintained in matrigel coated 75 cm^2 cell culture flasks.

3.2.2 Transfection and Cell Preparation for Total Internal Reflection Fluorescence (TIRF) Microscopy Imaging

For transfection with CFTR constructs, 3 x 10^6 cells were seeded into a matrigel coated T75 flask. The following day, the growth media in the HEK 293T flask was replaced with 10 mL of opti-MEM. Cells were transfected with 14 μL Lipofectamine-2000 mixed with 250 μL opti-MEM and separately 3.5 μg plasmid was mixed with 250 μL opti-MEM and incubated at room temperature for 5 min. The separate aliquots were then combined and allowed to incubate for 25 min at room temperature, and then added to the cells. After 24 h at 37 °C the cells were rinsed with PBS and dissociated with Trypsin. 200,000 cells were then plated onto matrigel coated 35 mm glass bottom dishes. In order to ensure the matrigel was thin enough for TIRFM, the 1% matrigel solution was left on the glass bottom dishes for 10 min at room temperature. The dishes were thoroughly rinsed with PBS prior to the addition of cells. Cells were incubated for an additional 24 h in growth medium at 37 °C before imaging.

3.2.3   Exposure to Pharmacological Agents

VX-809 treatment: After the transfected cells were seeded on a glass bottom dish, they were incubated at 37°C for 2 h for settling down. Then, growth medium in the dish was replaced by opti-MEM supplemented with 1% FBS, penicillin, and streptomycin containing 3 μM VX-809. The cells were incubated at 37°C for additional 24 h before imaging.

Reduced temperature correction: After the transfected cells were seeded on a glass bottom dish, they were incubated at 37°C for 2 h for settling down. Then, cells were incubated at the reduced temperature incubator for additional 24 h before imaging.

Azithromycin treatment: After the transfected cells were seeded on a glass bottom dish, they were incubated at 37°C for 2 h for settling down. Then, cell growth medium in the dish was replaced by opti-MEM supplemented with 1% FBS, penicillin, and streptomycin containing 5 μM azithromycin. The drug was incubated with the transfected cells at 37°C for 24 h before imaging. For the combined azithromycin and VX-809 treatment, cell growth medium in the dish was replaced by opti-MEM supplemented with 1% FBS, penicillin, and streptomycin containing both 5 μM azithromycin and 3 μM VX-809.

VX-770 treatment: Before imaging, medium in the cells seeded dish was replaced by an extracellular solution (recipe mentioned in section 3.2.5) containing 100 nM VX-770. Cells were incubated at 37 °C with VX-770 for 15 min before imaging. For the combined VX-770 and VX-809 or azithromycin treatment, cells were treated with VX-809 or

azithromycin 24 h before imaging as mentioned above. VX-770 was added 15 min before imaging.

3.2.4   TIRF imaging of Super Ecliptic pHluorin

Objective style total internal reflection fluorescence microscopy was utilized for all imaging studies. This setup is capable of detecting fluorophores to a depth of 200 nm above the cell-glass interface when excited by total internal reflection laser. CFTR-SEP localized on the PM, in the peripheral ER near the PM, and in the vesicles between PM and ER was within the TIRF excitation range. Super ecliptic pHluorin (SEP) was excited with a 488 nm DPSS laser through the objective (Olympus 1.49 NA 60x oil immersion). An electron multiplying charge coupled device (EMCCD) (Andor iXon Ultra 897) was employed to detect the SEP fluorescence signal. In order to obtain total internal reflection, the laser was focused on the back aperture of the objective lens and the angle was adjusted using a stepper motor to translate the beam laterally across the objective lens.

3.2.5   Measuring CFTR Expression and Distribution

SEP excited by the 488 nm laser was fluorescent at pH 7.4. Adjusting the pH to acidic conditions (pH<6) prevented SEP fluorescence. Before imaging, growth medium in the dish was replaced by a pH 7.4 extracellular solution (150 mM NaCl, 4 mM KCl, 2 mM MgCl2, 2 mM CaCl2, 10 mM HEPES and 10 mM glucose). CFTR on the PM and in the peripheral ER (pH>7) was visible under these conditions, while CFTR localized in the Golgi and trafficking vesicles at the lower pH were not visible. Initial images were

collected at pH 7.4, and then the extracellular solution was changed to an identical solution except that the pH had been adjusted to 5.4. Since SEP was located on the extracellular side of CFTR, it was exposed to pH 5.4. At pH 5.4 the observed fluorescence was solely from CFTR in the peripheral ER. TIRF images were collected for each cell at both pH 7.4 and pH 5.4. For quantitation, the integrated density (ID) for each image was determined. The ID is defined as the product of the average fluorescence intensity and the total number of pixels occupied by the cell. The ratio of CFTR on the plasma membrane was calculated from the integrated density of CFTR on the plasma membrane (pH 7.4 ID – pH 5.4 ID) divided by the total integrated density at pH 7.4. The plasma membrane integrated density (PMID) is a readout of the level of CFTR on the cell surface, where an increase in the PMID correlates to an increase in the number of CFTR-SEP channels on the plasma membrane. The ratio of CFTR on plasma membrane compared to the total (ER + PM) CFTR was used to quantify the distribution between the PM and peripheral ER. An increase in the percentage of receptors found on the plasma membrane (% PM) corresponds to a change in the distribution of receptors between the ER and PM. TIRF images were acquired using an exposure time of 200 ms, and a scanning stage was used to record the position of each cell to allow for a return to the exact same field of view for the images at pH 5.4 and 7.4. All experiments carried out with VX-809 used a concentration of 3 μM. Control experiments were performed with DMSO in the absence of VX-809.

Since the plasma membrane is permeable to NH_3, we altered the pH of the intracellular fluid by adding NH_4^+ to the extracellular solution. NH_3 moves into intracellular side of the cell until NH_3 equilibrates between the two sides of plasma membrane. Before imaging, growth medium in a dish was replaced with a pH 7.4 extracellular solution without NH_4^+

(150 mM NaCl, 4 mM KCl, 2 mM $MgCl_2$, 2 mM $CaCl_2$, 10 mM HEPES and 10mM glucose). After images were collected, the extracellular solution was changed to the exact same pH 7.4 extracellular solution but with NH_4^+ (100 mM NaCl, 4 mM KCl, 2 mM $MgCl_2$, 2 mM $CaCl_2$, 50 mM NH_4Cl, 10 mM HEPES and 10 mM glucose). When no NH_4^+ was in extracellular solution, only SEPs on the PM and in the ER were exposed to the pH 7.4 environment. NH_3 increases the pH in vesicles and turns on the fluorescence of SEPs in the vesicles. When NH_4^+ is in the extracellular solution, SEPs on the PM, in ER, and in vesicles are all visible. The integrated density of CFTR in vesicles was calculated by subtracting the images of pH 7.4 extracellular solution without NH_4^+ from those of pH 7.4 extracellular solution with NH_4^+.

3.2.6 Measuring CFTR Trafficking

To measure insertion events, real time images were acquired at a frame rate of 200 ms for 1000 frames to capture single vesicles integrating into the PM. Insertion events were counted by manually analyzing all 1000 frames. Insertion events were defined as a burst of fluorescence at the membrane lasting at least 2 frames (400 ms) and including lateral spreading of fluorescence to ensure transient full fusion of the delivery vesicle to the membrane. Persistent, continuously repeating bursts of fluorescence were not counted since a discrete exocytic event could not be ruled out.

3.2.7   CFTR PM Display Data Analysis

Quantification of fluorescence intensity was determined using ImageJ by manually selecting an intensity-based threshold and region of interest. All figures show results from a single imaging session that are representative of data collected on at least three separate occasions. All graphs show the mean with error bars representing SEM. P-values were determined using a two-tailed t test with equal variance not assumed.

3.3. Methods to Study CFTR-NBD1 Structure

3.3.1   CFTR-NBD1 Expression and Purification.

CFTR-NBD1 was expressed in *E.Coli* BL21 (DE3). *E.Coli* transformed with NBD1 plasmid were grown in 200 ml LB medium containing 50ug/ml Kanamycin. NBD1 expression was induced at 0.7 OD_{600} with a final concentration of 0.75mM isopropylthiogalactoside. Cells were shaking for additional 24 h at room temperature for protein expression. Then, cells were spinned down and resuspended in 10ml cold lysis buffer (50 mM Tris, 100 mM L-Arginine, 50 mM NaCl, 5 mM $MgCl_2$ hexahydrate, 12.5% Glycerol, 0.25% Triton X-100, 2 mM 2-Mercapto Ethanol, 2 mM ATP, pH 7.6, ATP was added right before use). Cells in lysis buffer were sonicated on ice for 1 min and cooled on ice for additional 5 min. Sonication was repeated for 3 times to ensure complete cell lysis. The lysed cells were centrifuged at 24,000 rpm, 4°C for 1 hour. The supernatant was mixed with 1ml Ni-NTA agarose resin (Invitrogen ProBond Resin) at 4°C under rotation in an end-over-end rotor. The protein-resin mixture was centrifuged at 700 g, 4 °C for 2 min and

then the supernatant was dumped as NBD1 protein was bound with Ni-NTA resin. The Ni-NTA resin binding with NBD1 was transferred to an empty Ni-NTA spin column and rinsed 3 times with 1.6 ml washing buffer (20 mM Tris, 500 mM NaCl, 60 mM Imidazole, 12.5% Glycerol, pH 7.6). NBD1 was eluted from the Ni-NTA resin by adding 400 ul elution buffer (20 mM Tris, 250 mM NaCl, 250 mM Imidazole, 12.5% Glycerol, pH 7.6) to the column and spinning at 700×g, 4°C for 2 min. The flow through was the purified NBD1 protein in elution buffer and stored at -80°C.

3.3.2   Labeling NBD1 with Cy3 and Cy5 and Remove Extra Dyes from the Protein

0.05 mg NBD1 in elution buffer was mixed with 0.8 ul 10 mM Cy3-maleimide and 0.8 ul 10 mM Cy5-maleimide, and the mixture was stored at 4°C overnight to allow the maleimide-thiol reaction to occur. Then, the mixture was dialyzed for 24 h using dialysis membrane (Spectra/Por Dialysis Membrane, Molecular weight cut-off: 10,000) in a dialysis buffer (20 mM Tris, 250 mM NaCl, 12.5% Glycerol final pH7.6). The dialysis buffer was replaced with new dialysis buffer after the first 4 h dialysis. Dialysis is to remove imidazole and the extra dyes from the protein.

3.3.3   Sample Preparation and Measurement

Protein samples were diluted to 35 pM in buffer containing 20 mM Tris, 250 mM NaCl, 12.5% Glycerol (final pH7.6).

Experiments were performed using an alternating light excitation (ALEX) confocal microscope system. The donor and acceptor tagged on a NBD1 molecule were excited alternatively with a pulsed 532 nm pulsed diode laser (20 MHz repetition rate, Picoquant) and a pulsed 640nm pulsed diode laser (20 MHz repetition rate, Picoquant). 100 ul protein solution was placed on a #1.5 cover glass and excited through a water immersion objective (60×, 1.20 NA, Nikon). The two excitation beams were completely overlapped and focused at a focal point 30 μm above the #1.5 cover glass. Donor and acceptor emissions were collected through the same objective and then they were separated from the excitation beam through a dichroic mirror. The pure emissions went through a spatial filter 100 μm diameter pinhole to remove the out- of focus beams. A second dichroic was then utilized to separate the donor and acceptor emission signals. The donor emission/acceptor emission was further cleaned by passing a 575 nm/40 nm band-pass filter (donor, Chroma)/ 667 nm/30 nm band pass filter (acceptor, Chroma). Single photons were collected using avalanche photodiodes (APDs), which converted light signals to electrical signals and then sent them to a photon counter (Picoharp 300, Picoquant). The photon counter converted electrical signals to digital signals and sent them to a PC where they were visualized in real-time (100 ms refresh rate) using the Symphotime 64 software (Picoquant).

3.3.4 Data Analysis

FRET efficiency was determined using Symphotime 64 software. Data were exported to Microsoft Excel and further exported to OriginPro8 (Origin Lab) where the FRET events were histogrammed.

3.4. Methods to Determine ENaC Half-life on the Plasma Membrane

3.4.1 Cell Culture

Human embryonic kidney (HEK) 293T cells were cultured using standard tissue culture techniques at 37 $^{\circ}$C and 5.6% CO_2. HEK 293T cells were maintained in growth media consisting of Dulbecco's Modified Eagle Medium (DMEM), 10% fetal bovine serum, and 1% penicillin, and streptomycin [128-129]. Culture flasks were coated with a matrigel solution consisting of 1% matrigel in DMEM media. The matrigel solution added to the flasks and allowed to incubate for 5-10 min, then aspirated before the addition of cells. Cells were maintained in matrigel coated 75 cm^2 cell culture flasks.

3.4.2 Transfection and Cell Preparation for TIRF Imaging

For transfection with CFTR constructs, 1 x 10^6 cells were seeded into a matrigel coated T25 flask. The following day, the growth media in the HEK 293T flask was replaced with 7 mL of opti-MEM. Cells were transfected with 5 μL Lipofectamine-2000 mixed with 250 μL opti-MEM and separately 1.5 μg plasmid was mixed with 250 μL opti-MEM and incubated at room temperature for 5 min. The separate aliquots were then combined and allowed to incubate for 25 min at room temperature, and then added to the cells. After 10 h of incubation at 37 °C, the transfection media was replaced with growth media. After an additional 12-14 h incubation, the transfected cells were dissociated with Trypsin and 5 × 10^5 cells were plated on a 35 mm matrigel coated glass bottom dish in growth medium. In order to ensure the matrigel was thin enough for TIRFM, the 1% matrigel solution was left

on the glass bottom dishes for 10 min at room temperature. Cells were incubated at 37 °C for an additional 24 h before imaging. For αβγ, SCNNIA, SCNNIB and SCNNIG were cotransfected in HEK 293T cells. Similarly, in the CFTR-ENaC interaction study, SCNNIA, SCNNIB SCNNIG and CFTR were cotransfected in HEK 293T cells.

3.4.3   TIRF Imaging of Dendra2

Objective-style TIRFM was utilized for all imaging studies. This setup is capable of detecting fluorophores on the plasma membrane and minimizes the fluorescence background from intracellular components. Dendra2 was excited with a 488 nm or 561 nm DPSS laser through the objective (Olympus 1.49 NA 60x oil immersion, Tokyo, Japan). In order to obtain total internal reflection, the laser was focused on the back aperture of the objective lens and the angle was adjusted using a stepper motor to translate the beam laterally across the objective lens. An electron multiplying charge coupled device (EMCCD) (Andor iXon Ultra 897, Belfast, United Kingdom) was employed to detect the Dendra2 fluorescence signal.

3.4.4   ENaC Half-Life Measurement

Photoconvertable fluorescent protein (Dendra2) was utilized to measure the ENaC half-life on the plasma membrane. Before imaging, growth media in the glass bottom dish was replaced with Leibovitz's L-15 with 100 uM ascorbic acid. At the start of each imaging session a control experiment was performed to correct for photobleaching during data collection. To obtain the correction curve, a randomly selected cell was photoconverted in

TIRF with a 405 nm laser; then 22 consecutive TIRF images were taken with 561 nm excitation. This was used to simulate the same level of laser exposure that occurs during the time-lapse imaging session. The fluorescence decay observed in these images results from 561 nm induced photobleaching. We assume on this time scale (<60 seconds) that protein endocytosis is negligible. Several cells in the same dish were then identified and the xy location was recorded. TIRF images of these selected cells were taken before Dendra2 photoconversion using both 561 nm and 488 nm excitation. This verified the absence of any fluorescence in the red emission channel prior to photoconversion. These cells were then exposed to TIRF oriented 405 nm laser (~16.5 mW at the objective) excitation for 3 seconds. Medium in the glass bottom dish was changed from Leibovitz's L-15 with 100 uM ascorbic acid to regular Leibovitz's L-15 after the photoconversion taking care to not move the position of the dish. Real-time TIRF images were then acquired for both 561 nm and 488 nm excitation to collect emission in both the red and green channels at 20 min interval for a total of 7 h. The intensity of both 488 nm and 561 nm lasers on the objective were ~ 1.0 mW and the 405 nm laser intensity on the objective was ~ 16.5 mW. The cells were kept at 37 °C for the duration of the experiment using a stage top incubator. For control studies with dynasore, 80uM dynasore was added to the imaging media containing ascorbic acid 20 minutes before imaging and the medium was then changed to L15 with 80 uM dynasore after photoconversion.

3.4.5 Data Analysis

Quantification of fluorescence integrated density (ID) was determined using ImageJ (NIH) by manually selecting an intensity-based threshold and region of interest. The decay in the

fluorescence ID of each image series using the decay constructed from the control images where the decay resulted from photobleaching. This removed the decay related to photobleaching in each data set. The resulting fluorescence decay in each data set after correction was then attributed to the departure of the fluorescently labeled protein from the TIRF field of view due to endocytosis. The measured protein intensity data was initially fit to the exponential equation to determine the half-life ($T_{1/2}$). All graphs show the mean with error bars representing SEM. P-values were determined using a two-tailed t test with equal variance not assumed.

CHAPTER 4: RESULTS

4.1 Correctors Alter Expression and Trafficking of CFTR

4.1.1   *Reduced Temperature and Second Site Suppressor (I539T) Promote ΔF508-CFTR*

   Expression on the PM

SEP, a pH-sensitive variant of green fluorescent protein (GFP)[128, 130-131], was used to quantify changes in CFTR distribution. A second site suppressor is defined as adding a second mutation to a mutant gene to partially revert the effect of the first mutation. In my study, we added I539T to ΔF508-CFTR to moderately revert the issue caused by ΔF508. SEP is emissive with 488 nm excitation at neutral pH but the emission is quenched under acidic conditions (pH <6). Previous studies showed that SEP-labeled receptors on the cell surface lost all detectable fluorescence upon exposure to low pH (5.4) extracellular solutions, while those localized in the ER membrane were not affected. Thus, SEP labeling allows for the measurement of only the receptor population localized to the cell surface[128].

The SEP tag was incorporated into the extracellular region of CFTR to allow for pH dependent fluorescence measurements to be made, whereby differentiation between intracellular and PM inserted CFTR could be quantified. HEK 293T cells expressing wild-type CFTR, ΔF508-CFTR, or I539T/ΔF508-CFTR were exposed to neutral (pH 7.4) and acidic (pH 5.4) conditions while recording TIRF images. Figure 4.1 shows representative TIRF images of cells expressing wild-type, ΔF508 at 30 °C, and I539T/ΔF508. The top row contains images of each cell at neutral pH, while the bottom shows the same cell at an acidic pH. At neutral pH, CFTR-SEP on the plasma membrane was fluorescent and visible

within the TIRF excitation volume. The peripheral ER that is within approximately 150 nm of the cell surface was also visible in TIRF. The ER population has the SEP-tag oriented on the luminal side of the organelle, which has a neutral pH, and is therefore fluorescent. As a result, the signal at this pH contains the PM as well as peripheral ER populations of CFTR-SEP. CFTR in the Golgi or in trafficking vesicles was not fluorescent due to the intra-organellar orientation of the SEP in these acidic environments. When the extracellular solution is replaced with an acidic solution the fluorescence of CFTR on the PM is eliminated. Thus, at an acidic pH the TIRF image is composed of fluorescence entirely from the peripheral ER (lower row of Figure 4.1). Calculating the fluorescence integrated density at pH 7.4 (ER+ PM ID) and subtracting the fluorescence integrated density at pH 5.4 (ER ID) allowed us to calculated the plasma membrane integrated density (PMID). This served as a real-time readout of CFTR levels on the PM.
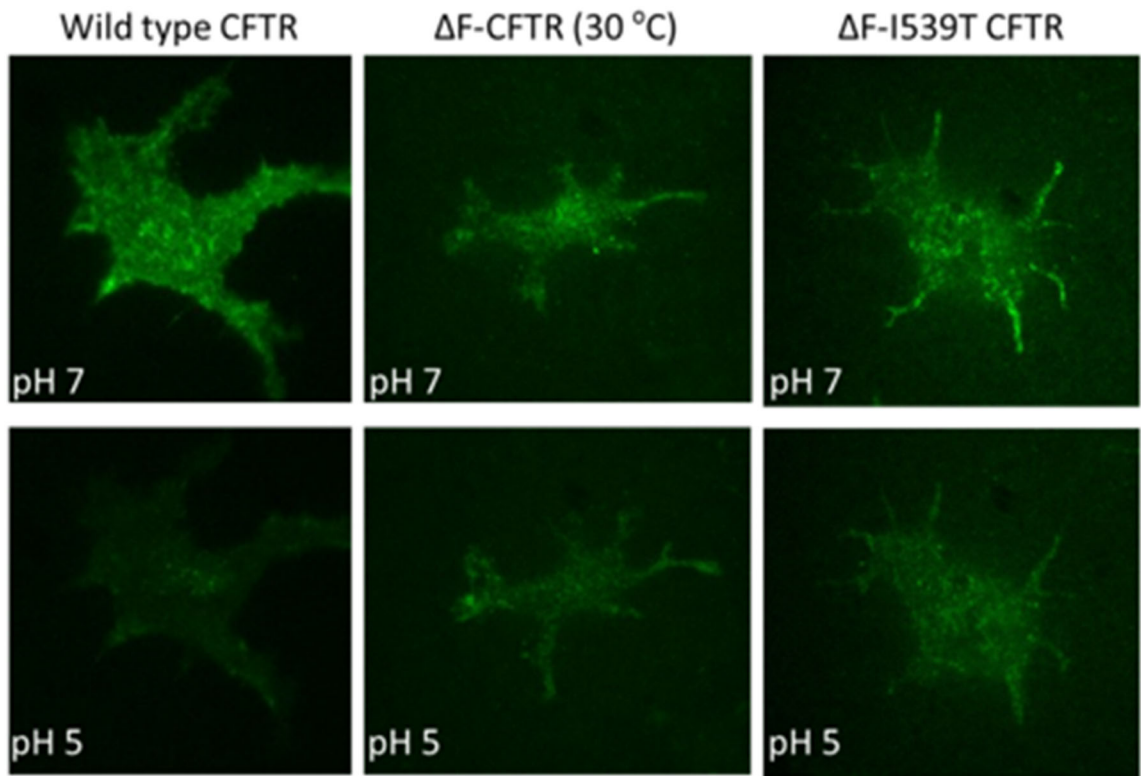
Figure 4.1: TIRFM Images Illustrating Increased CFTR Levels. TIRF images of HEK cells expressing wild-type CFTR-SEP, ΔF508-CFTR at 30°C, and I539T/ΔF508-CFTR. The top row shows images taken with an extracellular solution of pH 7.4 and the bottom row with pH 5.4. The loss of fluorescence at pH 5 represents the level of CFTR on the plasma membrane.

Distribution of CFTR within the cell was compared using percent plasma membrane (% PM), calculated by dividing the PM integrated density (difference between pH 7.4 and pH 5.4 images) with the total integrated density of receptors fluorescing on the PM and ER at pH 7.4. At 37 °C, we observed no detectable ΔF508-CFTR in the TIRF field of view. A 7 °C reduction in the temperature or adding a second site mutation, however, increased the ΔF508-CFTR expression and made the detection of ΔF508-CFTR possible. As shown in Figure 4.2, the PM fraction of ΔF508-CFTR at 30°C was ~ 30%, and total cell surface expression of ΔF508-CFTR in the same condition was ~10% of the wild-type level. CFTR containing both a ΔF508 mutation and the second site suppressor I539T mutation (I539T/ΔF508-CFTR) exhibited ~38% PM fraction, and total cell surface expression of ΔF508-CFTR increased to ~10% of the wild-type level.

A
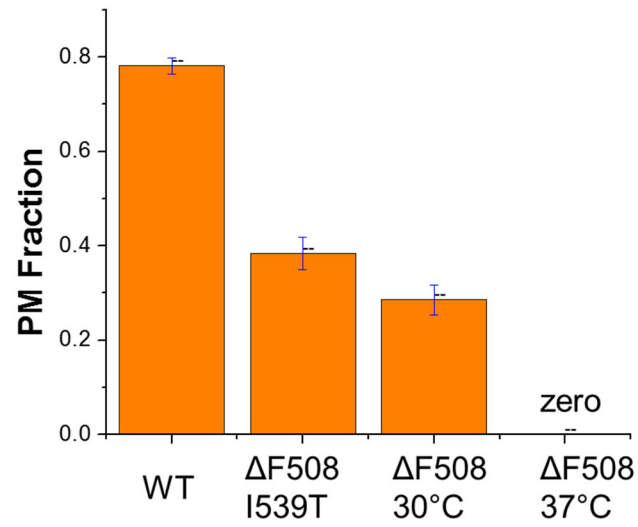
B
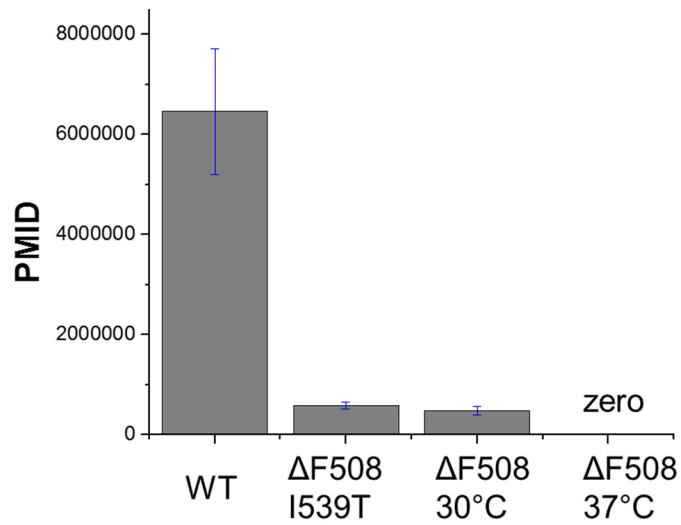
Figure 4.2: The CFTR Cell Surface Distribution and Expression. (A): the ratio of the plasma membrane to total fluorescence visible in the TIRF field of view. (B): the subtraction of ER ID from PM+ER ID. WT is short for wild-type.

4.1.2 VX-809 Works Synergistically with Reduced Temperature and a Second Site

Suppressor to Traffic ΔF508-CFTR

VX-809 ($C_{24}H_{18}F_2N_2O_5$), is an FDA approved drug for cystic fibrosis treatment. Currently, it is used in combination with VX-770 but has no medical use on its own. VX-809 acts as a chaperon during the protein folding, while the exact action mechanism remains unknown. We combined VX-809 with low temperature or I539T and showed the combination effects on ΔF508-CFTR trafficking. Approximately 75% of wild-type CFTR visible in the TIRF field of view was found on the PM. This fraction went up to 85% in the presence of 3 μM of VX-809 (Figure 4.3), while control experiments using DMSO (0.02%) showed no change in CFTR levels. This is consistent with reports of high levels of wild-type CFTR trafficking[132]. Similar studies showed that 35% of visible I539T/ΔF508-CFTR was displayed on the PM, and that this increased to nearly 60% in the presence of VX-809 (Figure 4.3). The same measurement with ΔF508-CFTR at 30 °C indicated that ~25% of the protein was displayed on the PM. This increased to approximately 55% in the presence of VX-809. In all cases there was a shift in the distribution of protein from the peripheral ER toward the plasma membrane. It should be noted that in this assay we did not detect any ΔF508-CFTR on the PM at 37 °C in the absence of VX-809, consistent with other reports using traditional techniques.
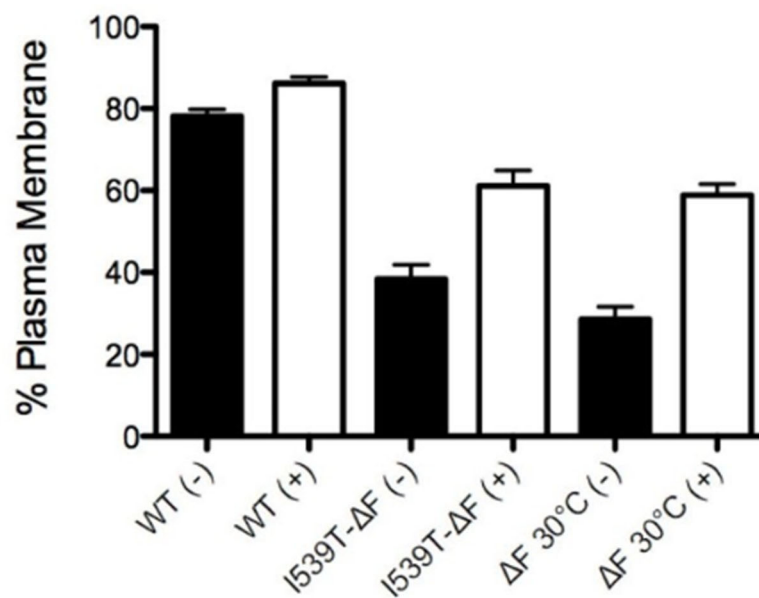
Figure 4.3: Plasma Membrane Fraction. Comparison of the ratio of plasma membrane to total fluorescence visible in the TIRF field of view. This reveals changes in the distribution of receptors from the peripheral ER to the PM. A large portion of intracellular CFTR is shifted to the PM for I539T/ΔF508 and ΔF508 when exposed to VX-809 (open bars designated with a + sign), suggesting the drug facilitates trafficking of a pool of CFTR stabilized by low temperature or second site suppressors.

To further quantify the cell-surface CFTR, we examined the integrated density of the fluorescence on the PM. This allows for quantifying only the amount of CFTR at the PM, eliminating any signal that may be coming from CFTR either in the ER or close to the PM. Figure 4.4 shows the raw integrated density (average fluorescence intensity multiplied by the number of pixels within a cell) for the same conditions in Figure 4.3. The high level of wild-type CFTR on the PM increased by approximately 20% in the presence of VX-809, showing that the compound affects the trafficking of wild-type CFTR. This indicates that a high percentage of CFTR does not form a conformation capable of ER export, but is amenable to export upon the addition of a chemical chaperone. CFTR containing both the disease causing ΔF508 mutation and the second site suppressor I539T mutation (I539T/ΔF508-CFTR) exhibited only ~10% of the level of PMID compared to wild-type CFTR. VX-809 corrected the trafficking of I539T/ΔF508-CFTR to ~40% of wild-type levels. This is substantially more than the sum of the protein levels seen for I539T/ΔF508-CFTR and VX-809 separately. Similar results were seen for ΔF508-CFTR at 30 °C. Consistent with previous studies that examined low temperature correction of ΔF508-CFTR, we show that approximately 8% of the wild-type population can be corrected[120, 133]. After exposure to VX-809 for 24 hours, the cells under the same conditions showed an increase in population at the plasma membrane, as ΔF508-CFTR at 30 °C in the presence of the compound exhibited ~40% of wild-type levels of PMID.
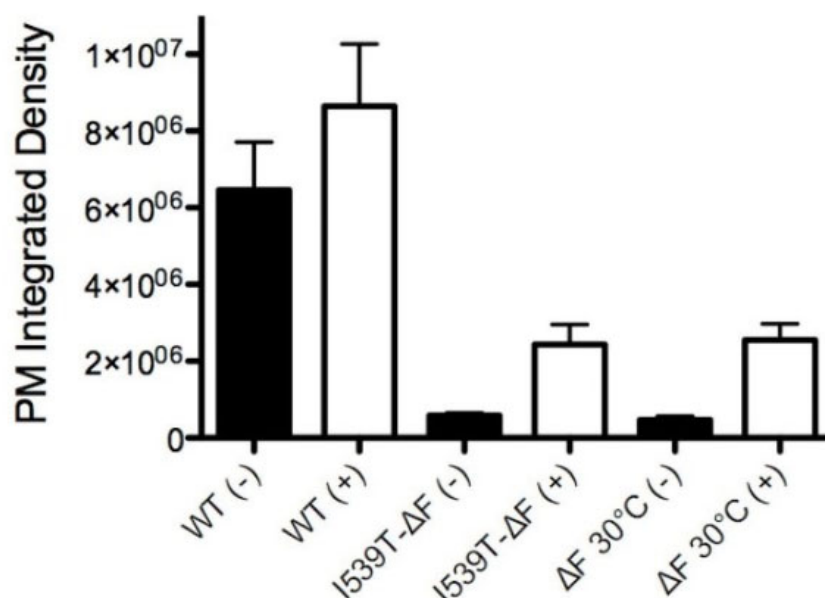
Figure 4.4. The Effect of VX-809 on Cell Surface CFTR. Comparison of the total amount of CFTR displayed on the plasma membrane as determined by the fluorescence change from the pH sensitive SEP label. A synergistic effect is observed for I539T/ΔF508 and ΔF508 when exposed to VX-809, as indicated by the large increase in CFTR PM level. Solid bars represent the data for CFTR in the absence of compound, while open bars are with VX-809.

4.1.3 The Immunomodulatory Mechanism of AZM is Different from That of Either Reduced Temperature or VX-809.

Azithromycin (AZM), a macrolide antibiotic, has medical use for the treatment of CF patients. Clinical studies show an improvement of patients treated with AZM compared with those receiving placebo, but the molecular mechanism remains unknown. Conflicted conclusions had been made over the years. Melotti's group showed the anti-inflammatory effect of azithromycin on the cystic fibrosis cell line[134], while Tabary's group described that azithromycin fails to reduce inflammation in cystic fibrosis airway epithelial cells[135]. Additionally, a few groups report that azithromycin is able to restore Cl⁻ efflux of CF cells, which is evidence to support azithromycin works as more than an antibiotic for CF patients[136-137]. Therefore, further study of the AZM action mechanism is required to determine the anti-inflammatory effect of azithromycin on CF. We performed experiments to test the effect of AZM on CFTR distribution and cell surface expression. AZM treatment was applied to I539T/ΔF508-CFTR. As seen in Figure 4.5 A, approximately 27% of I539T/ΔF508-CFTR was distributed across the plasma membrane, while this fraction went up to 50% in the presence of azithromycin. The two fraction values were significantly different from each other. Cells with treatment of VX-809 showed approximately 82% I539T/ΔF508-CFTR distributed on the plasma membrane and exhibited similar distribution with combined treatment of VX-809 and azithromycin. In addition, a combination of low temperature correction with azithromycin treatment was not statistically different in terms of the CFTR plasma membrane ratio as compared to low temperature correction on its own (Figure 4.5 A). I539T/ΔF508-CFTR cell surface expression showed the same results that AZM increase the amount of I539T/ΔF508-CFTR

on plasma membrane 2.5 fold compared with noncorrected I539T/ΔF508-CFTR. However,

AZM failed to alter I539T/ΔF508-CFTR cell surface expression when it is combined with

VX-809 or low temperature (Figure 4.5 B).

A
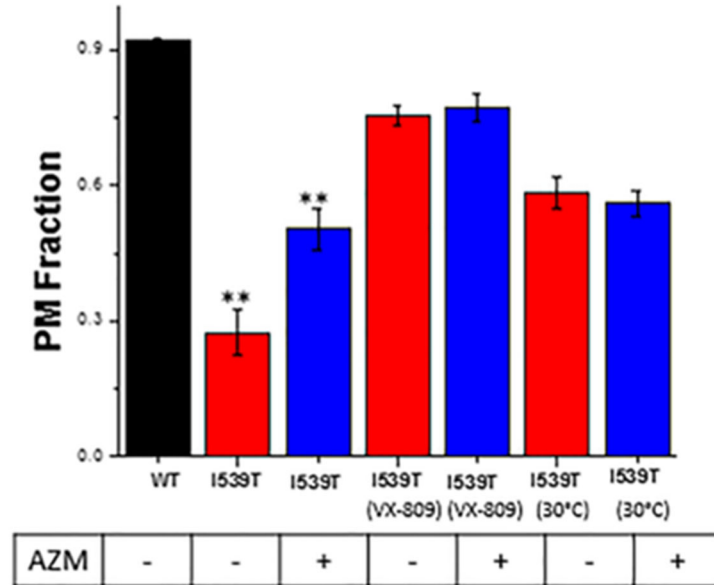
B
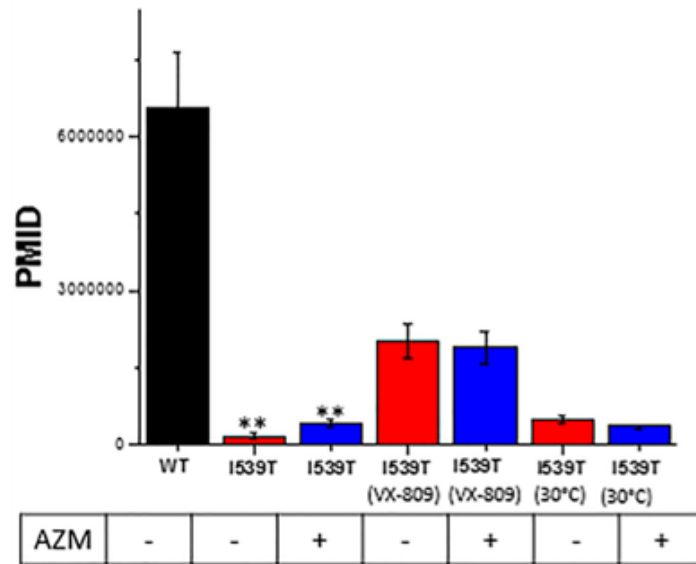
Figure 4.5: The Effects of Azithromycin on I539T/ΔF508-CFTR PM Fraction and PMID. The black bar is wild-type CFTR. Red bars are I539T/ΔF508-CFTR without azithromycin treatment. Blue bars are I539T/ΔF508-CFTR with azithromycin treatment. Azithromycin only changes the I539T/ΔF508-CFTR distribution and cell surface expression when no other correction is combined. (**, $p < 0.05$)

86

PM fraction and PMID experiments to study the AZM effect on ΔF508-CFTR were performed as well. We compared the effect of AZM on low temperature or VX-809 treated ΔF508-CFTR but not ΔF508-CFTR without correction since ΔF508-CFTR without correction showed undetectable levels of fluorescence on the cell surface. As seen in Figure 4.6 A, approximately 40% of reduced temperature corrected ΔF508-CFTR was distributed on the plasma membrane, and the presence of azithromycin did not statistically alter the fraction. Cells with treatment of VX-809 showed 68% ΔF508-CFTR distributed on the plasma membrane and exhibited a similar distribution with a combined treatment of VX-809 and azithromycin (57%). In addition, the PMID of VX-809 treated ΔF508-CFTR was $5.6 \times 10^5 \pm 1.1 \times 10^5$. Upon AZM exposure, this PMID value did not significantly change $(6.2 \times 10^5 \pm 1.8 \times 10^5)$. Similarly, no statistical change was seen in the AZM treated 30°C/ΔF508-CFTR compared with ΔF508-CFTR at 30°C (Figure 4.6 B).

A
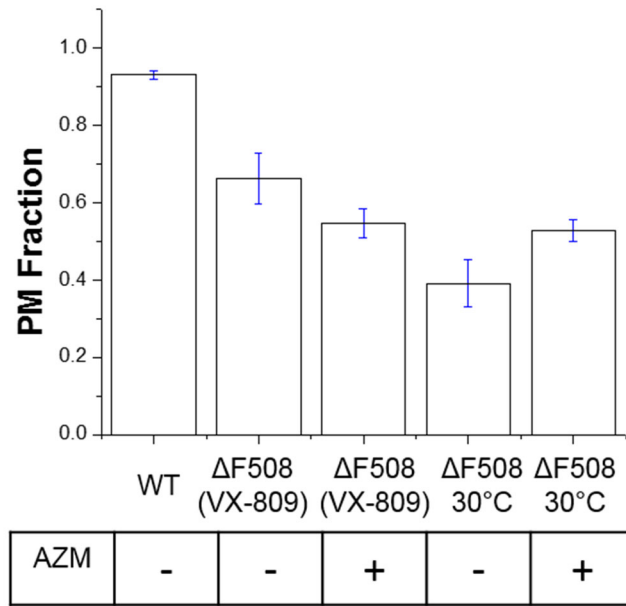
B
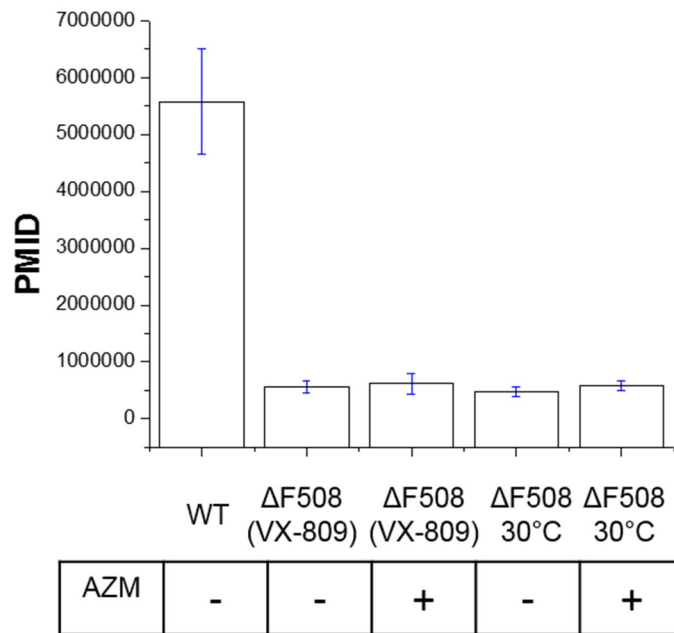
Figure 4.6: The Effects of Azithromycin on ΔF508-CFTR PM Fraction and PMID.
No statistical difference is seen in the AZM treated ΔF508-CFTR.

4.1.4   VX-770 does not Work Synergistically with VX-809 and Azithromycin

VX-770 ($C_{24}H_{28}N_2O_3$), trade name Kalydeco, is an FDA approved drug for cystic fibrosis treatment. Currently, it is used in conjunction with VX-809 to treat ΔF508-CFTR. It can also be used on its own for G551D-CFTR treatment, which accounts for 4–5% of cystic fibrosis cases. G551D results in a dysfunction of CFTR on the cell membrane. G551D-CFTR is able to traffic to the cell membrane, while it significantly reduces chloride transportation across the cell membrane. VX-770, a CFTR potentiator, facilitates chloride transportation by directly binding to the channels to induce a non-conventional mode of gating which increases the channel open probability[68, 70-71].

We performed experiments to test the effect of VX-770 on CFTR distribution and cell surface expression in the presence of VX-809 or azithromycin. As seen in Figure 4.7 A, approximately 40% of VX-809 corrected ΔF508-CFTR was distributed on the plasma membrane, and the presence of VX-770 did not statistically alter the fraction (~44%). Cells treated with azithromycin showed ~18% ΔF508-CFTR distributed on the plasma membrane, and the combined azithromycin and VX-809 failed to significantly increase the distribution value (~27%). In addition, the PMID of VX-809 treated ΔF508-CFTR was 7.7 x 10^5 ± 2.6 x 10^5. Upon VX-770 exposure, this PMID value did not significantly change (4.5 x 10^5 ± 1.2 x 10^5). Similarly, no statistical change was seen in the AZM corrected ΔF508-CFTR distribution or cell surface expression in the presence or absence of VX-770 (Figure 4.7 B).

A
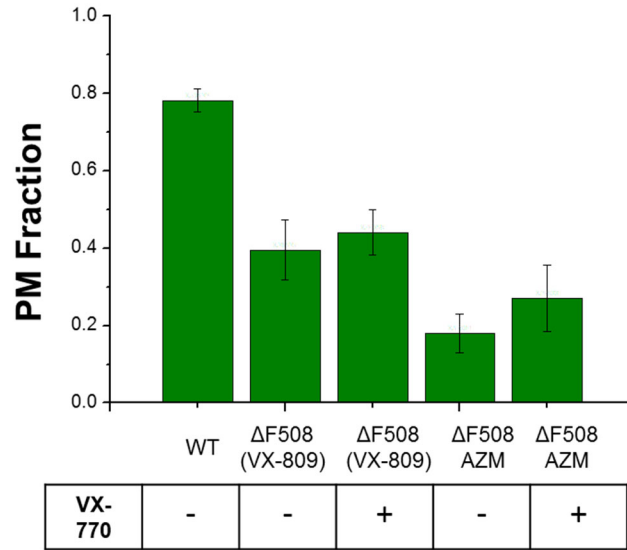
B
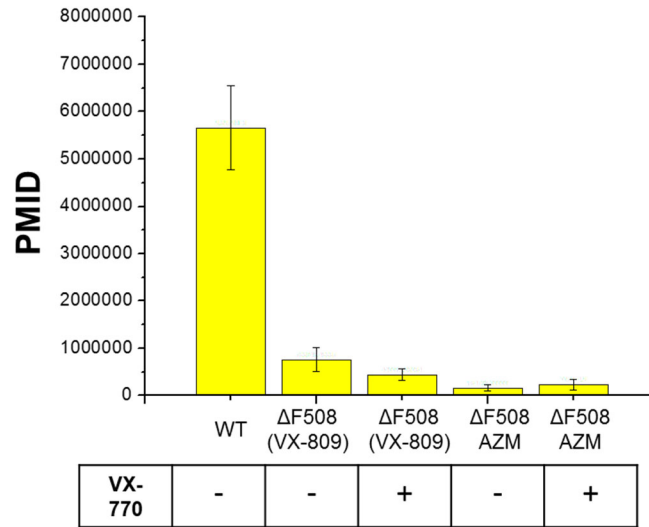
Figure 4.7: The Effects of VX-770 on ΔF508-CFTR PM Fraction and PMID. No statistical difference is seen in the VX-770 treated ΔF508-CFTR.

4.1.5 A Larger I539T/ΔF508-CFTR Pool in the Vesicles near The Cell Surface than That of Wild-Type CFTR

CFTRs are not only on the PM or in the ER, but also located in vesicles between the PM and ER. In order to determine the population of CFTR located in the acidic vesicles, we used an approach to equilibrate the pH of the lumen vesicles to that of the extracellular solution. NH_4Cl was utilized to increase the pH of the lumen vesicles. The pH of the intracellular fluid is changed by adding NH_4^+ to the extracellular solution since the plasma membrane is permeable to NH_3. NH_3 moves to the intracellular side of the cell until NH_3 equilibrates the two sides of the plasma membrane. Initially, growth medium in the imaging dish was replaced with pH 7.4 extracellular solution without NH_4^+. Images of the selected cells were taken, and then the extracellular solution was changed to the same pH 7.4 extracellular solution with NH_4^+. When no NH_4^+ is in the extracellular solution, only SEPs on the PM and in the ER are exposed to the pH 7.4 environment. As the additional NH_4^+ increases the pH of the lumen vesicles to above 6 with the additional NH_4^+, SEPs on the PM, in the ER, and in the vesicles are all visible. In this manner, we are able to quantify the integrated density (ID) of CFTR in the vesicles, which equals the difference between integrated density measured with NH_4^+ and that measured without NH_4^+. These experiments were performed for HEK 293T cells expressing I539T/ΔF508-CFTR. I539T/ΔF508-CFTR showed an approximately 10-fold vesicle ID increase compared to wild-type CFTR, which corresponded to the amount of I539T/ΔF508-CFTR in the vesicles near the cell surface, 10 times more than wild-type CFTR in the same place. In addition, I539T/ΔF508-CFTR with azithromycin treatment also exhibited a larger amount of I539T/ΔF508-CFTR than wild-type CFTR in the vesicles (Figure 4.8).
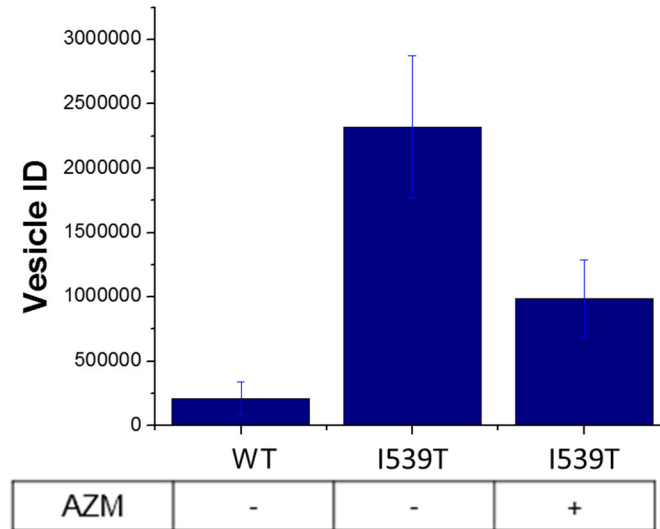
Figure 4.8: The Distribution of CFTR in the Vesicles. A 10 times more amount of I539T/ΔF508-CFTR was located in the vesicles than in wild-type CFTR. I539T/ΔF508-CFTR with azithromycin treatment correction showed 4 times the amount of wild-type CFTR in the vesicles.

4.1.6   Changes in PM CFTR Levels are Related To Differences in Trafficking Rates.

Changes observed in the presence of VX-809 or differences seen between mutations (I539T/ΔF508 and ΔF508) could be related either to differences in trafficking rates to the PM, or to the half-life of the protein on the cell surface. To determine if differences in trafficking rates accounted for the observed CFTR levels on the PM, we performed experiments to quantify the rate of transport of CFTR to the cell surface. In trafficking vesicles, the SEP tag is oriented toward the low pH interior, resulting in quenching of the fluorescence signal. When the vesicles merge with the PM the protein is exposed to a neutral pH extracellular solution, reactivating fluorescence. This results in a burst of light for each vesicle insertion. The supplementary movie shows an example of such insertion events in cells expressing wild-type CFTR-SEP. After the initial insertion and burst of fluorescence, we observed a spreading of the emission, corresponding to full fusion of the vesicle and diffusion into the PM.

We quantified the individual insertion events for cells expressing wild-type CFTR and I539T/ΔF508-CFTR with VX-809. Figure 4.9 A shows a time course of a single insertion event for wild-type CFTR. At time 0 the vesicle has just started to arrive, and the 200 ms per frame sequence of images shows a burst of fluorescence at 200 ms (shown inside the blue circle), which then begins to spread out as the protein diffuses into the plasma membrane. For the same time period, cells expressing wild-type CFTR exhibited twice as many insertion events as cells expressing I539T/ΔF508-CFTR with VX-809 (Fig. 4.9 B). This approximately matches the differences in the level of surface protein shown in Figure 4.4.

It is possible that the amount of CFTR loaded into each trafficking vesicle could also be different. To determine if this could be the case, we compared the relative fluorescence intensity of vesicles containing wild-type to I539T/ΔF508-CFTR. We selected a region of interest that encompassed the insertion event and determined the average fluorescence intensity the frame before vesicle arrival and again at the brightest point of vesicle insertion. The difference between these values was used to calculate the fluorescence signal from the insertion event and thus represented the relative number of channels in the vesicle. We found no difference between wild-type and I539T/ΔF508-CFTR signal intensities (Figure 4.9 C). Thus, the differences seen in the CFTR protein levels are consistent with the differences in the rate of arrival of CFTR on the plasma membrane, not the number of channels per vesicles.
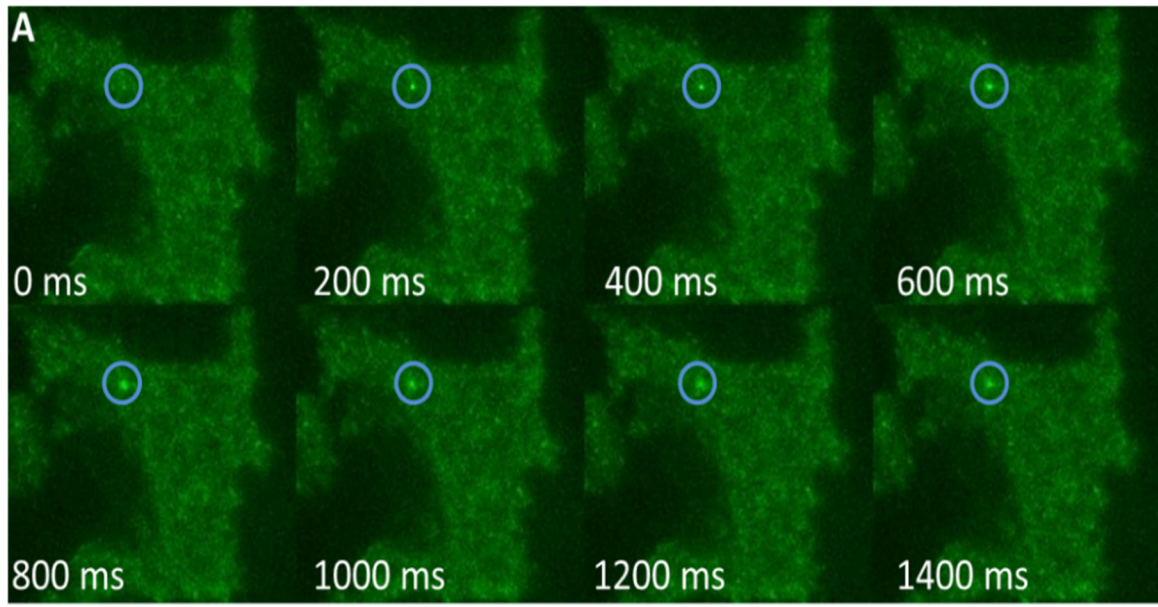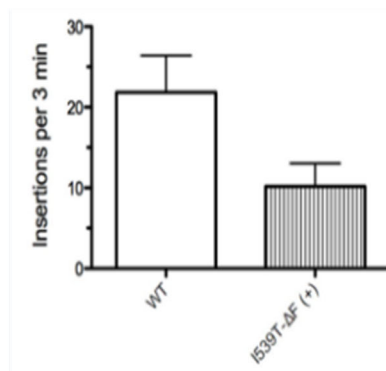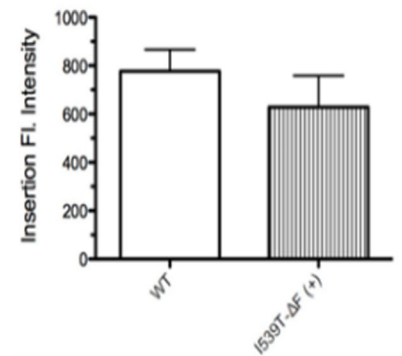
Figure 4.9: Quantifying Trafficking Rates via Counting Vesicle Insertion Events. (A) Series of images of wild-type CFTR-SEP showing an insertion event. The first frame shows just before the insertion event and the subsequent frames show the progression of the vesicle inserting. By 1.4 sec the vesicle has fully merged and the receptors are diffusing into the PM. (B) Comparison of the number of insertions per cell per 3 min for wild-type CFTR and I539T in the presence of VX-809. (C) A comparison of the average intensity of the insertion events. The trafficking rate of wild-type is roughly twice that of I539T with VX-809 which matches the relative PM levels. Conditions indicated as I539T represent ΔF508-I539T mutations.

4.1.7   A Range of Temperatures Stabilize ΔF508-CFTR and are Differentially Affected

   by VX-809

We performed a set of experiments to determine the effect of temperature in the presence

and absence of VX-809 on the levels of ΔF508-CFTR and ΔF508/I539T-CFTR on the PM.

Using our SEP assay, we measured the relative PMID of ΔF508-CFTR at 27, 30, 32, 34,

and 37 °C in the presence and absence of 3 µM VX-809. Cells cultured at 37 °C showed

no measurable levels of ΔF508-CFTR on the PM. However, cells cultured at all of the other

temperatures clearly displayed ΔF508-CFTR on the PM. In the absence of VX-809, values

ranging from 8 to 12% of wild-type were obtained for 27, 30, 32, and 34 °C (Figure 4.10

A). The combination of low temperature and exposure to 3 µM VX-809 resulted in 3 to 4-

fold higher levels of ΔF508-CFTR as compared to low temperature alone. Low temperature

caused no change in the levels of I539T/ΔF508-CFTR (Figure 4.10 B), with the exception

of a slight change at 34 °C; protein levels at all remaining temperatures were similar to that

observed at 37 °C. As shown earlier in Figure 4.3, VX-809 resulted in higher PM levels

of I539T/ΔF508-CFTR (50% of WT) at 37 °C. At reduced temperatures we also observed

an increase in I539T/ΔF508-CFTR. At 27 °C levels are increased to 45% of wild-type

levels. However, at 32 °C we achieved near 100% of wild-type in the presence of VX-809.

%PM DF and I539T
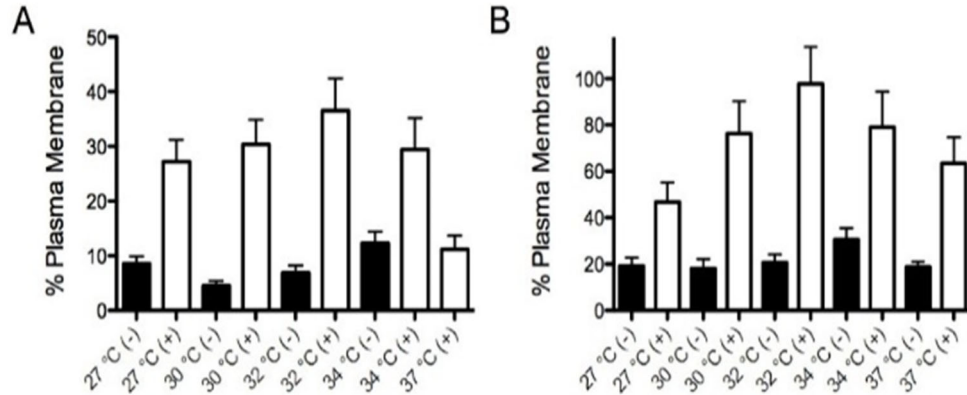
Figure 4.10: Temperature Dependence of VX-809 Activity on ΔF508 and I539T-ΔF508 CFTR. A. Total amount of ΔF508 CFTR displayed on the plasma membrane as determined by the fluorescence change from the pH sensitive SEP label. Experiments were performed across a range of temperatures, with (+) or without (-) VX-809. B. Total amount of I539T-ΔF508 CFTR on the plasma membrane as determined by the fluorescence change from the pH sensitive SEP label across a range of temperatures and with (+) and without (-) VX-809.

4.2 Single-Molecule FRET to Study NBD1 Structure

Single – molecule FRET is well suited to investigate the structure and dynamics of proteins. With this technique, a donor fluorophore and an acceptor fluorophore are both tagged on a protein molecule. When the protein is fully folded, the two fluorophores are close to each other, and energy can be transferred from the donor fluorophore to the acceptor fluorophore. As the protein is denatured, the distance between the two fluorophores is beyond the FRET distance range (1-10nm). Therefore, the energy transfer between the FRET pair is not efficient and low FRET efficiency events or even no FRET event is observed (Figure 4.11). A single fluorescent burst is observed as a single protein molecule labeled with a FRET pair freely diffusing through the detection volume under confocal microscopy. A burst gives rise to a FRET efficiency, E (details has been explained in Chapter 1). Thousands of fluorescent bursts are accumulated, and a histogram of FRET efficiencies are plotted resolving the folded and unfolded protein subpopulations (Figure 4.11).

In this study, CFTR-NBD1 was expressed in *E.Coli* and purified using Ni-NTA Agarose, as the NBD1 had a His tag at the C-terminus (NBD1 mentioned in this section refers to wild-type CFTR-NBD1). NBD1 consists of 291 amino acids from position 388 to 678 of CFTR. The Coomassie blue stain of purified NBD1 is shown in Figure 4.12 A. A FRET pair, Cyanine3 (Cy3) and Cyanine5 (Cy5), was utilized to label cysteines of NBD1 and worked as donors and acceptors, respectively. Cy3 and Cy5 are the most widely used FRET pair. Cy3 fluoresces greenish-yellow with a maxima of 550 nm excitation and 570 nm emission, and Cy5 is fluorescent in the red region with a maxima of 650 nm excitation and 670 nm emission. Maleimide conjugated to the fluorescent dye reacts with a sulfhydryl

group of the cysteine on NBD1 to tag the protein with the dye. The maleimide-thiol reaction took place as soon as the two fluorophores and purified protein were mixed together. Two cysteines at position 491 and 524 exist in NBD1. As a result, there were three differently labeled NBD1 populations: NBD1 molecules labeled with two Cy3s (25%); NBD1 molecules labeled with two Cy5s (25%); NBD1 molecules labeled with one Cy3 and one Cy5 (50%). FRET is impossible to occur in the first two populations since it is lacking the necessary fluorophore. When NBD1 is fully folded, the efficient energy transfer happens in the NBD1 molecules tagged with both Cy3 and Cy5. The distance between the two fluorophores, however, will be beyond the FRET distance range as the protein is unfolded (Figure 4.12 B).
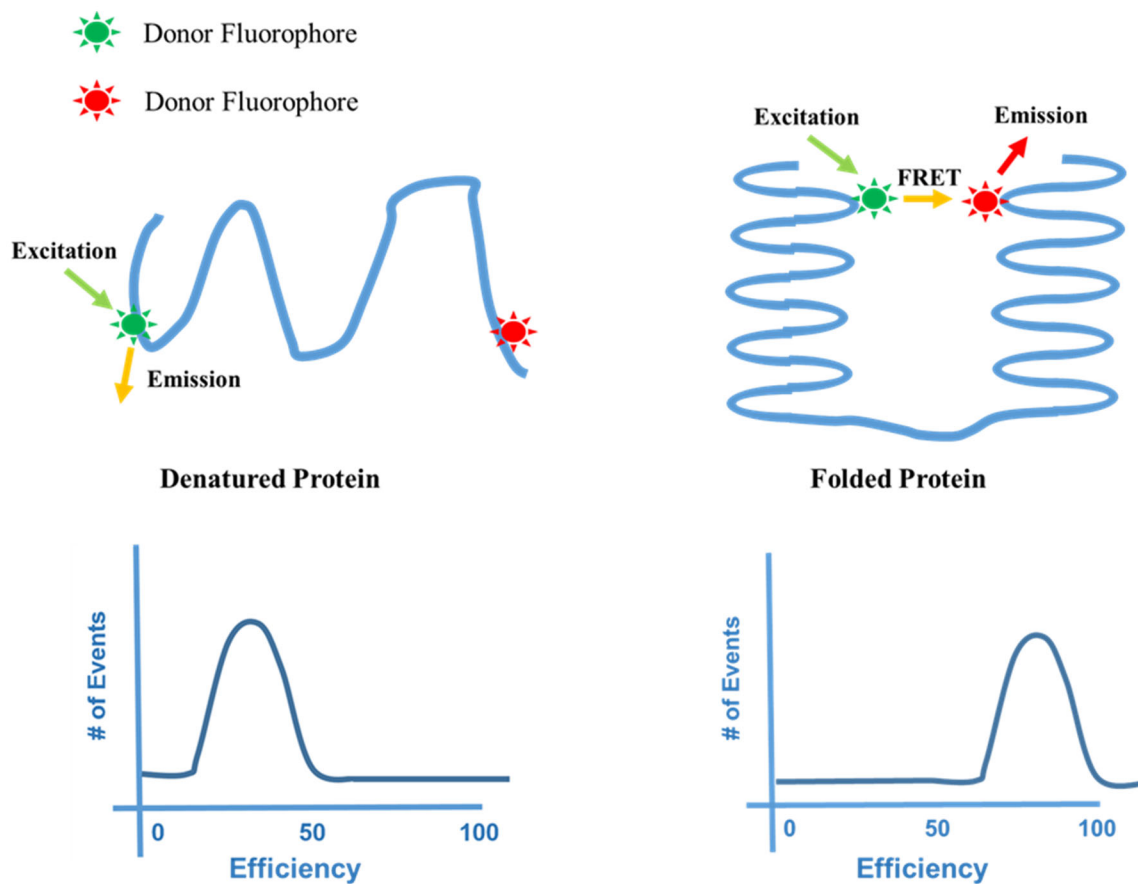
Figure 4.11: Cartoons Illustrating the Folding State of Protein and the Efficiency of FRET Events. When protein is denatured, low FRET efficiency events are observed. As protein is fully folded, high FRET efficiency events are seen.

A
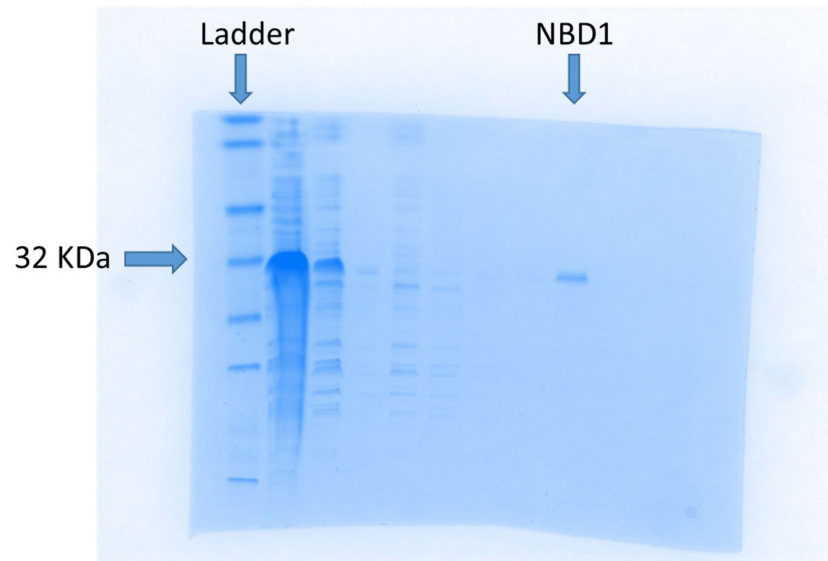
B
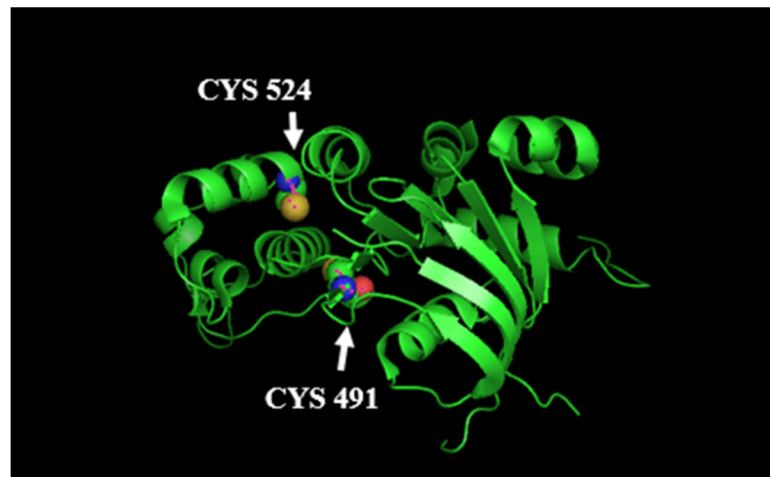
Figure 4.12: Wild-Type NBD1 Purification and Labeling. (A) Coomassie blue stain of wild-type CFTR-NBD1. (B) The structure of NBD1 and the position of the two cysteines. The structure is created from PBD 2BBO.

However, as the NBD1 molecules labeled with Cy3 and Cy5 diffused through the detection volume, only a low FRET efficiency protein population was observed (Figure 4.13). This result indicated that the NBD1 molecules were unfolded. To determine the reason for losing high FRET efficiency events, a positive control experiment was performed. Interleukin 1 beta (IL-1B) is a cytokine protein consisting of 157 amino acids. Previous studies showed that IL-1B remained fully folded after being isolated from *E. Coli*. In addition, IL-1B has two cysteines at position 8 and 71 and the distance between them is ~ 2 nm (Figure 4.14 A). Thus, IL-1B is perfect for being a positive control protein in this study. IL-1B with a His tag at the C-terminus was expressed in *E. Coli* BL21 (DE3) and purified using the same Ni-NTA Agarose (Figure 4.14 B). The FRET pair, Cy3 and Cy5, was utilized to label cysteines of IL-1B. High FRET efficiency events were observed (Figure 4.14 C), indicating the confocal microscopy system functioned well and the missing of high FRET efficiency events in the NBD1 experiment was caused by NBD1 losing its native structure.
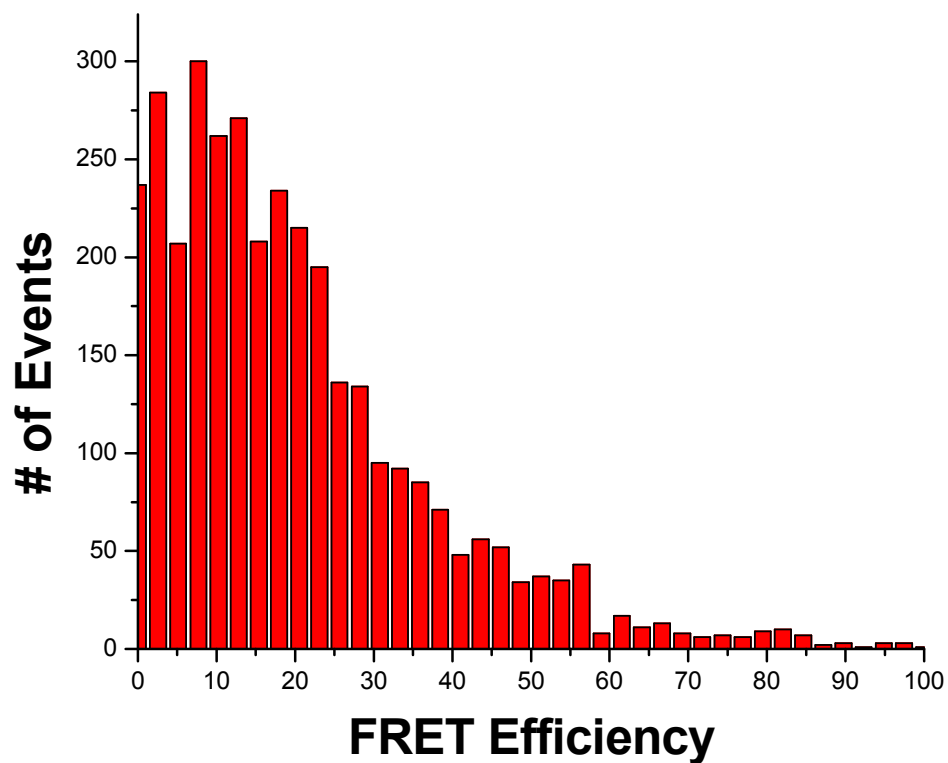
Figure 4.13: FRET Efficiency Histograms of NBD1. Only a low FRET efficiency NBD1 population is seen in this histogram.

A
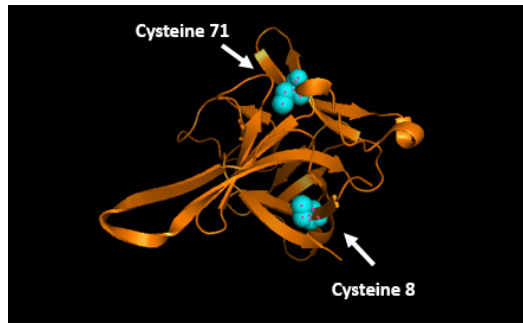
B
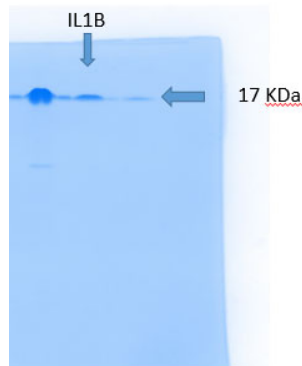
C
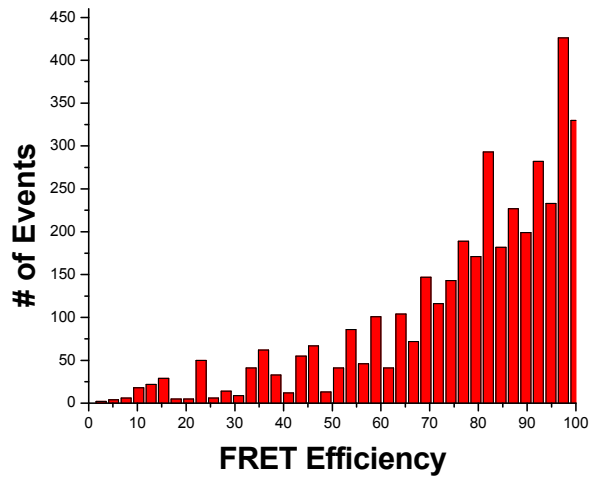
Figure 4.14: Interleukin 1 beta Structure and FRET Efficiency. (A) Structure of IL-1B and the positons of the two cysteines. The structure is created from PBD 3LTQ. (B) Coomassie blue stain of purified IL-1B. (C) FRET Efficiency Histograms of IL-1B. A high FRET efficiency IL-1B population is seen in this histogram.

To understand the reason for NBD1 unfolding, I utilized a different technique to further explore NBD1 structure. The secondary structure of NBD1 was determined by circular dichroism (CD) spectroscopy. I compared my CD data with published data from a previous CFTR-NBD1 publication wherein a similar NBD1 purification approach and CD spectroscopy protocol were utilized and the NBD1 molecules were assumed in their native folded state. The NBD1 sample was scanned from 195-260 nm. As seen in Figure 4.15, the CD spectroscopy curve I measured and the published CD curve have a positive band at 198 nm and two negative bands at 208 nm and 222 nm. In addition, the overall trend of the two curves is the same. This suggests that the purified NBD1 maintains its native secondary structure. Combined with the failure of seeing the expected high FRET efficiency NBD1 population, this indicates that the protein might not maintain its tertiary structure during the NBD1 purification process. A more thorough discussion of potential reasons for destabilized proteins is in chapter 5.

A
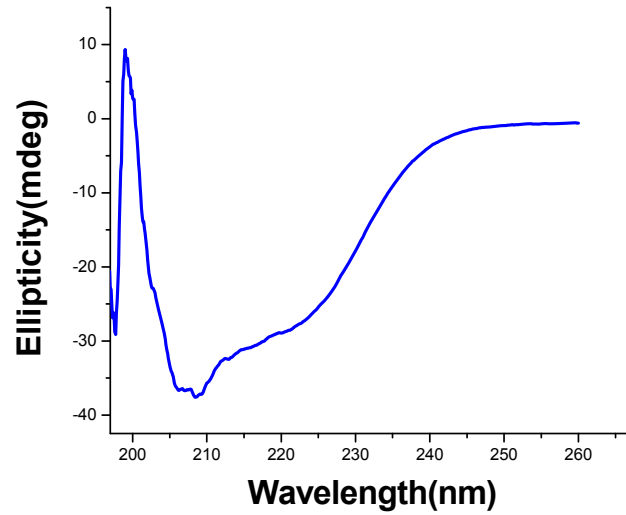
B
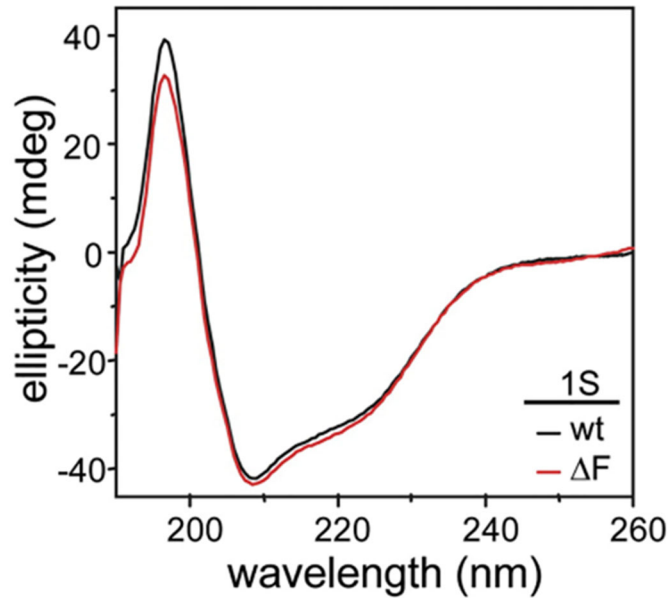
Figure 4.15: Comparison of the NBD1 CD Spectroscopy Data I Recorded with a Published One. (A): The wild-type NBD1 CD spectroscopy data I measured. (B): The NBD1 CD spectroscopy data from published literature (Reprinted with permission from Rabeh, Wael M, et al. *Cell* 148.1-2 (2012): 150-63.) This literature measured both wild-type and ΔF508 CFTR CD spectroscopy. We compared the wild-type NBD1 CD spectroscopy data in this same literature with the one I measured.

4.3 High Resolution Measurement of Membrane Protein Endocytosis

4.3.1   Principle of This Approach

We have developed a simple and straight-forward approach with high resolution to determine the half-life of protein on the plasma membrane using Dendra2. In response to 405 nm light, Dendra 2 undergoes irreversible photoconversion that alters the protein from emitting green light only to both green and red light when excited by the proper wavelength. Dendra2 is a stable and long-lived protein that does not alter the degradation of the fused protein[2]. Protein with Dendra2 tagged at the C-terminus was expressed in HEK 293T cells. We manually selected cells expressing membrane protein and photoconverted the population of protein residing on the cell membrane using TIRF oriented 405 nm light. As seen in Figure 2.8, a population of Dendra2 on the cell surface is fluoresces red after photoconversion. Then, real-time TIRF red fluorescence images were taken to monitor PM protein endocytosis. The endocytosis of Dendra2 tagged membrane protein causes the red fluorescence to decrease over time. Thus, the half-life of the protein on the PM is calculated by quantifying the decay in the red fluorescence over time. As proteins on the plasma membrane undergo endocytosis, newly synthesized proteins traffic to the plasma membrane at the same time. The new proteins have no influence on the monitoring of the red fluorescence since they are not photoconverted and exhibit green emission only. Figure 2.9 shows that cells were solely fluorescent in the green emission channel before being exposed to TIRF 405 nm light, and cells were fluorescent in both green and red emission channels after photoconversion. The green fluorescence intensity after photoconversion decreased compared with the pre-photoconversion intensity, which attributed to a fraction

of the population from green to red fluorophores (Figure 2.8). The representative images in Figure 2.9 B were selected from the time-lapse images, showing red fluorescence intensity decease over time. The quantified fluorescence intensity over time was plotted and fitted to an exponential equation to calculate the half-life of the PM protein.

4.3.2   Fluorescent Decay is not Caused by Lateral Diffusion

We used this approach to measure the half-life of the Epithelial Sodium Channel (ENaC) on the plasma membrane where time-lapse TIRF images were taken every 20 min. To verify that the loss of fluorescence intensity was due to endocytosis of the membrane protein rather than lateral diffusion along the cell surface, we performed control experiments with Dynasore, a small molecule dynamin inhibitor of GTPase activity which completely inhibits clathrin-mediated endocytosis in eukaryotic cells. Thus, any observed red fluorescence decay in the dynasore control experiment was caused by other sources such as diffusion of the protein along the cell surface outside of the TIRF field of view. As seen in Figure 4.16, a slight decay (less than 15%) is observed after 7 hours when α ENaC is treated with dynasore, indicating minimal loss of fluorescence due to diffusion or other sources. This indicates that the substantial fluorescence decay observed in the absence of dynasore can be attributed to endocytosis. Based on these studies, we assume that lateral diffusion has a negligible effect on the observed decrease in red fluorescence intensity.
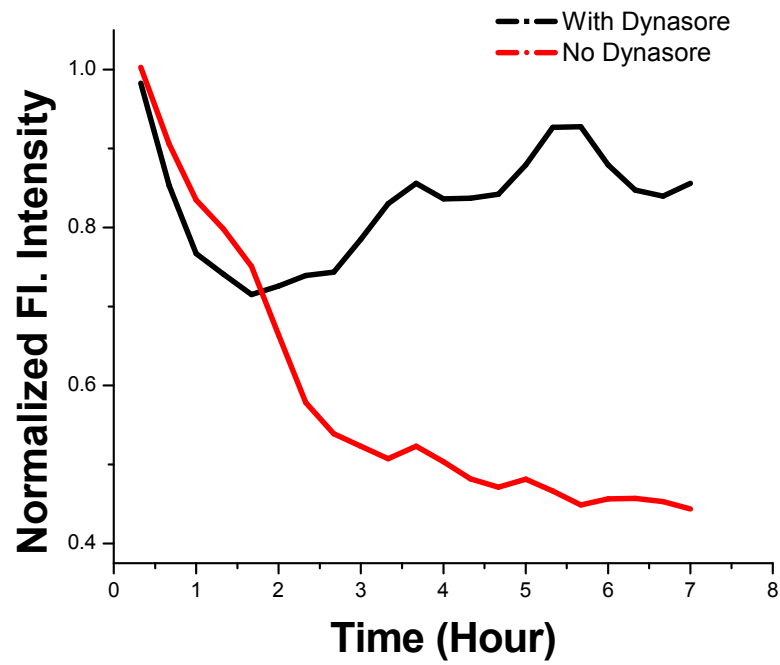
Figure 4.16: Compare Dynasore Treatment with Nondynasore Treatment A ENaC in Terms of Red Fluorescence Decay. Time course of red fluorescence intensity values of cells transfected with α ENaC -Dendra2 with or without Dynasore treatment. The values at time 0 were normalized.

4.3.3 Eliminating the Influence of Endosomes in the TIRF Field of View

The typical thickness of the plasma membrane is around 10 nm and the size of endosomes is in the range of 40-60 nm. TIRF allows us to illuminate fluorophores from the plasma membrane up to 150 nm. Thus, not only are the fluorophores on the plasma membrane illuminated, but also the endosomes. The fluorescent intensity of the TIRF images includes the fluorescence on the cell surface and the fluorescence from the endosomes. One concern was if the reduction in fluorescence in Figure 2.9 B was caused by the endosomes moving out of the evanescent field or by endocytosis. The final step of endocytosis is that a clathrin-coated pit must separate from the plasma membrane and move into the cytosol as a coated vesicle. Previous studies labeled fluorescent protein on the clathrin to observe the movement of single endosomes. Merrifield et al. tagged clathrin with DsRed in a Swiss 3T3 cell line and tracked the movement of single clathrin-coated pits under TIRF illumination and reported that the clathrin-coated structures significantly dimmed after 50 sec[138]. Another study showed similar results using AP2, an endocytic adaptor molecule which is colocalized with clathrin. Macro et al. labeled AP2 with GFP in *Dictyostelium*. They followed AP2 puncta for 10 minutes under the TIRF illumination. All puncta observed to appear on the surface disappeared within 6 minutes, with an average duration in the TIRF field of view of 56.3±4.2 seconds[139]. Merrifield et al. has examined *in vivo* clathrin does not uncoat the endosomes until the endosomes are separated from the plasma membrane by several hundred nanometers, which is far more than the depth of TIRF illumination[138]. Thus, the movement of clathrin or Ap2 represents the movement of cargo protein in the endosome.

In our study, we observed a dramatic fluorescence decrease minutes after the photoconversion. The fluorescence drop of the first 20 minutes is far bigger than that of the following 20 minutes time intervals. This is potentially caused by the disappearance of photoconverted protein in the endosomes. We observed the dot-like structures in the image taken right after photoconversion and the disappearance of them in the following images. This suggests photoconverted endosomes moving out of the TIRF field of view (Figure 4.17 A). To account for the loss of fluorescence by endosomes, we collected images with a 20 minutes delay after photoconversion. Previous studies showed that endosomes disappear from the evanescent field usually within 1-2 minutes after separation from the plasma membrane[138-141]. With this delay, all of the endosomes photoconverted in the TIRF field were gone from the following time-lapse images. Thus, the red fluorescence disappearance was caused by the endocytosis of protein on the cell surface. The half-life of protein was quantified by fitting the curve of fluorescence intensity over time to an exponential equation.
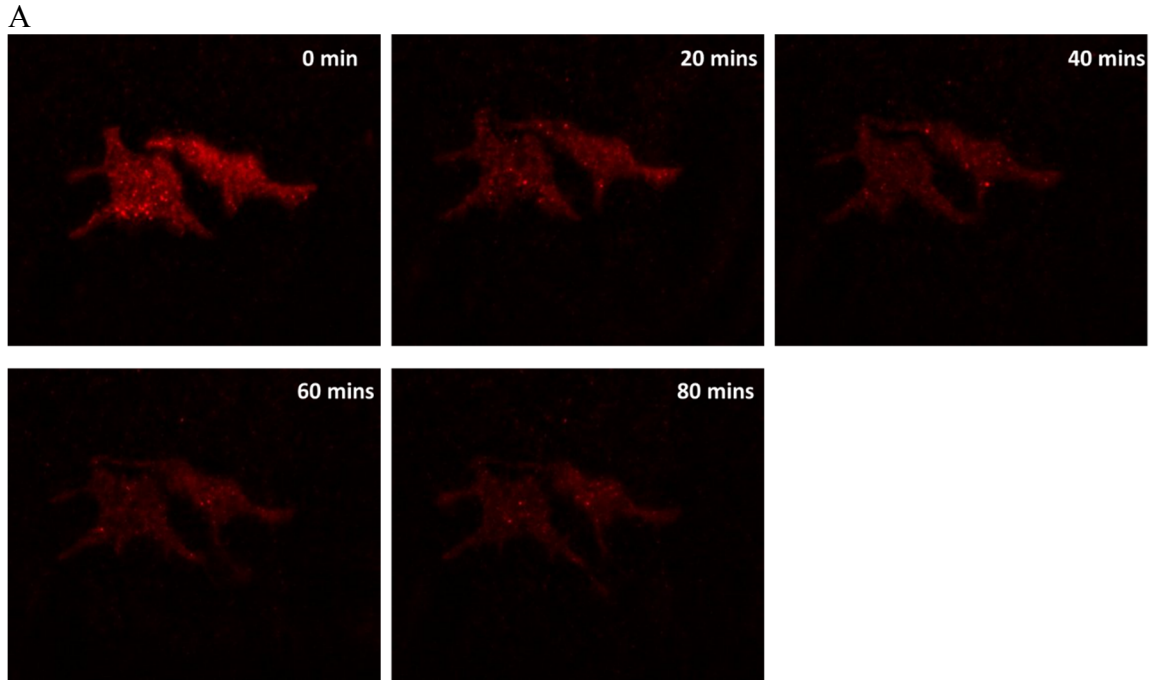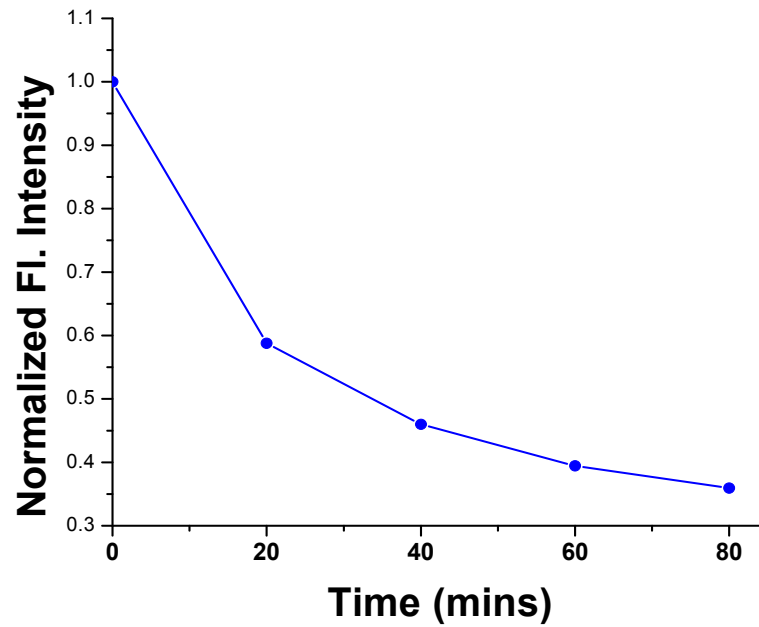
Figure 4.17: Red Fluorescence Drops Dramatically in the First 20 minutes. (A) Example of TIRF images taken at different time points for the same cell. (B) The fluorescence intensities of images in (A) are plotted in (B).

113

4.3.4   Half-Life of ENaC Subunits on the Plasma Membrane

Time-lapse images were taken for a total 7 hours with 20 minutes time intervals, meaning a single cell would be exposed to TIRF 561 nm light for 22 frames. Therefore, another factor we need to consider is the influence of photobleaching on the observed fluorescence intensity. A control experiment was performed to eliminate influence caused by laser induced photobleaching. In the control studies, a randomly selected cell was photoconverted by TIRF 405 nm; then 22 TIRF 561 nm images were acquired with a time interval of 1 sec. A ~10-20% fluorescence decay was usually observed in the 22 images (Figure 4.18), which is caused by the 561 nm light photobleaching as we assume protein endocytosis in this short time is negligible. Thus, it is necessary to remove photobleaching influence from the time-lapse images. The fluorescence integrated density of the control images was normalized with the first one assumed to be 1. The fluorescence intensities of each time-lapse image were divided by that of the corresponding number image in the control experiment. The new fluorescence intensities after correction were used for further data analysis.

We measured the plasma membrane half-life of α, β, and γ subunits on their own. The subunits on the PM exhibited similar half-life on the cell membrane where α, β, and γ gave a half-life of 1.52 h, 1.62 h and 1.49 h, respectively (Figure 4.19). However, when α, β, and γ subunits were expressed together, the half-life (2.41h) was significantly longer than that of those subunits on its own. A mutation in the PY motif (PPxY) of β subunit (β_{Y618A}) is connected with a heritage disease, Liddle's syndrome, which is caused by the longer residing time of ENaC on the cell membrane. The PY motif serves as the binding sites of

protein ubiquitin E3 ligase such as nedd4, which ubiquitylates the channel and promotes its endocytosis. The single mutation in the PY motif of the β subunit makes protein ubiquitin E3 ligase fail to bind to it and disrupts the following endocytosis and degradation. The β subunit had 1.62 h half-life on the PM, while the Y618A mutant increased the half-life to 3.58 h. We also compared the half-life when α and γ were expressed with the mutant β. Though a statistically significant increase in the residence time on the cell surface was seen, the presence of the other subunits compensated for the effect of the mutation. The half-life of $\alpha\beta_{Y618A}\gamma$ was 2.97 h, and the half-life of $\alpha\beta\gamma$ was 2.41 h. Figure 4.19 A is the plots of red fluorescence intensity values over time. The half-life calculated in Figure 4.19 B was based on the red fluorescence decay curves of Figure 4.19 A.
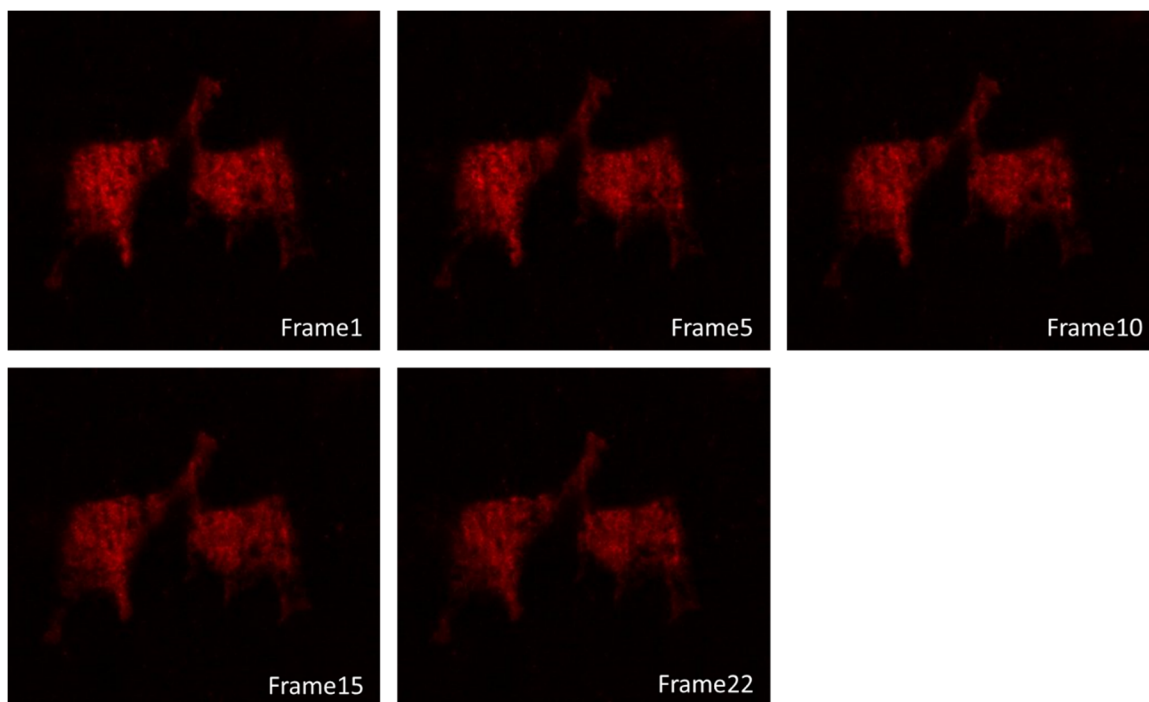
Figure 4.18: Representative TIRF Images of Photobleaching Control Experiment. The control TIRF Images are taken with a 1 second time interval. ~10-20% intensity decay is usually observed due to the photobleaching caused by the 561 nm laser. In the representative images, a 19% fluorescent intensity decay is seen in frame 22.

A
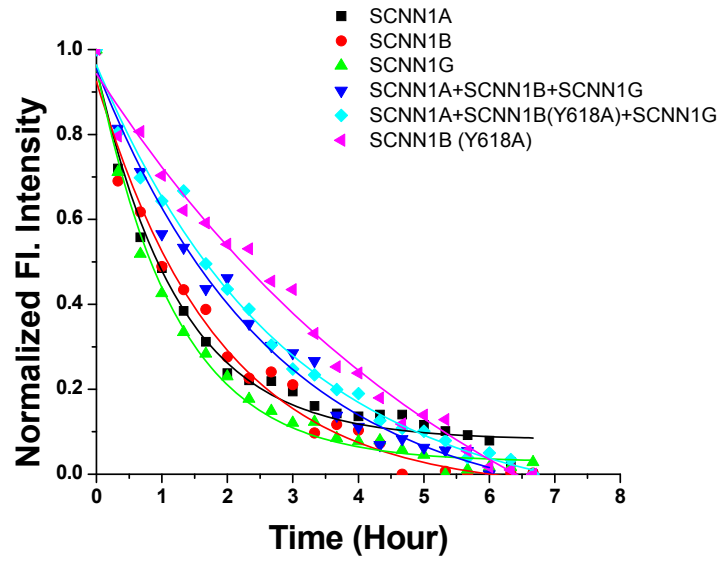
B
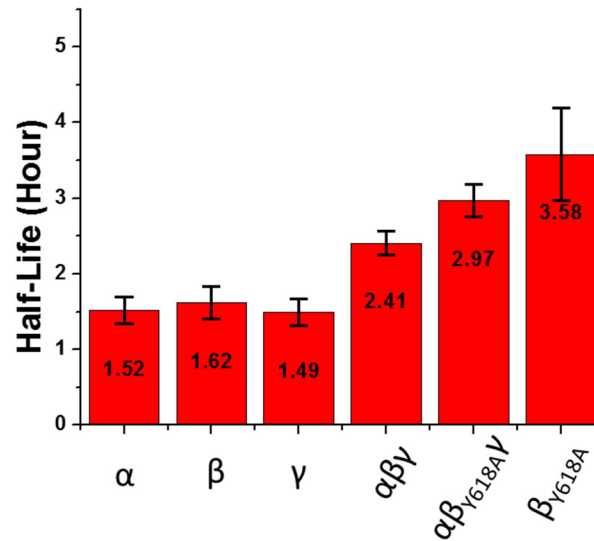
Figure 4.19: Half-Life of ENaC Subunits on the Plasma Membrane. (A) Time course of red fluorescence intensity values of cells transfected with Dendra2 labeled different ENaC subunit(s). Values were fitted to a single exponential equation and the values at time 0 were normalized. (B) Bar diagram of ENaC subunits half-life. Values are average ± SE (10-15 cells were measured for each experiment). Two tails t-tests (P=0.05) were performed with unequal variance assumed.

4.3.5 Both Wild-Type CFTR and ΔF508 CFTR do not Alter ENaC Half-Life

Previous studies showed that the cystic fibrosis transmembrane regulator (CFTR) interacted through scaffold proteins to indirectly regulate ENaC. Inhibited ENaC function was seen in the presence of CFTR. One hypothesis contends presence of CFTR may alter the residence time of ENaC on the cell surface. Thus, we measured the half-life of ENaC in the presence of wild-type CFTR and in the presence of a CFTR mutation (ΔF508) that prevented it from reaching the cell surface. CFTR wild-type or ΔF508 were co-transfected with ENaC in HEK 293T cells. As shown in Figure 4.20, the half-lives of the α subunit with CFTR WT and CFTR ΔF508 were 1.49 h, 1.54 h, respectively, which were not significantly different from that of the α subunit on its own (1.52 h). We also measured the half-lives of αβγ with CFTR wild-type (2.11 h) and CFTR ΔF508 (2.56 h). These results were not significantly different from that of αβγ (2.41 h) as well (Figure 4.21). This indicates that the bridging scaffold proteins between CFTR and ENaC do not sense the loss of CFTR by influencing the residence time of ENaC on the cell surface. The time course of red fluorescence intensity values of the cells expressing Dendra2 labeled ENaC subunit(s) with or without CFTR are also shown in Figure 4.20 A and Figure 4.21 A.

A
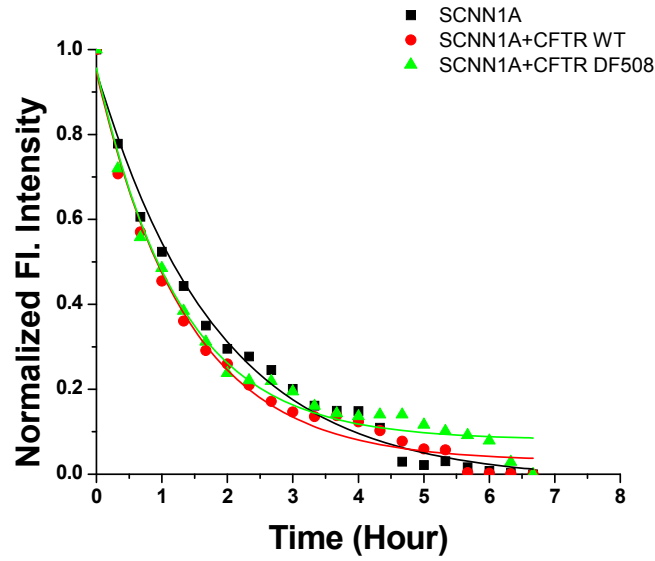
B
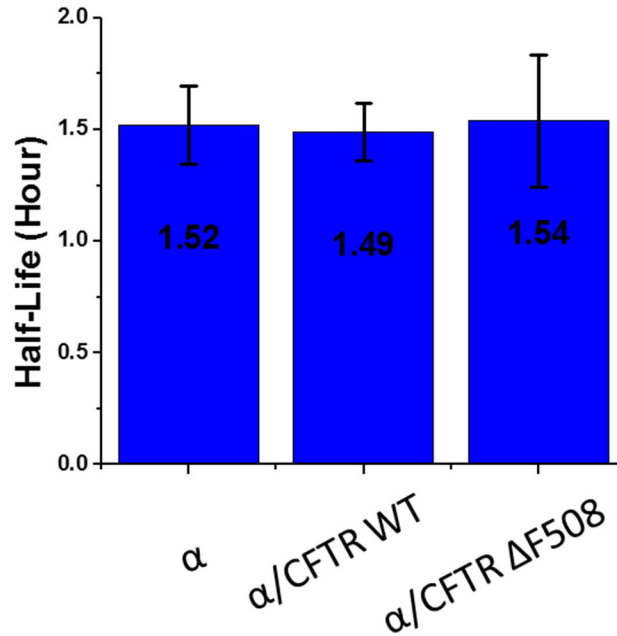
Figure 4.20: Half-Life of α Subunit on the Plasma Membrane in the Presence of Wild-Type CFTR or ΔF508 CFTR. (A) Time course of red fluorescence intensity values of cells expressing Dendra2 labeled α subunit with or without CFTR. Values were fitted to a single exponential equation and the values at time 0 were normalized. (B) Bar diagram of α Subunit half-life with or without CFTR. Values are average ± SE (10-15 cells were measured for each experiment). Two tails t-tests (P=0.05) were performed with unequal variance assumed.

A
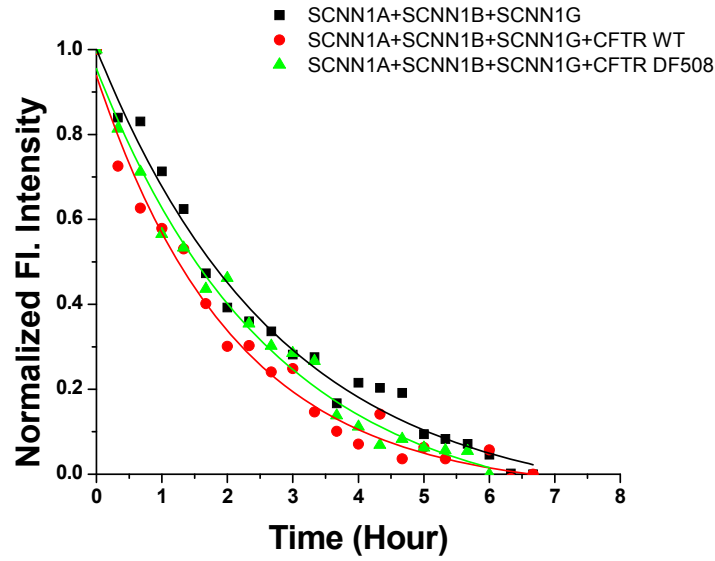
B
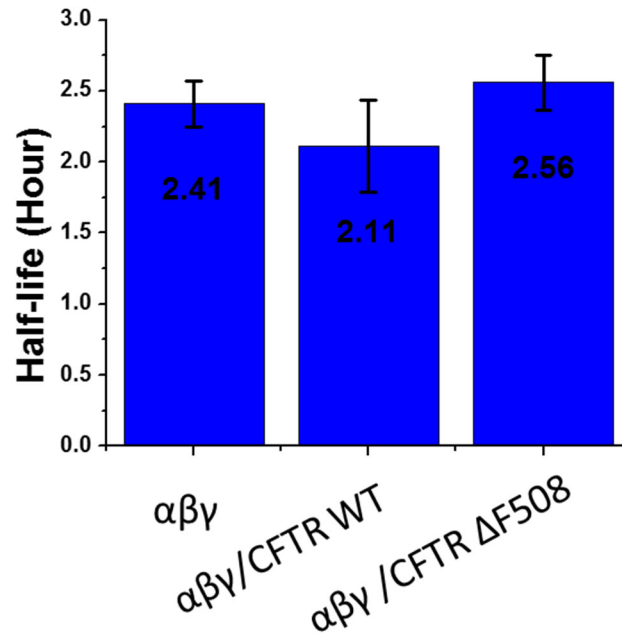
Figure 4.21: Half-Life of αβγ ENaC on the Plasma Membrane in the Presence of Wild-Type CFTR or ΔF508 CFTR. (A) Time course of red fluorescence intensity values of cells expressing Dendra2 labeled αβγ ENaC with or without CFTR. Values were fitted to a single exponential equation and the values at time 0 were normalized. (B) Bar diagram of αβγ ENaC half-life with or without CFTR. Values are average ± SE (10-15 cells were measured for each experiment). Two tails t-tests (P=0.05) were performed with unequal variance assumed.

CHAPTER 5: DISCUSSION AND CONCLUSIONS

5.1 Correctors Alter Expression and Trafficking of CFTR

Recent studies have suggested that multiple therapeutics that target different CFTR domains may be used in combination to correct ΔF508-CFTR trafficking and function[43, 142]. Previous work has primarily focused on the use of chaperones that can increase protein trafficking out of the ER in combination with sensitizers that improve ion channel function at the plasma membrane. Much remains to be understood, however, as to the mechanistic details of these chemical chaperones. Most reports have primarily hypothesized that the compounds act by stabilizing CFTR at different domains or domain-domain interfaces.

The work presented here suggests that therapeutic small molecules that could stabilize ΔF508-CFTR in the ER, interrupting protein degradation, could be used in combination with a second compound that facilitates transport out of the ER. The first compound in effect would mimic the mechanism that provides the stability conferred by I539T and low temperatures. There are thus two distinct mechanisms to improve levels of CFTR on the plasma membrane.

5.1.1 VX-809 Works Synergistically with Temperature and a Second Site Suppressor to Traffic ΔF508-CFTR

In this study we performed real-time experiments to determine the cellular distribution, trafficking rates, and action of CFTR in the presence of the corrector molecule, VX-809,

alone and in combination with conditions known to stabilize ΔF508-CFTR. Using TIRF, we measured the distribution of CFTR between the PM and the peripheral ER, and clearly showed that 75% of wild-type CFTR was present on the PM and very little was located in the peripheral ER. We were unable to detect any ΔF508-CFTR at 37 °C on the PM, indicating that all of the protein was in the ER. We did observe clear temperature dependent changes in PM ΔF508-CFTR and ΔF508-CFTR containing the second site suppressor mutation. In both cases, approximately 30% of the protein visible in TIRF was located on the PM. This suggests that these conditions are able to stabilize the protein, protecting it from degradation and moderately shifting distribution to the cell surface.

The TIRF measurement was restricted to protein within 200 nm of the cell surface, so does not represent total protein within the cell. It does, however, demonstrate large differences in distribution between the peripheral ER and PM for wild-type and mutant CFTR. Traditionally, comparison of core glycosylated and complex glycosylated protein via western blot has been used to determine distributions between protein in the ER and protein that has trafficked out of the ER. However, complex glycosylation does not mean that the protein has been inserted into the plasma membrane. The PM insertion was directly visualized by utilizing SEP emission in this study.

Electrophysiology measurements of CFTR function compare fully functional wild-type and defective CFTR, which has been shown to exhibit temperature dependent functional properties. In contrast to individual channel function measurements, the trafficking studies presented here directly quantify protein populations. In the presence of VX-809, a clear shift of the protein from the ER to the PM was observed for low temperature ΔF508 and

ΔF508/I539T, with approximately 60% of the visible protein on the cell surface. This suggests that low temperature and second site suppressors are capable of creating an export-ready pool of CFTR in the ER that VX-809 can act on. This export-ready pool is likely to be more stable, but not stable enough for ER export without VX-809[52].

In our studies it appears that VX-809 acts synergistically with other stabilizing conditions, increasing the amount of PM protein from less than 10% to 40% of wild-type levels. At 37 °C, VX-809 results in approximately 10% of wild-type levels of protein on the cell surface. In the absence of VX-809, low temperatures led to 5-10% of wild-type levels. If these effects were additive, we would expect to see 15-20% of wild-type levels. This study is the first to report on the synergistic activity of the second site mutation (I539T), and further, provides an imaging approach to directly measure protein populations in different sub-cellular locals. The disparity between this finding and previous measurements using electrophysiology and western blots which showed additive effects is likely because these prior reports were not directly measuring the amount of cell surface protein.

We also examined the total amount of protein on the cell surface for several other conditions. Similar to studies by other groups, our data showed that at 37 °C VX-809 increased the trafficking of ΔF508-CFTR to approximately 10% of wild-type levels. When we reduced the temperature (30 °C) to stabilize the protein through thermal effects, we observed approximately 10% of wild-type levels. The biochemical approach to stabilization using ΔF508/I539T yielded similar levels (10% of wild-type) at 37 °C. However, we saw a marked increase in the level of mutant CFTR at the surface when either of the stabilizing conditions (reduced temperature or I539T) was combined with VX-809.

Interestingly, the combination of low temperature and the I539T mutation did not alter the levels of ΔF508 beyond what was seen separately with low temperature or the secondary mutation. These results suggest that the second site mutation and lowered temperature work via the same mechanism and each induces a maximal effect, while the chemical chaperone functions through a complementary process.

The lack of temperature correction for ΔF508/I539T suggests that low temperature assists the protein to adopt a similar, partially stable conformation as seen with I539T. In contrast, the ΔF508 defect appears to be partially restored through manipulation of temperature. A synergistic increase in PM ΔF508-CFTR occurred when temperature manipulation or the second site suppressor mutation were combined with VX-809. Combined with the subcellular distribution measurements, this again points to a mechanism where VX-809 could be acting on a stabilized pool of CFTR that is protected from degradation, but unable to traffic efficiently in the absence of a chemical chaperone. This is supported by our observation that for both the second site suppressor and low temperature that in the presence of VX-809 the distribution of CFTR shifts significantly toward the plasma membrane. In the absence of the compound 25-30% of CFTR is on the plasma membrane within in our assay. In the presence of compound this shifts to 55-60% indicating a release of protein from the ER to the plasma membrane.

In order to determine the distribution of the stabilized ΔF508-CFTR, we also quantified the amount of ΔF508-CFTR in the vesicles and the Golgi complex, where SEPs are not visible in the pH studies. The integrated density (ID) of CFTR in the vesicles was quantified by measuring the difference between ID measured in the presence and absence of NH_4^+.

This experiments were performed for HEK 293T cells expressing I539T/ΔF508-CFTR. I539T/ΔF508-CFTR showed an approximately 10-fold vesicle ID increase compared to wild-type CFTR, which corresponded to 10 times the amount of wild-type CFTR in the vesicles. This further supports the hypothesis we made that the second site suppressor I539T stabilizes ΔF508-CFTR in ER. Furthermore, the stabilized ΔF508-CFTR is not only located in ER, but also in the trafficking vesicles. Now it is clear that a large population of ΔF508-CFTR stabilized by the second site suppressor I539T is located in the Golgi complex and the trafficking vesicles, while the stabilized ΔF508-CFTRs fail to reach the cell membrane.

5.1.2   The Immunomodulatory Mechanism of AZM is Different from That of Either

Reduced Temperature or VX-809

Azithromycin (AZM) is a macrolide antibiotic, which was initially used to treat inflammation for CF patients. Later, it was reported that azithromycin had both immunomodulatory and anti-inflammatory properties that were able to reduce the lung damage associated with CF. In this dissertation, the influences of AZM on CFTR distribution and cell surface expression were quantified using TIRF microscopy. AZM shifted I539T/ΔF508-CFTR distribution from the ER to the PM and improved I539T/ΔF508-CFTR cell surface expression. However, when AZM was combined with the reduced temperature or VX-809, the conjugated treatment did not alter I539T/ΔF508-CFTR distribution or cell surface expression compared to reduced temperature or VX-809 on its own. As we have seen in our previous results, I539T/ΔF508-CFTR is stabilized in the reduced temperature condition and thus additional trafficking promotors like VX-809

strongly facilitate I539T/ΔF508-CFTR traffic from the ER to the cell surface. However, in the AZM study, the improvement caused by AZM is not addable with that resulted from reduced temperature. Hence, we infer that AZM does not promote the trafficking of I539T/ΔF508-CFTR to the cell surface. On the other hand, when I539T/ΔF508-CFTR was treated with a trafficking promotor VX-809, the additional AZM did not make significant changes in I539T/ΔF508-CFTR distribution and cell surface expression. Therefore, AZM is not capable of stabilizing I539T/ΔF508-CFTR in ER, either. Similar observations were seen when ΔF508-CFTR was treated with AZM. The immunomodulatory mechanism of AZM is different from that of either reduced temperature or VX-809.

5.1.3 No Additional Influence of VX-770 on ΔF508-CFTR Observed

The FDA approved drug VX-770 is a CFTR potentiator, which has been known to facilitate CFTR channel activities by directly binding to the channel to induce a non-conventional mode of gating which increases the channel open probability[68, 70-71]. Now it is used combined with VX-809 for the treatment of CF patients with the ΔF508 mutation. In this study, the effect of VX-770 on CFTR distribution and cell surface expression was quantified using TIRF microscopy. VX-770 neither altered VX-809 corrected ΔF508-CFTR distribution nor cell surface expression. Similarly, no statistical change was seen in the AZM corrected ΔF508-CFTR distribution or cell surface expression in the presence or absence of VX-770. No influence of VX-770 on CFTR trafficking was observed. Hence, VX-770 is only known to promote CFTR channel activities.

5.1.4   A Range of Temperatures Stabilize ΔF508-CFTR and are Differentially Affected

by VX-809

While standard low temperature experiments with ΔF508-CFTR use 27 °C, we found that

intermediate temperatures between 27 °C and 37 °C were as good or better at stabilizing

the mutant protein. While at 37 °C we observed no detectable ΔF508-CFTR on the PM,

just a 3 °C reduction in the temperature results in the detection of 10% of wild-type levels.

Lower temperatures (27-32 °C) did not further improve trafficking. This suggests that a

moderate change in temperature is sufficient to stabilize mutant CFTR to assume a

conformation that is partially export-ready, and that further reduction in temperature does

not assist the protein in assuming a more stable conformation or does not increase the pool

of mutant CFTR that obtains a stable conformation. Thus, increasing stability by reducing

the temperature to 34 °C represents a thermodynamic plateau.

The addition of VX-809 also showed that intermediate temperatures were superior for the

synergistic effect of temperature and drug to 27 °C. A 2 to 4 °C reduction in temperature

yielded an increase to roughly 10% of wild-type in the absence of the compound, but when

the compound was added these same temperatures yielded near 40% of wild-type. The

same conditions at 27 °C showed less than 30% of wild-type. The results were even more

striking for I539T/ΔF508-CFTR. This further supports the idea that reduced temperature

or second site suppressor mutations result in a high degree of stabilization, but little

trafficking.

5.1.5   Changes in PM CFTR Levels are Related to Differences in Trafficking Rates

Increases in cell surface numbers could result from changes in trafficking or from changes in residence time on the plasma membrane. To differentiate these two possible mechanisms, we performed a set of experiments to quantify the arrival of CFTR to the cell surface. We quantified trafficking rates by counting the number of insertion events and determined the number of channels in vesicles by the average emission intensity. Figure 4B shows that wild-type CFTR traffics at roughly twice the rate seen for ΔF508/I539T in the presence of VX-809. This matches the differences observed in surface protein levels, suggesting that I539T and VX-809 alter surface levels by increasing trafficking rates. This may be due to an increase in the percentage of stable protein that is trafficking ready.

Overall, these studies show that certain conditions that stabilize ΔF508-CFTR, specifically low temperature or the introduction of a secondary mutation, result in an increase in the population of protein that can be corrected by VX-809, resulting in higher levels of CFTR at the PM than the sum of the conditions alone. This is consistent with a mechanism where low temperature or key mutations increases a stable pool of ΔF508-CFTR in the ER that is more resistant to degradation but not fully export-ready. The interaction of VX-809 with this stable pool leads to the synergistic effects observed in these studies. As seen in recent clinical trials, existing therapeutics such as VX-809 can partially correct the trafficking of ΔF508-CFTR, but on their own are not sufficient to eliminate the majority of CF symptoms. However, therapeutics that could achieve the levels of correction seen with the combination of I539T and VX-809 in this study would be sufficient to eliminate the majority of CF related symptoms[143]. This suggests that a 2 step therapeutic approach might

be an ideal treatment for CF. The first step would be composed of a compound that mimics the mechanism of stabilization provided by low temperature or the I539T mutation, while the second step would be VX-809 or a similar corrector compound. These studies suggest that understanding how low temperature and second site suppressors alter ΔF508-CFTR could be key to the development of future therapeutics for the effective treatment of CF.

5.2 Single-Molecule FRET to Study NBD1 Structure

The fundamental cause of ΔF508 related cystic fibrosis is that the deletion of phenylalanine in position 508 affects the proper folding of CFTR and alters its stability. Understanding the detailed wild-type CFTR folding and ΔF508-CFTR misfolding actions will be greatly beneficial to the development of CF therapies. Single molecule techniques offer new access to information unavailable from bulk measurements such that it is capable of providing dynamic information at the single molecule resolution. By combining fluorescence correlation spectroscopy (FCS) with single molecule techniques, it is not necessary to immobilize protein molecules on a glass surface, which is required for TIRF-single molecule measurement with the downside of altering the native properties of protein molecules. Whereas, protein molecules can diffuse freely in solution in the FCS-single molecule study with no external force. Therefore, the native properties of protein molecules are best maintained.

Previous CFTR studies usually monitored CFTR in cells, which provided essential information for CFTR expression, distribution, channel activities and degradation. Protein in cells maintains its native properties and exhibits real response to external stimuli.

However, in that case, measurements can only be taken at single cell resolution. Single molecule studies require the isolation of protein molecules from the cell. The isolated molecules provide more straight forward responses upon external stimuli. The single molecule NBD1 project goal was to directly collect structural information from isolated NBD1. In this study, NBD1 molecules were tagged with a FRET pair Cy3 and Cy5 on the sites of two cysteines. As the protein is denatured, the distance between the two fluorophores is not in the FRET distance range (1-10nm)[99, 105]. As a result, the energy transfer between the FRET pair is not efficient, and thus only low FRET efficiency events are observed. With the protein fully folded, the two-fluorophore distance is reduced and high FRET efficiency events are observed. As a single protein molecule labeled with a FRET pair freely diffuses through the detection volume of confocal microscopy, a single fluorescent burst is captured and gives rise to a FRET efficiency, E. Thousands of fluorescent bursts are accumulated and a histogram of efficiencies of those FRET events is plotted resolving the folded and unfolded protein subpopulations.

However, only low FRET efficiency events were observed in my study, suggesting NBD1 molecules failed to maintain its tertiary structure. To determine the reason of losing high FRET efficiency events, a positive control experiment with interleukin 1 beta (IL-1B) was performed. IL-1B is a cytokine protein consisting of 157 amino acids and it is capable of maintaining its fully folded structure in the isolated condition. In addition, the existence of two cysteines in IL-1B makes it a perfect protein for the positive control experiment. IL-1B showed a high FRET efficiency population, which demonstrated the confocal microscopy system functioned well. Thus, the low FRET efficiency population we saw in the NBD1 study indicated the NBD1 molecules were unfolded. The reason could be: (1)

other CFTR domains are required to initiate NBD1 folding or to maintain its fully folded state; (2) the protein purification protocol I used may not be ideal for NBD1 isolation.

The presence of other CFTR domains might be required for NBD1 folding. Previous CFTR studies had successfully purified the whole human CFTR and zebrafish CFTR[57, 144-145]. The channel function of isolated whole CFTR was verified, which demonstrated that the whole CFTR was capable of maintaining its folded state in the isolated condition[144]. It has been demonstrated that domain-domain interactions are essential for CFTR folding. The deletion of phenylalanine at position 508 disrupts the proper interactions as Phe508 provides hydrophobic contacts for domain-domain interactions that are indispensable for stabilization of CFTR[146]. As the CFTR single domain study is very limited so far, it is still obscure if the existence of other CFTR domains is demanded for the proper NBD1 folding or maintaining its folded state. Further CFTR domain interactions information is necessary to answer the question, which provides a direction for the future CFTR research.

There is another possibility that NBD1 was fully folded in *E Coli* but lost its native conformation during the protein purification process. The NBD1 purification protocol was reproduced from a previous publication (Rabeh, Wael M, et al. *Cell* 148.1-2 (2012): 150-63.). I compared my circular dichroism (CD) data with a published CD curve wherein a similar NBD1 purification approach and CD spectroscopy protocol were utilized and the NBD1 molecules were assumed in their native folded state. The two CD curves both exhibited a positive band at 198 nm and two negative bands at 208 and 222 nm. In addition, the overall trend of the two curves were the same. If the CD data in that publication revealed NBD1's native secondary structure, it was reasonable to claim that the NBD1 in my study

maintained its secondary structure. That literature, however, neither showed the tertiary structure of the isolated NBD1 nor demonstrated its folding state. Thus, there is a possibity that the isolated NBD1 they measued lost its folded state during the purfication process. Since we cannot validate the realiblity of the NBD1 purfication protocal, it is possible to be the reason causing NBD1 unfolding. The NBD1 purification protocol might need to be modified to stabilize NBD1 and maintain its native state.

5.3 High Resolution Measurement of Membrane Protein Endocytosis

The precise pathology of cystic fibrosis is not well studied with many unanswered questions. The involvement of another transport protein, epithelial sodium channel (ENaC), makes the situation more complicated. ENaC and CFTR are colocalized on the apical surface of epithelia cells and have tissue specific functional interactions. The presence of CFTR reduced the Na^+ current in the airways, while it increased ENaC-mediated sodium transport in the sweat duct[147-149]. In addition, when CFTR and ENaC were co-expressed in oocytes cells, reduced functional expression of ENaC was observed even before activation of CFTR[150]. Therefore, the CFTR-ENaC interaction is an interesting topic to study. Previous studies mostly showed the presence of CFTR altered the channel activities of ENaC. With our fluorescence microscopy techniques, we would like to explore the effects of CFTR on the residence time of ENaC on the cell membrane. The approaches currently used to determine protein half-life showed discrepant measured ENaC half-lives. Yu et al did single-channel analysis of ENaC to quantify the half-life of ENaC and reported that the average half-life of ENaC in CHX-treated cells was 1.45 ± 0.24 h, while it was 3.28 ± 0.89 h with the puromycine treatment [125]. Additionally, these techniques suffer from

low temporal resolution of membrane protein half-life and can be low throughput. Therefore, an approach with high temporal resolution is highly needed.

We developed a new approach to quantify the half-life of protein on the cell surface, through labeling the protein with the photoconvertible fluorescent protein, Dendra2. Previous studies demonstrated the application of Dendra2 to study the protein degradation in the cytoplasm utilizing confocal microscope [151]. However, it could not be applied to study protein on the plasma membrane due to the confocal microscopy visualization limitation. In this dissertation, we extended the application of Dendra2 to monitor protein on the plasma membrane by utilizing TIRF microscopy, which makes it possible to limit the visualization to a narrow region near the plasma membrane.

Using this approach, we measured the half-life of different ENaC subunits and mutations. Typically, ENaC on the cell membrane turns over rapidly, with a reported half-life of ~40-120 min in cultured cells [152-155]. The half-life we measured for ENaC α, β, γ subunits were 1.52 h, 1.62 h, and 1.49 h, respectively, indicating near identical stability on the plasma membrane. When α, β, γ subunits coexpressed together, the half-life increased to ~2.41h. The heterotrimic ENaC structure exhibited increased stability on the plasma membrane compared with homo trimer. Additionally, it has been reported that the mutation in the PY motif of β subunit results in a longer half-life on the membrane [156]. Our observations were consistent with this. The 3.58 h half-life of βY618A was more than two-fold of that of β wild-type. However, the residence time of α, γ subunits coexpressing with βY618A (~2.97h) was just slightly longer than that of α, γ subunits with wild-type β subunit (~2.41h). In a homo trimer, the mutation is sufficient to disrupt interactions with cellular machinery responsible

for the endocytosis of ENaC, while the presence of the other subunits appears to compensate for the effect of the mutation.

To determine the influence of CFTR on the half-life of ENaC subunits, we also measured the half-lives in the presence of CFTR WT or ΔF508. The half-life we measured for ENaC α in the presence of CFTR WT and ΔF508 were 1.49 h, and 1.54 h, which were not statistically different from that of α ENaC subunit alone (1.52 h). Similar results were seen for the co-expressed α, β, γ subunits that the presence of wild-type or ΔF508 CFTR did not alter the half-life of α, β, γ heterotrimer ENaC. The presence of CFTR has influences on the channel activities of ENaC, while, it fails to alter the half-life of ENaC on the cell membrane. As the CFTR-ENaC interaction mechanism is still not fully understood, future studies could be developed to determine if the changing of ENaC function in the presence of CFTR is caused by changes of ENaC trafficking and cell surface expression, which can be studied using the SEP pH approach.

Although the CFTR-ENaC interaction is not resolved, apparent advantages of the proposed methods should be noted. This approach has a simple and straight forward experimental procedure. Time-lapse images of individual cells were automatically taken with a program set up, which not only saved time but also made it possible to take as many as data points(images) as needed. The currently used techniques such as biotinylation-western blotting, radioactive pulse-chase and electrophysiology approach have complicated experimental procedures, which limits number of data points taken and thus limits the temporal resolution. Hence, our method has a much higher temporal resolution compared to the current approaches. On the other hand, we avoid the errors caused by compounds

that may alter cellular metabolism. Protein translation inhibitor or trafficking inhibitor is required in the electrophysiology related approaches. The additional compounds may strongly affect cellular metabolism and have influences on the protein half-life measurement. In contrast, our technique does not require them, and avoids the errors caused by that. Our method provides a unique opportunity to observe real-time protein turnover at the single cell level without addition of protein synthesis inhibitors. This technique will be extremely valuable for studying the protein half-life on the cell membrane.

The work in this dissertation provides strong evidence for a synergistic effect of VX-809 with either reduced temperature or the second site suppressor I539T. The increase in the population of CFTR on the cell surface is not sufficient to eliminate the majority of CF related symptoms when ΔF508-CFTR is treated with VX-809, reduced temperature or I539T alone. However, the levels of correction seen with the combination of I539T and VX-809 in this study would be adequate for the CF symptoms elimination. Therefore, we proposed a two steps therapeutic approach that the first step would be a compound that mimicked the mechanism of stabilization provided by low temperature or the I539T mutation, and the second step would be VX-809 or a similar corrector compound. This proposed approach provides a direction for the future CF drug development. Further CF research could focus on the mechanism of reduced temperature and I539T, as well as screening compounds that mimic the mechanism of reduced temperature or I539T.

In this dissertation, we also developed a new method to measure the half-life of protein on the cell membrane with less labor intense but much higher temporal resolution. It changes

the situation that all half-life measurements suffer from low temporal resolution and are even influenced by the errors resulting from additional compounds. Our method can be expanded to a variety of classes of membrane proteins. For instance, this technique can be employed to study the stability of CFTR on the cell surface. Ideally, this technique will impact research related to any membrane protein half-life studies.

REFERENCES

1. Revyakin, A.; Liu, C.; Ebright, R. H.; Strick, T. R., Abortive initiation and productive initiation by RNA polymerase involve DNA scrunching. *Science* **2006,** *314* (5802), 1139-1143.

2. Hodges, C.; Bintu, L.; Lubkowska, L.; Kashlev, M.; Bustamante, C., Nucleosomal fluctuations govern the transcription dynamics of RNA polymerase II. *Science* **2009,** *325* (5940), 626-628.

3. Mandal, S. S.; Chu, C.; Wada, T.; Handa, H.; Shatkin, A. J.; Reinberg, D., Functional interactions of RNA-capping enzyme with factors that positively and negatively regulate promoter escape by RNA polymerase II. *Proc. Natl. Acad. Sci. U. S. A.* **2004,** *101* (20), 7572-7577.

4. Raffaelle, M.; Kanin, E. I.; Vogt, J.; Burgess, R. R.; Ansari, A. Z., Holoenzyme switching and stochastic release of sigma factors from RNA polymerase in vivo. *Molecular cell* **2005,** *20* (3), 357-366.

5. Lykke-Andersen, S.; Jensen, T. H., Overlapping pathways dictate termination of RNA polymerase II transcription. *Biochimie* **2007,** *89* (10), 1177-1182.

6. Richardson, J. P., Rho-dependent termination and ATPases in transcript termination. *Biochimica et Biophysica Acta (BBA)-Gene Structure and Expression* **2002,** *1577* (2), 251-260.

7. Lippincott-Schwartz, J.; Roberts, T. H.; Hirschberg, K., Secretory protein trafficking and organelle dynamics in living cells. *Annual review of cell and developmental biology* **2000,** *16* (1), 557-589.

8. Crowley, K. S.; Reinhart, G. D.; Johnson, A. E., The signal sequence moves through a ribosomal tunnel into a noncytoplasmic aqueous environment at the ER membrane early in translocation. *Cell* **1993,** *73* (6), 1101-1115.

9. Fitz, V.; Shin, J.; Ehrlich, C.; Farnung, L.; Cramer, P.; Zaburdaev, V.; Grill, S. W., Nucleosomal arrangement affects single-molecule transcription dynamics. *Proceedings of the National Academy of Sciences* **2016,** *113* (45), 12733-12738.

10. Goodrich, J. A.; Tjian, R., Transcription factors IIE and IIH and ATP hydrolysis direct promoter clearance by RNA polymerase II. *Cell* **1994,** *77* (1), 145-156.

11. Anfinsen, C. B.; Haber, E., Studies on the reduction and re-formation of protein disulfide bonds. *J Biol Chem* **1961,** *236* (5), 1361-1363.

12. Anfinsen, C. B.; Haber, E.; Sela, M.; White, F., The kinetics of formation of native ribonuclease during oxidation of the reduced polypeptide chain. *Proceedings of the National Academy of Sciences* **1961,** *47* (9), 1309-1314.

13. White, F. H., Regeneration of native secondary and tertiary structures by air oxidation of reduced ribonuclease. *Journal of Biological Chemistry* **1961,** *236* (5), 1353-1360.

14. Netzer, W. J.; Hartl, F. U., Protein folding in the cytosol: chaperonin-dependent and-independent mechanisms. *Trends in biochemical sciences* **1998,** *23* (2), 68-73.

15. Fersht, A., *Structure and mechanism in protein science: A Guide to enzyme catalysis and protein folding*. World Scientific: 2017; Vol. 9.

16. Balchin, D.; Hayer-Hartl, M.; Hartl, F. U., In vivo aspects of protein folding and quality control. *Science* **2016,** *353* (6294), aac4354.

17. Dobson, C. M., Protein folding and misfolding. *Nature* **2003,** *426* (6968), 884.

18. Lippincott-Schwartz, J.; Donaldson, J. G.; Schweizer, A.; Berger, E. G.; Hauri, H.-P.; Yuan, L. C.; Klausner, R. D., Microtubule-dependent retrograde transport of proteins into the ER in the presence of brefeldin A suggests an ER recycling pathway. *Cell* **1990,** *60* (5), 821-836.

19.   Gatta, A. T.; Wong, L. H.; Sere, Y. Y.; Calderón-Noreña, D. M.; Cockcroft, S.; Menon, A. K.; Levine, T. P., A new family of StART domain proteins at membrane contact sites has a role in ER-PM sterol transport. *Elife* **2015,** *4*.

20.   Georgiev, A. G.; Sullivan, D. P.; Kersting, M. C.; Dittman, J. S.; Beh, C. T.; Menon, A. K., Osh proteins regulate membrane sterol organization but are not required for sterol movement between the ER and PM. *Traffic* **2011,** *12* (10), 1341-1355.

21.   Plemper, R. K.; Bordallo, J.; Deak, P. M.; Taxis, C.; Hitt, R.; Wolf, D. H., Genetic interactions of Hrd3p and Der3p/Hrd1p with Sec61p suggest a retro-translocation complex mediating protein transport for ER degradation. *J Cell Sci* **1999,** *112* (22), 4123-4134.

22.   Lee, M. C.; Miller, E. A.; Goldberg, J.; Orci, L.; Schekman, R., Bi-directional protein transport between the ER and Golgi. *Annu. Rev. Cell Dev. Biol.* **2004,** *20*, 87-123.

23.   Barlowe, C.; Schekman, R., SEC12 encodes a guanine-nucleotide-exchange factor essential for transport vesicle budding from the ER. *Nature* **1993,** *365* (6444), 347.

24.   Rocks, O.; Peyker, A.; Kahms, M.; Verveer, P. J.; Koerner, C.; Lumbierres, M.; Kuhlmann, J.; Waldmann, H.; Wittinghofer, A.; Bastiaens, P. I., An acylation cycle regulates localization and activity of palmitoylated Ras isoforms. *Science* **2005,** *307* (5716), 1746-1752.

25.   Pastan, I.; Willingham, M. C., The pathway of endocytosis. In *Endocytosis*, Springer: 1985; pp 1-44.

26.   Claing, A.; Laporte, S. A.; Caron, M. G.; Lefkowitz, R. J., Endocytosis of G protein-coupled receptors: roles of G protein-coupled receptor kinases and ß-arrestin proteins. *Progress in neurobiology* **2002,** *66* (2), 61-79.

27.   Gao, Y.; Zhang, Y.; Zhang, D.; Dai, X.; Estelle, M.; Zhao, Y., Auxin binding protein 1 (ABP1) is not required for either auxin signaling or Arabidopsis development. *Proceedings of the National Academy of Sciences* **2015,** *112* (7), 2275-2280.

28.   Petreska, N.; Smallwood, J., Defining Protein Kinase C Substrates Involved in the Na-K-2Cl Cotransporter 1 Endocytosis in Colonic Epithelial Cells. **2016**.

29.   Schwartz, O.; Maréchal, V.; Le Gall, S.; Lemonnier, F.; Heard, J.-M., Endocytosis of major histocompatibility complex class I molecules is induced by the HIV–1 Nef protein. *Nature medicine* **1996,** *2* (3), 338-342.

30.   McMahon, H. T.; Boucrot, E., Molecular mechanism and physiological functions of clathrin-mediated endocytosis. *Nature reviews Molecular cell biology* **2011,** *12* (8), 517.

31.   Yu, A.; Shibata, Y.; Shah, B.; Calamini, B.; Lo, D. C.; Morimoto, R. I., Protein aggregation can inhibit clathrin-mediated endocytosis by chaperone competition. *Proceedings of the National Academy of Sciences* **2014,** *111* (15), E1481-E1490.

32.   O'Sullivan, B. P.; Freedman, S. D., Cystic fibrosis. *The Lancet* **2009,** *373* (9678), 1891-1904.

33.   Busch, R., On the history of cystic fibrosis. *Acta Universitatis Carolinae. Medica* **1990,** *36* (1-4), 13-15.

34.   Andersen, D. H., Cystic fibrosis of the pancreas and its relation to celiac disease: a clinical and pathologic study. *American Journal of Diseases of Children* **1938,** *56* (2), 344-399.

35.   Massie, J.; Delatycki, M. B., Cystic fibrosis carrier screening. *Paediatric respiratory reviews* **2013,** *14* (4), 270-275.

36.   Davidson, D. J.; Porteous, D. J., The genetics of cystic fibrosis lung disease. *Thorax* **1998,** *53* (5), 389-397.

37.   Frizzell, R. A.; Hanrahan, J. W., Physiology of Epithelial Chloride and Fluid Secretion. *Cold Spring Harbor Perspectives in Medicine* **2012,** *2* (6), a009563.

38.   Cohen, T. S.; Prince, A., Cystic fibrosis: a mucosal immunodeficiency syndrome. *Nat Med* **2012,** *18* (4), 509-19.

39.   Cohn, J. A., Reduced CFTR function and the pathobiology of idiopathic pancreatitis. *J Clin Gastroenterol* **2005,** *39* (4 Suppl 2), S70-7.

40.   Bombieri, C.; Claustres, M.; De Boeck, K.; Derichs, N.; Dodge, J.; Girodon, E.; Sermet, I.; Schwarz, M.; Tzetis, M.; Wilschanski, M.; Bareil, C.; Bilton, D.; Castellani, C.; Cuppens, H.; Cutting, G. R.; Drevinek, P.; Farrell, P.; Elborn, J. S.; Jarvi, K.; Kerem, B.; Kerem, E.; Knowles, M.; Macek, M., Jr.; Munck, A.; Radojkovic, D.; Seia, M.; Sheppard, D. N.; Southern, K. W.; Stuhrmann, M.; Tullis, E.; Zielenski, J.; Pignatti, P. F.; Ferec, C., Recommendations for the classification of diseases as CFTR-related disorders. *J Cyst Fibros* **2011,** *10 Suppl 2,* S86-102.

41.   Rowe, S. M.; Miller, S.; Sorscher, E. J., Cystic fibrosis. *N Engl J Med* **2005,** *352* (19), 1992-2001.

42.   Rowe, S. M.; Pyle, L. C.; Jurkevante, A.; Varga, K.; Collawn, J.; Sloane, P. A.; Woodworth, B.; Mazur, M.; Fulton, J.; Fan, L.; Li, Y.; Fortenberry, J.; Sorscher, E. J.; Clancy, J. P., DeltaF508 CFTR processing correction and activity in polarized airway and non-airway cell monolayers. *Pulmonary Pharmacology & Therapeutics* **2010,** *23* (4), 268-78.

43.   Okiyoneda, T.; Veit, G.; Dekkers, J. F.; Bagdany, M.; Soya, N.; Xu, H.; Roldan, A.; Verkman, A. S.; Kurth, M.; Simon, A.; Hegedus, T.; Beekman, J. M.; Lukacs, G. L., Mechanism-based corrector combination restores DeltaF508-CFTR folding and function. *Nat Chem Biol* **2013,** *9* (7), 444-54.

44.   Turnbull, E. L.; Rosser, M. F.; Cyr, D. M., The role of the UPS in cystic fibrosis. *BMC Biochem* **2007,** *8 Suppl 1,* S11.

45.   Wang, X.; Matteson, J.; An, Y.; Moyer, B.; Yoo, J. S.; Bannykh, S.; Wilson, I. A.; Riordan, J. R.; Balch, W. E., COPII-dependent export of cystic fibrosis transmembrane conductance regulator from the ER uses a di-acidic exit code. *J Cell Biol* **2004,** *167* (1), 65-74.

46.   Sharma, M.; Pampinella, F.; Nemes, C.; Benharouga, M.; So, J.; Du, K.; Bache, K. G.; Papsin, B.; Zerangue, N.; Stenmark, H.; Lukacs, G. L., Misfolding diverts CFTR from recycling to degradation: quality control at early endosomes. *J Cell Biol* **2004,** *164* (6), 923-33.

47.   Younger, J. M.; Chen, L.; Ren, H. Y.; Rosser, M. F.; Turnbull, E. L.; Fan, C. Y.; Patterson, C.; Cyr, D. M., Sequential quality-control checkpoints triage misfolded cystic fibrosis transmembrane conductance regulator. *Cell* **2006,** *126* (3), 571-82.

48.   Du, K.; Lukacs, G. L., Cooperative Assembly and Misfolding of CFTR Domains In Vivo. *Molecular Biology of the Cell* **2009,** *20* (7), 1903-1915.

49.   Cui, L.; Aleksandrov, L.; Chang, X. B.; Hou, Y. X.; He, L.; Hegedus, T.; Gentzsch, M.; Aleksandrov, A.; Balch, W. E.; Riordan, J. R., Domain interdependence in the biosynthetic assembly of CFTR. *J Mol Biol* **2007,** *365* (4), 981-94.

50.   Du, K.; Sharma, M.; Lukacs, G. L., The DeltaF508 cystic fibrosis mutation impairs domain-domain interactions and arrests post-translational folding of CFTR. *Nat Struct Mol Biol* **2005,** *12* (1), 17-25.

51.   Lukacs, G. L.; Chang, X. B.; Bear, C.; Kartner, N.; Mohamed, A.; Riordan, J. R.; Grinstein, S., The delta F508 mutation decreases the stability of cystic fibrosis transmembrane conductance regulator in the plasma membrane. Determination of functional half-lives on transfected cells. *J Biol Chem* **1993,** *268* (29), 21592-8.

52.   Hoelen, H.; Kleizen, B.; Schmidt, A.; Richardson, J.; Charitou, P.; Thomas, P. J.; Braakman, I., The Primary Folding Defect and Rescue of ΔF508 CFTR Emerge during Translation of the Mutant Domain. *PLoS ONE* **2010,** *5* (11), e15458.

53.   He, L.; Aleksandrov, A. A.; Serohijos, A. W. R.; Hegedüs, T.; Aleksandrov, L. A.; Cui, L.; Dokholyan, N. V.; Riordan, J. R., Multiple Membrane-Cytoplasmic Domain Contacts in the Cystic Fibrosis Transmembrane Conductance Regulator (CFTR) Mediate Regulation of Channel Gating. *Journal of Biological Chemistry* **2008,** *283* (39), 26383-26390.

54.	He, L.; Aleksandrov, L. A.; Cui, L.; Jensen, T. J.; Nesbitt, K. L.; Riordan, J. R., Restoration of domain folding and interdomain assembly by second-site suppressors of the ΔF508 mutation in CFTR. *The FASEB Journal* **2010,** *24* (8), 3103-3112.

55.	Cant, N.; Pollock, N.; Ford, R. C., CFTR structure and cystic fibrosis. *The international journal of biochemistry & cell biology* **2014,** *52*, 15-25.

56.	Adam, V.; Nienhaus, K.; Bourgeois, D.; Nienhaus, G. U., Structural basis of enhanced photoconversion yield in green fluorescent protein-like protein Dendra2. *Biochemistry* **2009,** *48* (22), 4905-4915.

57.	Liu, F.; Zhang, Z.; Csanády, L.; Gadsby, D. C.; Chen, J., Molecular structure of the human CFTR ion channel. *Cell* **2017,** *169* (1), 85-95. e8.

58.	Riordan, J. R., CFTR function and prospects for therapy. *Annu. Rev. Biochem.* **2008,** *77*, 701-726.

59.	Chang, X.-b.; Mengos, A.; Hou, Y.-x.; Cui, L.; Jensen, T. J.; Aleksandrov, A.; Riordan, J. R.; Gentzsch, M., Role of N-linked oligosaccharides in the biosynthetic processing of the cystic fibrosis membrane conductance regulator. *Journal of cell science* **2008,** *121* (17), 2814-2823.

60.	Ostedgaard, L. S.; Baldursson, O.; Vermeer, D. W.; Welsh, M. J.; Robertson, A. D., A functional R domain from cystic fibrosis transmembrane conductance regulator is predominantly unstructured in solution. *Proceedings of the National Academy of Sciences* **2000,** *97* (10), 5657-5662.

61.	Dulhanty, A. M.; Riordan, J. R., Phosphorylation by cAMP-dependent protein kinase causes a conformational change in the R domain of the cystic fibrosis transmembrane conductance regulator. *Biochemistry* **1994,** *33* (13), 4072-4079.

62.	Van Goor, F.; Straley, K. S.; Cao, D.; González, J.; Hadida, S.; Hazlewood, A.; Joubran, J.; Knapp, T.; Makings, L. R.; Miller, M., Rescue of ΔF508-CFTR trafficking and gating in human cystic fibrosis airway primary cultures by small molecules. *American Journal of Physiology-Lung Cellular and Molecular Physiology* **2006,** *290* (6), L1117-L1130.

63.	Heda, G. D.; Tanwani, M.; Marino, C. R., The ΔF508 mutation shortens the biochemical half-life of plasma membrane CFTR in polarized epithelial cells. *American Journal of Physiology-Cell Physiology* **2001,** *280* (1), C166-C174.

64.	Ameen, N.; Silvis, M.; Bradbury, N. A., Endocytic trafficking of CFTR in health and disease. *Journal of Cystic Fibrosis* **2007,** *6* (1), 1-14.

65.	Farinha, C. M.; Canato, S., From the endoplasmic reticulum to the plasma membrane: mechanisms of CFTR folding and trafficking. *Cellular and molecular life sciences* **2017,** *74* (1), 39-55.

66.	Holleran, J. P.; Zeng, J.; Frizzell, R. A.; Watkins, S. C., Regulated recycling of mutant CFTR partially restored by pharmacological treatment. *J Cell Sci* **2013**, jcs. 120196.

67.	Accurso, F. J.; Rowe, S. M.; Clancy, J.; Boyle, M. P.; Dunitz, J. M.; Durie, P. R.; Sagel, S. D.; Hornick, D. B.; Konstan, M. W.; Donaldson, S. H., Effect of VX-770 in persons with cystic fibrosis and the G551D-CFTR mutation. *New England Journal of Medicine* **2010,** *363* (21), 1991-2003.

68.	Eckford, P. D.; Li, C.; Ramjeesingh, M.; Bear, C. E., Cystic fibrosis transmembrane conductance regulator (CFTR) potentiator VX-770 (ivacaftor) opens the defective channel gate of mutant CFTR in a phosphorylation-dependent but ATP-independent manner. *Journal of Biological Chemistry* **2012,** *287* (44), 36639-36649.

69.	Jih, K.-Y.; Hwang, T.-C., Vx-770 potentiates CFTR function by promoting decoupling between the gating cycle and ATP hydrolysis cycle. *Proceedings of the National Academy of Sciences* **2013**, 201215982.

70.	Van Goor, F.; Hadida, S.; Grootenhuis, P. D.; Burton, B.; Cao, D.; Neuberger, T.; Turnbull, A.; Singh, A.; Joubran, J.; Hazlewood, A., Rescue of CF airway epithelial cell function in vitro by a

CFTR potentiator, VX-770. *Proceedings of the National Academy of Sciences* **2009,** *106* (44), 18825-18830.

71.   Sloane, P. A.; Rowe, S. M., Cystic fibrosis transmembrane conductance regulator protein repair as a therapeutic strategy in cystic fibrosis. *Current opinion in pulmonary medicine* **2010,** *16* (6), 591.

72.   Eckford, P. D.; Ramjeesingh, M.; Molinski, S.; Pasyk, S.; Dekkers, J. F.; Li, C.; Ahmadi, S.; Ip, W.; Chung, T. E.; Du, K., VX-809 and related corrector compounds exhibit secondary activity stabilizing active F508del-CFTR after its partial rescue to the cell surface. *Chemistry & biology* **2014,** *21* (5), 666-678.

73.   Ren, H. Y.; Grove, D. E.; De La Rosa, O.; Houck, S. A.; Sopha, P.; Van Goor, F.; Hoffman, B. J.; Cyr, D. M., VX-809 corrects folding defects in cystic fibrosis transmembrane conductance regulator protein through action on membrane-spanning domain 1. *Molecular biology of the cell* **2013,** *24* (19), 3016-3024.

74.   Van Goor, F.; Hadida, S.; Grootenhuis, P. D.; Burton, B.; Stack, J. H.; Straley, K. S.; Decker, C. J.; Miller, M.; McCartney, J.; Olson, E. R., Correction of the F508del-CFTR protein processing defect in vitro by the investigational drug VX-809. *Proceedings of the National Academy of Sciences* **2011,** *108* (46), 18843-18848.

75.   Boyle, M. P.; De Boeck, K., A new era in the treatment of cystic fibrosis: correction of the underlying CFTR defect. *The Lancet Respiratory Medicine* **2013,** *1* (2), 158-163.

76.   Donaldson, S.; Pilewski, J.; Griese, M.; Dong, Q.; Lee, P.-S., WS7. 3 VX-661, an investigational CFTR corrector, in combination with ivacaftor, a CFTR potentiator, in patients with CF and homozygous for the F508Del-CFTR mutation: Interim analysis. *Journal of Cystic Fibrosis* **2013,** *12*, S14.

77.   Donaldson, S. H.; Pilewski, J. M.; Griese, M.; Cooke, J.; Viswanathan, L.; Tullis, E.; Davies, J. C.; Lekstrom-Himes, J. A.; Wang, L. T., Tezacaftor/ivacaftor in subjects with cystic fibrosis and F508del/F508del-CFTR or F508del/G551D-CFTR. *American journal of respiratory and critical care medicine* **2018,** *197* (2), 214-224.

78.   Mijnders, M.; Kleizen, B.; Braakman, I., Correcting CFTR folding defects by small-molecule correctors to cure cystic fibrosis. *Current opinion in pharmacology* **2017,** *34*, 83-90.

79.   Hussar, D. A.; Hussar, E. F., New therapeutic agents marketed in 2018: Part 1. *Pharmacy Today* **2018,** *24* (7), 45-58.

80.   Hanukoglu, I.; Hanukoglu, A., Epithelial sodium channel (ENaC) family: phylogeny, structure–function, tissue distribution, and associated inherited diseases. *Gene* **2016,** *579* (2), 95-132.

81.   Hanukoglu, A.; Hanukoglu, I., In systemic pseudohypoaldosteronism type 1 skin manifestations are not rare and the disease is not transient. *Clinical Endocrinology* **2018**.

82.   Hanukoglu, I.; Boggula, V. R.; Vaknine, H.; Sharma, S.; Kleyman, T.; Hanukoglu, A., Expression of epithelial sodium channel (ENaC) and CFTR in the human epidermis and epidermal appendages. *Histochemistry and cell biology* **2017,** *147* (6), 733-748.

83.   Kubitscheck, U., *Fluorescence microscopy: from principles to biological applications*. John Wiley & Sons: 2017.

84.   Schulman, S. G., *Fluorescence and phosphorescence spectroscopy: physicochemical principles and practice*. Elsevier: 2017.

85.   Lichtman, J. W.; Conchello, J.-A., Fluorescence microscopy. *Nature methods* **2005,** *2* (12), 910.

86.   Plaetzer, K.; Krammer, B.; Berlanda, J.; Berr, F.; Kiesslich, T., Photophysics and photochemistry of photodynamic therapy: fundamental aspects. *Lasers in medical science* **2009,** *24* (2), 259-268.

87.   Valeur, B.; Berberan-Santos, M. N., *Molecular fluorescence: principles and applications*. John Wiley & Sons: 2012.

88.   Eastmond, D. A.; Schuler, M.; Rupa, D., Advantages and limitations of using fluorescence in situ hybridization for the detection of aneuploidy in interphase human cells. *Mutation Research Letters* **1995,** *348* (4), 153-162.

89.   Toman, K., What are the advantages and disadvantages of fluorescence microscopy. *Toman's tuberculosis: case detection, treatment, and monitoring—questions and answers. 2nd ed. Geneva: World Health Organization* **2004**, 31-34.

90.   Mattheyses, A. L.; Simon, S. M.; Rappoport, J. Z., Imaging with total internal reflection fluorescence microscopy for the cell biologist. *J Cell Sci* **2010,** *123* (21), 3621-3628.

91.   Yildiz, A.; Vale, R. D., Total internal reflection fluorescence microscopy. *Cold Spring Harbor Protocols* **2015,** *2015* (9), pdb. top086348.

92.   Axelrod, D., [1] Total internal reflection fluorescence microscopy in cell biology. In *Methods in enzymology*, Elsevier: 2003; Vol. 361, pp 1-33.

93.   Guthoff, R. F.; Zhivov, A.; Stachs, O., In vivo confocal microscopy, an inner vision of the cornea–a major review. *Clinical & experimental ophthalmology* **2009,** *37* (1), 100-117.

94.   Sheppard, C.; Shotton, D.; Sheppard, C., *Confocal Laser Scanning Microscopy. Microscopy Handbook*. New York: BIOS Scientific Publishers Ltd: 1997.

95.   Martin, W. E.; Srijanto, B. R.; Collier, C. P.; Vosch, T.; Richards, C. I., A Comparison of Single-Molecule Emission in Aluminum and Gold Zero-Mode Waveguides. *The Journal of Physical Chemistry A* **2016,** *120* (34), 6719-6727.

96.   Murphy, D. B.; Davidson, M. W., Confocal laser scanning microscopy. *Fundamentals of Light Microscopy and Electronic Imaging, Second Edition* **2012**, 265-305.

97.   Taraska, J. W.; Zagotta, W. N., Fluorescence applications in molecular neurobiology. *Neuron* **2010,** *66* (2), 170-89.

98.   Hohlbein, J.; Kapanidis, A., Probing the Conformational Landscape of DNA Polymerases Using Diffusion-Based Single-Molecule FRET. In *Methods in enzymology*, Elsevier: 2016; Vol. 581, pp 353-378.

99.   Roy, R.; Hohng, S.; Ha, T., A practical guide to single-molecule FRET. *Nature methods* **2008,** *5* (6), 507.

100.   Elf, J.; Li, G.-W.; Xie, X. S., Probing transcription factor dynamics at the single-molecule level in a living cell. *Science* **2007,** *316* (5828), 1191-1194.

101.   Schwille, P.; Korlach, J.; Webb, W. W., Fluorescence correlation spectroscopy with single‐molecule sensitivity on cell and model membranes. *Cytometry: The Journal of the International Society for Analytical Cytology* **1999,** *36* (3), 176-182.

102.   Foster, R. A., An analysis of the action of proflavine on bacteriophage growth. *Journal of bacteriology* **1948,** *56* (6), 795.

103.   Schaufele, F.; Demarco, I.; Day, R. N., FRET imaging in the wide-field microscope. In *Molecular Imaging*, Elsevier Inc.: 2005.

104.   Dos Remedios, C. G.; Moens, P. D., Fluorescence resonance energy transfer spectroscopy is a reliable" ruler" for measuring structural changes in proteins: dispelling the problem of the unknown orientation factor. *Journal of structural biology* **1995,** *115* (2), 175-185.

105.   Piston, D. W.; Kremers, G.-J., Fluorescent protein FRET: the good, the bad and the ugly. *Trends in biochemical sciences* **2007,** *32* (9), 407-414.

106.   Hohlbein, J.; Craggs, T. D.; Cordes, T., Alternating-laser excitation: single-molecule FRET and beyond. *Chemical Society Reviews* **2014,** *43* (4), 1156-1171.

107.   Nagai, T.; Sawano, A.; Park, E. S.; Miyawaki, A., Circularly permuted green fluorescent proteins engineered to sense Ca2+. *Proceedings of the National Academy of Sciences* **2001,** *98* (6), 3197-3202.

108.   Miesenböck, G.; De Angelis, D. A.; Rothman, J. E., Visualizing secretion and synaptic transmission with pH-sensitive green fluorescent proteins. *Nature* **1998,** *394* (6689), 192.

109.   Labas, Y. A.; Gurskaya, N.; Yanushevich, Y. G.; Fradkov, A.; Lukyanov, K.; Lukyanov, S.; Matz, M., Diversity and evolution of the green fluorescent protein family. *Proceedings of the National Academy of Sciences* **2002,** *99* (7), 4256-4261.

110.   Gurskaya, N. G.; Verkhusha, V. V.; Shcheglov, A. S.; Staroverov, D. B.; Chepurnykh, T. V.; Fradkov, A. F.; Lukyanov, S.; Lukyanov, K. A., Engineering of a monomeric green-to-red photoactivatable fluorescent protein induced by blue light. *Nature biotechnology* **2006,** *24* (4), 461.

111.   Heidary, D. K.; Fox, A.; Richards, C. I.; Glazer, E. C., A High-Throughput Screening Assay Using a Photoconvertable Protein for Identifying Inhibitors of Transcription, Translation, or Proteasomal Degradation. *SLAS DISCOVERY: Advancing Life Sciences R&D* **2017,** *22* (4), 399-407.

112.   Zhang, L.; Gurskaya, N. G.; Merzlyak, E. M.; Staroverov, D. B.; Mudrik, N. N.; Samarkina, O. N.; Vinokurov, L. M.; Lukyanov, S.; Lukyanov, K. A., Method for real-time monitoring of protein degradation at the single cell level. *Biotechniques* **2007,** *42* (4), 446.

113.   Akai, S.; Okayama, H.; Shimura, S.; Tanno, Y.; Sasaki, H.; Takishima, T., F508 mutation of cystic fibrosis gene is not found in chronic bronchitis with severe obstruction in Japan. *Am Rev Respir Dis* **1992,** *146*, 781-783.

114.   Van Goor, F.; Hadida, S.; Grootenhuis, P. D.; Burton, B.; Stack, J. H.; Straley, K. S.; Decker, C. J.; Miller, M.; McCartney, J.; Olson, E. R.; Wine, J. J.; Frizzell, R. A.; Ashlock, M.; Negulescu, P. A., Correction of the F508del-CFTR protein processing defect in vitro by the investigational drug VX-809. *Proc Natl Acad Sci U S A* **2011,** *108* (46), 18843-8.

115.   Rowe, S. M.; Verkman, A. S., Cystic fibrosis transmembrane regulator correctors and potentiators. *Cold Spring Harb Perspect Med* **2013,** *3* (7).

116.   McPhail, G. L.; Clancy, J. P., Ivacaftor: the first therapy acting on the primary cause of cystic fibrosis. *Drugs Today (Barc)* **2013,** *49* (4), 253-60.

117.   Zhang, L.; Button, B.; Gabriel, S. E.; Burkett, S.; Yan, Y.; Skiadopoulos, M. H.; Dang, Y. L.; Vogel, L. N.; McKay, T.; Mengos, A.; Boucher, R. C.; Collins, P. L.; Pickles, R. J., CFTR Delivery to 25% of Surface Epithelial Cells Restores Normal Rates of Mucus Transport to Human Cystic Fibrosis Airway Epithelium. *PLoS Biology* **2009,** *7* (7), e1000155.

118.   Dalemans, W.; Barbry, P.; Champigny, G.; Jallet, S.; Dott, K.; Dreyer, D.; Crystal, R. G.; Pavirani, A.; Lecocq, J.-P.; Lazdunski, M., Altered chloride ion channel kinetics associated with (Δ)F508 cystic fibrosis mutation. *Nature* **1991,** *354*, 526-528.

119.   Drumm, M. L.; Wilkinson, D. J.; Smit, L. S.; Worrell, R. T.; Strong, T. V.; Frizzell, R. A.; Dawson, D. C.; Collins, F. S., Chloride conductance expressed by delta F508 and other mutant CFTRs in Xenopus oocytes. *Science* **1991,** *254* (5039), 1797-9.

120.   Farinha, Carlos M.; King-Underwood, J.; Sousa, M.; Correia, Ana R.; Henriques, Bárbara J.; Roxo-Rosa, M.; Da Paula, Ana C.; Williams, J.; Hirst, S.; Gomes, Cláudio M.; Amaral, Margarida D., Revertants, Low Temperature, and Correctors Reveal the Mechanism of F508del-CFTR Rescue by VX-809 and Suggest Multiple Agents for Full Correction. *Chemistry & Biology* **2013,** *20* (7), 943-955.

121.   Deniz, A. A.; Laurence, T. A.; Beligere, G. S.; Dahan, M.; Martin, A. B.; Chemla, D. S.; Dawson, P. E.; Schultz, P. G.; Weiss, S., Single-molecule protein folding: diffusion fluorescence resonance energy transfer studies of the denaturation of chymotrypsin inhibitor 2. *Proceedings of the National Academy of Sciences* **2000,** *97* (10), 5179-5184.

122.   Colley, B. S.; Biju, K.; Visegrady, A.; Campbell, S.; Fadool, D. A., Neurotrophin B receptor kinase increases Kv subfamily member 1.3 (Kv1. 3) ion channel half-life and surface expression. *Neuroscience* **2007,** *144* (2), 531-546.

123.   Zhou, P., Determining protein half-lives. *Signal Transduction Protocols* **2004**, 67-77.

124.   De La Rosa, D. A.; Li, H.; Canessa, C. M., Effects of aldosterone on biosynthesis, traffic, and functional expression of epithelial sodium channels in A6 cells. *The Journal of general physiology* **2002,** *119* (5), 427-442.

125.   Yu, L.; Helms, M. N.; Yue, Q.; Eaton, D. C., Single-channel analysis of functional epithelial sodium channel (ENaC) stability at the apical membrane of A6 distal kidney cells. *Am J Physiol Renal Physiol* **2008,** *295* (5), F1519-27.

126.   Kleyman, T. R.; Zuckerman, J. B.; Middleton, P.; McNulty, K. A.; Hu, B.; Su, X.; An, B.; Eaton, D. C.; Smith, P. R., Cell surface expression and turnover of the α-subunit of the epithelial sodium channel. *American Journal of Physiology-Renal Physiology* **2001,** *281* (2), F213-F221.

127.   Mohan, S.; Bruns, J. R.; Weixel, K. M.; Edinger, R. S.; Bruns, J. B.; Kleyman, T. R.; Johnson, J. P.; Weisz, O. A., Differential current decay profiles of epithelial sodium channel subunit combinations in polarized renal epithelial cells. *Journal of Biological Chemistry* **2004,** *279* (31), 32071-32078.

128.   Richards, C. I.; Srinivasan, R.; Xiao, C.; Mackey, E. D. W.; Miwa, J. M.; Lester, H. A., Trafficking of α4* Nicotinic Receptors Revealed by Supercliptic Phluorin. *J. Biol. Chem.* **2011,** *286* (36), 31241-31249.

129.   Srinivasan, R.; Richards, C. I.; Dilworth, C.; Moss, F. J.; Dougherty, D. A.; Lester, H. A., Forster Resonance Energy Transfer (FRET) Correlates of Altered Subunit Stoichiometry in Cys-Loop Receptors, Exemplified by Nicotinic alpha 4 beta 2. *Int. J. Mol. Sci.* **2012,** *13* (8), 10022-10040.

130.   Yudowski, G. A.; Puthenveedu, M. A.; Leonoudakis, D.; Panicker, S.; Thorn, K. S.; Beattie, E. C.; von Zastrow, M., Real-time imaging of discrete exocytic events mediating surface delivery of AMPA receptors. *Journal of Neuroscience* **2007,** *27* (41), 11112-21.

131.   Araki, Y.; Lin, D. T.; Huganir, R. L., Plasma membrane insertion of the AMPA receptor GluA2 subunit is regulated by NSF binding and Q/R editing of the ion pore. *Proc. Natl. Acad. Sci. U. S. A.* **2010,** *107* (24), 11080-11085.

132.   Ameen, N.; Silvis, M.; Bradbury, N. A., Endocytic Trafficking of CFTR in Health and Disease. *Journal of cystic fibrosis : official journal of the European Cystic Fibrosis Society* **2007,** *6* (1), 1-14.

133.   Sondo, E.; Tomati, V.; Caci, E.; Esposito, A. I.; Pfeffer, U.; Pedemonte, N.; Galietta, L. J., Rescue of the mutant CFTR chloride channel by pharmacological correctors and low temperature analyzed by gene expression profiling. *Am J Physiol Cell Physiol* **2011,** *301* (4), 13.

134.   Cigana, C.; Nicolis, E.; Pasetto, M.; Assael, B. M.; Melotti, P., Anti-inflammatory effects of azithromycin in cystic fibrosis airway epithelial cells. *Biochemical and biophysical research communications* **2006,** *350* (4), 977-982.

135.   Saint-Criq, V.; Ruffin, M.; Rebeyrol, C.; Guillot, L.; Jacquot, J.; Clement, A.; Tabary, O., Azithromycin fails to reduce inflammation in cystic fibrosis airway epithelial cells. *European journal of pharmacology* **2012,** *674* (1), 1-6.

136.   Oliynyk, I.; Varelogianni, G.; Schalling, M.; Asplund, M. S.; Roomans, G. M.; Johannesson, M., Azithromycin increases chloride efflux from cystic fibrosis airway epithelial cells. *Experimental lung research* **2009,** *35* (3), 210-221.

137.   Saint-Criq, V.; Rebeyrol, C.; Ruffin, M.; Roque, T.; Guillot, L.; Jacquot, J.; Clement, A.; Tabary, O., Restoration of chloride efflux by azithromycin in CF human airway epithelial cells. *Antimicrobial agents and chemotherapy* **2011**.

138.   Merrifield, C. J.; Feldman, M. E.; Wan, L.; Almers, W., Imaging actin and dynamin recruitment during invagination of single clathrin-coated pits. *Nature cell biology* **2002,** *4* (9), 691.

139.   Macro, L.; Jaiswal, J. K.; Simon, S. M., Dynamics of clathrin-mediated endocytosis and its requirement for organelle biogenesis in Dictyostelium. *J Cell Sci* **2012,** *125* (23), 5721-5732.

140.   Gaidarov, I.; Santini, F.; Warren, R. A.; Keen, J. H., Spatial control of coated-pit dynamics in living cells. *Nature cell biology* **1999,** *1* (1), 1.

141.   Toshima, J. Y.; Toshima, J.; Kaksonen, M.; Martin, A. C.; King, D. S.; Drubin, D. G., Spatial dynamics of receptor-mediated endocytic trafficking in budding yeast revealed by using fluorescent α-factor derivatives. *Proceedings of the National Academy of Sciences* **2006,** *103* (15), 5793-5798.

142.   Holleran, J. P.; Zeng, J.; Frizzell, R. A.; Watkins, S. C., Regulated recycling of mutant CFTR is partially restored by pharmacological treatment. *Journal of Cell Science* **2013,** *126* (Pt 12), 2692-703.

143.   Raju, S. V.; Jackson, P. L.; Courville, C. A.; McNicholas, C. M.; Sloane, P. A.; Sabbatini, G.; Tidwell, S.; Tang, L. P.; Liu, B.; Fortenberry, J. A.; Jones, C. W.; Boydston, J. A.; Clancy, J. P.; Bowen, L. E.; Accurso, F. J.; Blalock, J. E.; Dransfield, M. T.; Rowe, S. M., Cigarette smoke induces systemic defects in cystic fibrosis transmembrane conductance regulator function. *Am J Respir Crit Care Med* **2013,** *188* (11), 1321-30.

144.   Zhang, Z.; Chen, J., Atomic structure of the cystic fibrosis transmembrane conductance regulator. *Cell* **2016,** *167* (6), 1586-1597. e9.

145.   Zhang, Z.; Liu, F.; Chen, J., Conformational changes of CFTR upon phosphorylation and ATP binding. *Cell* **2017,** *170* (3), 483-491. e8.

146.   Du, K.; Sharma, M.; Lukacs, G. L., The ΔF508 cystic fibrosis mutation impairs domain-domain interactions and arrests post-translational folding of CFTR. *Nature Structural and Molecular Biology* **2005,** *12* (1), 17.

147.   Ismailov, I.; Berdiev, B.; Shlyonsky, V. G.; Fuller, C.; Prat, A.; Jovov, B.; Cantiello, H.; Ausiello, D.; Benos, D., Role of actin in regulation of epithelial sodium channels by CFTR. *American Journal of Physiology-Cell Physiology* **1997,** *272* (4), C1077-C1086.

148.   Ji, H.-L.; Chalfant, M. L.; Jovov, B.; Lockhart, J. P.; Parker, S. B.; Fuller, C. M.; Stanton, B. A.; Benos, D. J., The cytosolic termini of the β-and γ-ENaC subunits are involved in the functional interactions between cystic fibrosis transmembrane conductance regulator and epithelial sodium channel. *Journal of Biological Chemistry* **2000,** *275* (36), 27947-27956.

149.   Ling, B. N.; Zuckerman, J. B.; Lin, C.; Harte, B. J.; McNulty, K. A.; Smith, P. R.; Gomez, L. M.; Worrell, R. T.; Eaton, D. C.; Kleyman, T. R., Expression of the cystic fibrosis phenotype in a renal amphibian epithelial cell line. *Journal of Biological Chemistry* **1997,** *272* (1), 594-600.

150.   Rubenstein, R. C.; Lockwood, S. R.; Lide, E.; Bauer, R.; Suaud, L.; Grumbach, Y., Regulation of endogenous ENaC functional expression by CFTR and ΔF508-CFTR in airway epithelial cells. *American Journal of Physiology-Lung Cellular and Molecular Physiology* **2010,** *300* (1), L88-L101.

151.   Zhang, L.; Gurskaya, N. G.; Merzlyak, E. M.; Staroverov, D. B.; Mudrik, N. N.; Samarkina, O. N.; Vinokurov, L. M.; Lukyanov, S.; Lukyanov, K. A., Method for real-time monitoring of protein degradation at the single cell level. *Biotechniques* **2007,** *42* (4), 450.

152.   May, A.; Puoti, A.; Gaeggeler, H.-P.; Horisberger, J.-D.; Rossier, B. C., Early effect of aldosterone on the rate of synthesis of the epithelial sodium channel alpha subunit in A6 renal cells. *Journal of the American Society of Nephrology* **1997,** *8* (12), 1813-1822.

153.   Rotin, D.; Kanelis, V.; Schild, L., Trafficking and cell surface stability of ENaC. *American Journal of Physiology-Renal Physiology* **2001,** *281* (3), F391-F399.

154.   Staub, O.; Gautschi, I.; Ishikawa, T.; Breitschopf, K.; Ciechanover, A.; Schild, L.; Rotin, D., Regulation of stability and function of the epithelial Na+ channel (ENaC) by ubiquitination. *The EMBO journal* **1997,** *16* (21), 6325-6336.

155.   Weisz, O. A.; Wang, J.-M.; Edinger, R. S.; Johnson, J. P., Non-coordinate regulation of endogenous epithelial sodium channel (ENaC) subunit expression at the apical membrane of A6 cells in response to various transporting conditions. *Journal of Biological Chemistry* **2000,** *275* (51), 39886-39893.

156.   Yang, K.-Q.; Xiao, Y.; Tian, T.; Gao, L.-G.; Zhou, X.-L., Molecular genetics of Liddle's syndrome. *Clinica Chimica Acta* **2014,** *436*, 202-206.

VITA

Education:

2009-2013   **B.S. in Pharmacy**   Hebei University, China

Publication:

Zhang, Z.; Heidary, D; Richards, C.I., High Resolution Quantification of Receptor Endocytosis. Manuscript Accepted

Zhang, Z.; Baksh, M. M.; Finn, M.; Heidary, D. K.; Richards, C. I., Direct Measurement of Trafficking of the Cystic Fibrosis Transmembrane Conductance Regulator to the Cell Surface and Binding to a Chemical Chaperone. Biochemistry 2016, 56 (1), 240-249.

Sun, Y.; Heidary, D.K.; **Zhang, Z.**; Richards, C.I.; Glazer, E.C., Bacterial Cytological Profiling Reveals the Mechanism of Action of Anticancer Metal Complexes Molecular Pharmaceutics, 2018.

Ma, G.; Li, Y.; Dong, J.; Zou, Y.; **Zhang, Z.**; Sun, Y., The dynamic nature of incubation solution after cooling to room temperature in amyloid formation of hen egg white lysozyme: An FTIR assessment. Vibrational Spectroscopy 2013**,** 64, 44-50.

Conference Presentations:

Zhang Z. et al., "Small Molecule Induced Changes in the Trafficking of the Cystic Fibrosis Conductance Regulator", 6th Bluegrass Molecular Biophysics Symposium, May 2017, Lexington, KY. Oral Presenter.

Zhang Z. et al., "Small Molecule Induced Changes in the Trafficking of the Cystic Fibrosis Conductance Regulator", 61st Biophysical Society Annual Meeting, Feb 2017, New Orleans, LA. Poster Presenter.

Zhang Z. et al., "Quantifying Membrane Protein Endocytosis with Photoconvertible Fluorophores", 62nd Biophysical Society Annual Meeting, Feb 2018, San Francisco, CA. Poster Presenter

Zhang Z. et al., "Quantifying Membrane Protein Endocytosis with Photoconvertible Fluorophores", 255th ACS National Meeting, March 2018, New Orleans, LA. Poster Presenter